Effects of Varying Material Properties on the Available Rotation Capacity of a One-Way Slab

By
Sascha Prein
Steven L. McCabe

Structural Engineering and Engineering Materials
SM Report No. 50
June 1998

THE UNIVERSITY OF KANSAS CENTER FOR RESEARCH, INC.
2291 Irving Hill Drive - Campus West, Lawrence, Kansas 66045

Effects Of Varying Material Properties On The Available Rotation Capacity Of A One-Way Slab

By

Sascha Prein
Steven L. McCabe

Structural Engineering and Engineering Materials
SM Report No. 50

UNIVERSITY OF KANSAS CENTER FOR RESEARCH, INC.
LAWRENCE, KANSAS
June 1998

ABSTRACT

Effects of Varying Material Properties on the Available Rotation Capacity of a One-Way Slab

Sascha Prein and Steven L. McCabe
Department of Civil and Environmental Engineering
University of Kansas
Lawrence, KS 66045

The influence of reinforcing steel properties on the behavior of a one-way slab is investigated. A number of European and American reinforcing steels are evaluated at different effective reinforcing ratios and their influence on the rotation capacity of the slab is determined. The effect of high strength concrete in a slab with large effective reinforcing ratios also is addressed. Analytical work is performed using a nonlinear finite element approach in a three-dimensional model. To simulate the behavior of concrete in tension, the smeared crack approach is used, while compression softening is approximated with the Willam-Warnke model. The stress-strain behavior of the reinforcing steel is incorporated using a multilinear elastic strain-hardening model and a model for bond-slip is adapted to take the structural response at the steel-concrete interface into account. During preliminary studies different models for compression softening and concrete behavior under tension were investigated. Also, the effects of the mesh, convergence tolerances and load step size were studied.

Analyses are performed for three point bending and the load is applied by imposing displacements on the system. To calibrate the finite element model, the results are compared to experimental data. Load-displacement curves are generated to measure the response of the system and the maximum amounts of carrying capacity obtained from the finite element analysis are compared to predictions using ACI 318-95 (1995) design equations.

The results of this study suggest that the influence of the ductility characteristics of the reinforcing steel on the rotation capacity of the structure depend on the effective reinforcing ratio of the specimen. At low reinforcing levels, the structural behavior is governed by the ductility characteristics of the steel, thus, the amount of deflection at failure depends on the ultimate elongation capability of the steel. By increasing the amounts of steel in the structure, the overall behavior is shifted from a ductile to a brittle failure mode. Therefore, in structures with moderate amounts of reinforcement the choice of reinforcing steel determines whether the structural behavior is governed by the steel characteristics or the concrete behavior. At high reinforcing levels, the concrete characteristics completely determine the structural behavior and generally all specimens with high effective reinforcing ratios exhibit a failure of the compression strut in the concrete - a brittle failure mode while the steel does not reach its yield capacity. The carrying capacity for all analysis cases with large amounts of reinforcement was found significantly under the capacities calculated with the ACI equations. Finally, all analyzed cases exhibited insensitivity to the effects of bond-slip.

ACKNOWLEDGEMENTS

The Authors wish to acknowledge the support of the Department of Civil and Environmental Engineering at the University of Kansas for their support of this research. The computing facilities provided by the Department enabled the analytical studies to be carried out. Moreover, their financial support for the first Author was essential to this research.

The Authors also wish to thank Prof. Dr.-Ing. Horst Schäfer of the Beton und Stahlbeton Lehrstuhl at the Univerisity of Dortmund for his support. The first author attended the University of Kansas on a DAAD Scholarship for this first year of study. The authors greatly appreciate the support that enabled the first Author to come to Kansas to pursue graduate study.

The support of Mr. Ken Pearce, Director of the KU School of Engineering Computing Service, is gratefully acknowledged. His help during the course of this study was of great importance in maintaining a reliable computing environment.

Lastly, the Authors wish to thank Task Group 2/2 of the Committee Euro-International du Beton (CEB), chaired by Prof. Dr.-Ing. Rolf Eligehausen of the University of Stuttgart, for their work on the ductility question. The round robin problem proposed by the Task Group was the inspiration for this research.

TABLE OF CONTENTS

CHAPTER 1

INTRODUCTION

CHAPTER 2

FINITE ELEMENT ANALYSIS - MATERIAL MODEL CONSIDERATIONS

TABLE OF CONTENTS CONT'D

TABLE OF CONTENTS CONT'D

TABLE OF CONTENTS CONT'D

APPENDIX B

COMPUTER ANALYSIS - INPUT FILES

LIST OF TABLES

* Copies of the Table/ Figure are placed in the text and in the Tables/Figures Section

LIST OF FIGURES

LIST OF FIGURES CONT'D

LIST OF FIGURES CONT'D

CHAPTER 1

INTRODUCTION

1.1 General

The ductility of concrete structures is an important issue in structural design. It is desirable to provide the ability to support large amounts of rotation capacity in plastic hinge regions to save the structural integrity of a building in case of emergency loading. Current studies suggest that the use of ductile reinforcing steel can provide additional rotation capacity in case of overloading (Comité Euro-International du Béton, 1993b).

Current building codes like the EC2 (1991) and the ACI 318-95 (1995) do not explicitly include provisions for ductility-based design. Thus, design according to the guidelines in the building codes may result in members that do not have the necessary ductility actually needed especially in highly reinforced members. Of critical concern is the role of the material properties in design. To investigate the influence of changes in the material properties a task group of the Comité Euro-International du Béton (CEB TG II/2 "Ductility") is in the process of developing a reliable relation between the steel ductility characteristics and the available rotation capacity of plastic hinges in concrete structures. It is proposed to quantify this relation as a function of the effective mechanical reinforcing ratio. The task group is gathering results from experiments performed mainly in Europe and the United States and recently initiated

a round robin proposal. The goal is to obtain analytical results from a broad scale of studies, so that general conclusions and design provisions can be derived. The issue of ductility behavior is a complex matter and many aspects influence the rotation capacity. The material characteristics of concrete and reinforcing steel, effective reinforcing ratio, member size and scale, influence of confining reinforcement and compression reinforcement all are important aspects to consider. The objective of this research project is to study the effects of changes in the stress-strain relations of the reinforcing steel and the influence of the reinforcing percentage on the rotation capacity of a one-way slab. Also, the effects of high strength concrete in a highly reinforced slab are investigated. It is of special interest how American reinforcing bars perform compared to typical European reinforcing steel. Differences in performance are expected since American reinforcing steel is characterized by significant amounts of strain-hardening, whereas European reinforcement tends to have a higher yield capacity but little strain-hardening capabilities.

The Finite Element Method can be utilized as a powerful tool to investigate the behavior of reinforced concrete structures. The response of the structure objected to loading can be studied on either a microscopic or macroscopic level. A microscopic analysis usually focuses on the evaluation of local structural behavior phenomena (e.g. local crack response) and, therefore, requires extremely detailed modeling. Macroscopic types of analysis on the other hand aim at representing the general behavior of the structure. Since this study investigates the overall member performance under monotonic loading and load-displacement relations are obtained, a

macroscopic analysis is performed. The major aspects of nonlinear behavior of the composite material reinforced concrete (cracking and crushing of the concrete, steel ductility and bond between the reinforcing steel and the concrete) are incorporated in the study. However, long-term concrete behavior such as creep and shrinkage and the microscopic effects of aggregate interlock are purposely neglected, since those additional aspects would not affect the overall performance but significantly influence and complicate the computational efforts.

1.2 Previous Work

In the early years of concrete design around the turn of the 19th century, it was realized that the complexity of concrete behavior could neither be described nor predicted with classical strength of materials principals. Concrete exhibits severe discontinuities, such as cracks, which occur at low tensile stress levels. Under the assumption of elastic material behavior, the stresses at a crack tip tend to infinity. Since no material is capable of resisting infinite stresses, a region of inelastic material behavior must surround this area. This behavior presents a level of complexity, which cannot be handled using the classical mechanics of material techniques. Methods to accurately describe this kind of material behavior (i.e. crack propagation) were developed in the field of fracture mechanics during the course of this century. In the 1930s the methods found in the area of fracture mechanics were first applied to investigate the behavior of reinforced concrete beams (Westergaard, 1934).

The invention of the computer in the 1940s and the development of the Finite Element Method in the 1950s, present the next milestones for the research of concrete behavior. First attempts to apply these powerful tools to analyze concrete structures were undertaken during the course of the 1960s (Clough, 1962; Ngo and Scordelis, 1967; Nilson, 1967 and 1968; Rashid, 1968). Even though the computational tools had advanced, certain problems in modeling this complex material behavior remained. It became apparent that concrete structures do not behave according to the principals of continuum mechanics, which is in part due to the strain-softening nature of the concrete (Bazant, 1976).

The Finite Element Method allows modeling continuum mechanical phenomena as well as discrete phenomena. This approach led to the development of two significantly different approaches to represent the concrete behavior in a finite element analysis. Discrete modeling techniques treat the cracking of the concrete as a geometrical entity, whereas the smeared crack approach applies an equivalent theory of continuum mechanics and treats cracking as a material property. Hillerborg (1976) introduced the fictitious crack method where a predefined crack was located and allowed to form, incorporating fracture mechanics principals at the crack face. A recent addition to these established modeling techniques was introduced by Bazant (1990) as the Micro-Plane Model and involves modeling the heterogeneous constituents of the concrete at the size scale of the aggregate. Currently attempts are made to combine the discrete and smeared crack modeling approaches. Since both

methods have their limitations, a combination could yield an excellent numerical representation of the concrete behavior phenomenon.

1.3 Finite Element Approaches

The two most common modeling approaches, namely discrete crack modeling and the smeared crack modeling approach are discussed here. The historical development of both methods and their analytical assumptions are presented.

1.3.1 Discrete Crack Modeling

The first attempt to utilize discrete modeling of cracks in a finite element analysis of reinforced concrete beams was undertaken by Ngo and Scordelis (1967). Concrete and steel were modeled with triangular finite elements in two-dimensional space and bond-link elements were used to connect the reinforcing steel to the concrete (Fig. 1.1). Cracks were introduced in the finite element model by separating elements along predefined crack trajectories. Once the tensile capacity was exceeded those cracks were introduced into the model. Thus, the finite element model was no longer continuous and stresses could no longer be transferred at the crack plane. However, the Ngo and Scordelis model did not account for crack propagation.

Nilson (1967 and 1968) first considered this important issue in a finite element analysis. Nonlinear material properties were introduced and applied to the model using an incremental loading technique. The analysis process required user intervention when a predefined cracking criterion was reached. Cracks were then

manually introduced in the finite element model by separating the nodes of the finite element mesh at the location where the cracking criterion was exceeded. The modified model was then incrementally reloaded from zero. Thus, crack propagation could be studied and the extent of cracking at any loading stage was obtained.

This modeling technique of discrete crack propagation had three major shortcomings: (a) crack propagation is a gradual rather than abrupt process (Hillerborg et al., 1976), (b) crack formation is mesh dependent (i.e. cracks are forced to coincide with element boundaries), and (c) the dissipated energy during crack propagation is unlikely to resemble that in the actual structure.

Further research was needed to eliminate the shortcomings in the field of discrete crack modeling. A singular crack tip element was proposed by Wilson (1969), which had the capability to model linear elastic cracks more accurately. Several improvements and additions to singular crack tip elements were developed during the following decade (Tracey, 1971; Tong et al., 1973; Barsoum, 1976). A virtual crack extension method to calculate opening mode stress intensity factors was carried out by Parks (1974) and Hellen (1975). This approach did not require the use of singular crack tip elements. After the development of the capability of computing stress intensity factors with the Finite Element Method, the next big step was to incorporate linear elastic crack propagation into the modeling approach. Fracture mechanics principals to describe this phenomenon of concrete structures were first developed by Ingraffea (1977). Numerous researchers (Ingraffea and Manu, 1980; Saouma, 1981; Gerstle, 1982 and 1986; Wawrzynek and Ingraffea, 1986; Swenson

and Ingraffea, 1988) further investigated the aspect of crack propagation by developing automatic crack trajectory algorithms and semi-automatic remeshing schemes. For a two-dimensional analysis, reasonably successful applications were developed and lately sophisticated automatic remeshing routines have been evolved from numerous research projects (ACI Committee 446, 1998). However, several problems with this method still remain to be solved for the 3-D regime, where the computational efforts are immense. Over the years is has been realized that the use approach of the linear elastic fracture mechanics approach to investigate crack propagation does not apply to concrete structures of normal size because the fracture process zone in concrete is relatively large compared to the member size. The need for a more appropriate method led to the development of a finite element model for nonlinear discrete fracture.

The fictitious crack modeling approach introduced by Hillerborg (1976) treated the crack as a strain-softening zone, which was modeled by using interface elements or cohesive nodal forces. It has become a popular tool to model the fracture behavior of concrete. The fracture process zone (Fig. 1.2) is assumed to be long and infinitesimally narrow. In this modeling approach cracking behavior is described based upon fracture energy considerations and a 'normal stress versus crack opening displacement curve' (Fig. 1.3) which is treated as a material property. The area under this curve represents the fracture energy, G_f, of the system. When the tensile stresses in the concrete exceed the tensile capacity of the material, microcracks are introduced in the model, which still can transfer stresses at the cracking plane. As the cracks

develop into larger cracks, less stress can be transferred. Once the full fracture energy is developed, the crack opening has developed into a structural discontinuity and stresses can no longer be transferred.

Since the fracture process zone is assumed to be of infinitesimal width, this phenomenon can easily be incorporated in a finite element analysis by using interface elements. Most commonly interface elements of zero thickness are used, which incorporate normal and shear stresses and relative displacements across the interface as constitutive variables. The stiffness of the element is defined by a nonlinear function following the curve of the envelope of the fracture energy as illustrated in Fig. 1.3 (Ma, T., Niwa, J., McCabe, S.L., 1991 and 1992).

Finally, situations where the fictions crack modeling approach is inappropriate to realistically represent the fracture processing zone exist. In those cases other methods of modeling the concrete behavior need to be applied. The smeared crack approach can be implemented as described next.

1.3.2 Smeared Crack Modeling

In many cases the representation of concrete cracking with a smeared crack model presents a convenient alternative to the discrete cracking approach. Rashid (1968) was the first to pursue this approach where the constitutive properties of the finite elements are altered during the analysis process rather than the topography of the finite element grid. His initial procedure involved dropping the material stiffness in the direction of the principle stress to zero, once the calculated stress exceeded the

tensile strength of the concrete. Simultaneously, the stresses in the concrete were released and redistributed in the structure as residual loads.

The material was assumed to behave initially linear elastic and isotropic. After cracking the material was treated as incrementally linear and orthotropic (material directions parallel and perpendicular to the crack). Commonly the stress-strain relationship for post-cracking behavior contains a shear retention factor that was introduced to eliminate numerical difficulties and to reflect the capability of the cracked material to carry some residual load across the crack plane. To make the analysis more realistic, a descending branch was introduced to the tensile stress-strain curves of the concrete because the concrete strength decreases gradually upon cracking rather than dropping immediately to zero. This phenomenon is often referred to as tension stiffening. Several ways of describing the downward slope of the stress-strain curve have been used in finite element analyses. Some common stress-strain curve approximations are illustrated in Fig. 1.4. Thus, the smeared crack modeling approach is capable of representing crack propagation of single and distributed cracks with reasonable accuracy.

Over the years, the smeared crack modeling approach has become the most widely used method to represent concrete behavior in a finite element analysis. The main reason being the computationally convenient way to manipulate the material stiffness matrices rather than the finite element mesh. Moreover, the highly irregular crack propagation of concrete can be investigated more realistically than with the discrete crack modeling approach. However, a downside of this modeling technique

is its mesh sensitivity (Bazant, 1976). The size of the finite elements can directly influence the outcome of an analysis. Cracking localizes in a one element wide section. Hence, the crack tends to become longer and narrower when mesh refinements as illustrated in Fig. 1.5 are implemented (Bazant and Cedolin, 1979 and 1980; Bazant and Oh, 1983; Rots et al., 1984; Darwin, 1985). Structures where the yielding of the reinforcement governs the failure proved to be insensitive to mesh size effects (Dodds et al., 1984). For all other cases the issue of mesh sensitivity can be eliminated by using a numerical tool often referred to as 'localization limiter'. The easiest localization limiter to implement is by defining a relationship between the element size and the constitutive material model. The dissipated energy has to match the energy of the material modeled. Therefore, the downward slope of the tensile stress-strain curve can be adjusted in such a way that the area below the curve represents the fracture energy of the structure. Other approaches to address the issues of localization limitation have been developed and are presented in a recent ACI report (ACI Committee 446, 1998).

1.4 Computational Tools

Reinforced concrete behavior is characterized by the combination of several nonlinearities, such as cracking and crushing of the concrete, strain-hardening of the reinforcing steel and bond-slip relationships at the interface from the steel to the concrete. Thus, analysis tools able to model this complex matter need to be utilized. The Finite Element Method has proven to be an adequate technique to model and

investigate the behavior of reinforced concrete by replacing the actual structural system by a system of small (finite) elements connected at their nodal points. Each element incorporates material properties and mathematical relationships that describe the element deformation under loading. Solutions are obtained at the node points and, therefore, the level of computational complexity increases with the number of elements. A nonlinear analysis type is required to yield reasonable solutions for cases where material properties vary over time. Hence, the solution is obtained by gradually applying loads to the system and measuring the reactions for each load increment. This type of iterative solution procedure has high demands on computation speed and storage space. In this study HP Apollo 9000 workstations (Series 700, Model 730, Model 715/50 and Model 715/80) served as the operating platforms.

The finite element software is the backbone of the analysis. Therefore, it is of great importance that features needed for a nonlinear analysis are built into the program. ANSYS53 is a commercial finite element code with built-in capabilities for nonlinear types of analysis. It provides several methods for defining incremental loading patterns and convergence criteria. Moreover, a finite element capable of modeling cracking and crushing of brittle material, such as concrete, is readily available in the program. Therefore, ANSYS53 was selected to be used in this study and testing its performance was part of the project.

1.5 Proposed Study

This project investigates the influence of changes in the ductility of the reinforcement and changes of the reinforcing percentage on the structural behavior of a one-way slab. Therefore, a range of members incorporating low to large amounts of reinforcement is evaluated. Also, the performance of a highly reinforced test specimen with high strength concrete is analyzed. The research is conducted using the Finite Element Method as an analytical tool to model the structural behavior of reinforced concrete.

The following chapter outlines the numerical models implemented in the finite element analysis to represent the material behavior of reinforced concrete. In Chapter 3 the investigated structure is introduced and the process of obtaining an accurate finite element model is described. Issues concerning the finite element mesh topology and solution techniques also are addressed and experimental data used to calibrate the finite element model is presented. The analysis cases investigated in this study are outlined in Chapter 4, which also discusses the obtained results. A summary of the research project with conclusions and interpretations of the analysis results is presented in the last chapter.

CHAPTER 2

FINITE ELEMENT ANALYSIS – MATERIAL MODEL CONSIDERATIONS

2.1 General

Several approaches to represent concrete behavior in a finite element analysis exist (Section 1.2). In this study the smeared crack approach was selected to model the concrete behavior on a macroscopic level using material constituencies that are defined to be applied as nonlinear material properties during the analysis process. This chapter outlines the constitutive models used in this study. The material models for concrete in tension and compression, reinforcing steel and bond-slip are discussed. For the numerical implementation of the concrete behavior, this research takes advantage of a finite element capable of cracking and crushing. Its mathematical model and assumptions are outlined in this chapter.

2.2 Concrete Behavior

The common approach to model the behavior of concrete in a smeared crack finite element analysis is to separately define the cracking and crushing behavior as material properties.

2.2.1 Concrete in Tension

Concrete is a brittle material characterized by a tensile strength significantly lower than the compressive capacity. European and American building codes provide relations between the compressive and the tensile capacity. The EC2 (1991) defines the mean tensile strength as

$$f_{ctm} = 0.3\, f_{ck}^{2/3} \qquad \text{[MPa]} \tag{2.1}$$

where,

f_{ck}= concrete cylinder compressive strength (5% fractile characteristic value)

The ACI 318-95 Building Code (1995) defines a modulus of rupture, which takes the form

$$f_t = 0.7\sqrt{f'_c} \qquad \text{[MPa]} \tag{2.2}$$

where,

f'_c= concrete cylinder compressive strength

The definitions of f_{ck} and f'_c are elaborated in Appendix A.

Under tensile loading the material is assumed to be initially linear elastic. Cracking occurs normal to the principal stress direction when the first principal stress exceeds the tensile strength of the material. Microcracks, which can still partially transfer stresses, start forming in the structure. Under increasing loads these microcracks develop into larger macrocracks until the fully cracked state is reached and load can no longer be transferred at the crack face. After cracking, the material exhibits orthotropic behavior normal and parallel to the crack. The residual shear

transfer at the mirocracks can be incorporated into the material stiffness matrix by using a shear retention factor. The stress in the post-cracking region can be modeled in several ways. The use of a descending branch in the stress-strain relation makes the analysis more realistic since the capacity decreases gradually, and does not just drop to zero immediately after initial cracking (Fig. 1.4).

2.2.2 Concrete in Compression

The behavior of concrete in compression was studied extensively by numerous researchers and an explicit form of a failure function was defined (Chen and Han, 1988). Its essential features are illustrated in Fig. 2.1. From that several mathematical models have been derived and successfully used in analytical applications. A common material model is the two-parameter model by Drucker and Prager (Chen, 1982). Its simplicity makes it easy to use in a finite element analysis. The yield surface created by this criterion is a right circular cone in principal stress space to approximate the actual yield surface. However, the Drucker-Prager yield criterion has two basic shortcomings in connection with concrete modeling: The independence of the angle of similarity, θ, and the linear approximation between the variables r and ξ, which define the tensile and compressive meridians (Fig. 2.2a). Therefore, the Willam-Warnke five-parameter model was selected for this analysis (Fig. 2.2b). This model has curved tensile and compressive meridians expressed by quadratic parabolas. The failure curves are convex and smooth everywhere and the hydrostatic axis are defined at $\theta = 0°$ and $\theta = 60°$, respectively.

To incorporate both tension and compression behavior in a finite element model, a decision where tension or compression behavior is expected needs to be made a priori. The appropriate material behavior is then assigned to the elements in those regions.

In this study that modeling process could be avoided, because an element capable of cracking and crushing was used. The following paragraph describes the features of this finite element in greater detail.

2.3 Reinforced Concrete Element

The finite element software ANSYS provides a three-dimensional 8 node isoparametric finite element (SOLID65) capable of cracking and element crushing. Cracking is represented by using the smeared crack modeling approach, which treats the tensile behavior as a material property. The concrete behavior under compression is modeled by evaluating a three-dimensional yield criterion developed by Willam and Warnke (1975) at each step of the solution process. Additional plasticity behavior can be incorporated into the model by applying the Drucker-Prager material model to the element. Thus, two criteria for the behavior of concrete in compression are in place, which may result in a higher accuracy of the analysis. During preliminary studies it was found, that using this combined plasticity option could predict the behavior of the structure quite well. However, a major drawback was the significantly increased required computation time, along with significant convergence difficulties during the analysis process. Hence, this additional plasticity model was not

considered in this study. Reinforcement also can be represented in the element. When used with reinforcement capabilities, the reinforcing material is distributed over the volume of the element. Thus, perfect bond between the reinforcement and the concrete would be assumed. Because of these major generalizations, this study does not make use of the built-in reinforcement modeling capability. Instead the reinforcing steel is modeled as a separate entity connected to the concrete using bond-link elements, so that bond-slip behavior can be discretely accounted for, as discussed later on in the chapter.

The finite element incorporates the smeared crack modeling approach and is capable of cracking in three orthogonal directions at each integration point. The material softening behavior after cracking follows a discontinuous stress-stain curve (Fig. 1.4b). The material stiffness matrix of the initially linear elastic isotropic material takes the form

$$[D]=\frac{E}{(1+\upsilon)(1-2\upsilon)}\begin{bmatrix} (1-\upsilon) & \upsilon & \upsilon & 0 & 0 & 0 \\ \upsilon & (1-\upsilon) & \upsilon & 0 & 0 & 0 \\ \upsilon & \upsilon & (1-\upsilon) & 0 & 0 & 0 \\ 0 & 0 & 0 & \frac{(1-2\upsilon)}{2} & 0 & 0 \\ 0 & 0 & 0 & 0 & \frac{(1-2\upsilon)}{2} & 0 \\ 0 & 0 & 0 & 0 & 0 & \frac{(1-2\upsilon)}{2} \end{bmatrix} \tag{2.3}$$

where,

E= modulus of elasticity

υ= Poisson's ratio

Cracks in the material start forming as the tensile concrete strength is exceeded. To account for the changed material behavior a plane of weakness is introduced in the direction perpendicular to the crack face. Thus, orthotropic material behavior is assumed. Since this element is defined in three-dimensional space, three cases of orthotropic material behavior need to be addressed, namely cracking in one, two and three directions. Those relations refer to a coordinate system parallel to the principal stress direction where the x-axis is normal to the cracking plane. Thus, the stress-strain relation for material that has cracked in one direction becomes

$$[D^{ck}]=\frac{E}{(1+\upsilon)}\begin{bmatrix} \frac{R^{t}(1+\upsilon)}{E} & 0 & 0 & 0 & 0 & 0 \\ 0 & \frac{1}{1-\upsilon} & \frac{\upsilon}{1-\upsilon} & 0 & 0 & 0 \\ 0 & \frac{\upsilon}{1-\upsilon} & \frac{1}{1-\upsilon} & 0 & 0 & 0 \\ 0 & 0 & 0 & \frac{\beta_t}{2} & 0 & 0 \\ 0 & 0 & 0 & 0 & \frac{1}{2} & 0 \\ 0 & 0 & 0 & 0 & 0 & \frac{\beta_t}{2} \end{bmatrix} \quad (2.4)$$

where,

R^t= secant modulus

β_t= shear stiffness retention factor (reduction for open crack)

The case of cracking in two directions is characterized by the following stress-strain relation

$$[D^{ck}] = E \begin{bmatrix} \frac{R^t}{E} & 0 & 0 & 0 & 0 & 0 \\ 0 & \frac{R^t}{E} & 0 & 0 & 0 & 0 \\ 0 & 0 & 1 & 0 & 0 & 0 \\ 0 & 0 & 0 & \frac{\beta_t}{2(1+\upsilon)} & 0 & 0 \\ 0 & 0 & 0 & 0 & \frac{\beta_t}{2(1+\upsilon)} & 0 \\ 0 & 0 & 0 & 0 & 0 & \frac{\beta_t}{2(1+\upsilon)} \end{bmatrix} \tag{2.5}$$

The third case with three directions cracked is described by

$$[D^{ck}] = E \begin{bmatrix} \frac{R^t}{E} & 0 & 0 & 0 & 0 & 0 \\ 0 & \frac{R^t}{E} & 0 & 0 & 0 & 0 \\ 0 & 0 & \frac{R^t}{E} & 0 & 0 & 0 \\ 0 & 0 & 0 & \frac{\beta_t}{2(1+\upsilon)} & 0 & 0 \\ 0 & 0 & 0 & 0 & \frac{\beta_t}{2(1+\upsilon)} & 0 \\ 0 & 0 & 0 & 0 & 0 & \frac{\beta_t}{2(1+\upsilon)} \end{bmatrix} \tag{2.6}$$

In case a crack is completely closed, compressive stresses perpendicular to the crack face are fully transmitted. However, the shear strength is reduced by a shear transfer coefficient, β_c. From experiments with different shear transfer coeffiecients on the calibration model (Section 3.3.4; Fig. 3.6) values of β_c= 0.8 (80%), and β_t= 0.6 (60%) for opening cracks, proved to yield the most accurate results. All together sixteen cases of changes in the stress-strain relationships cover all possible combinations of crack arrangement and are part of the element formulation (ANSYS Inc., 1996).

In addition to representing the cracking behavior, a concrete material model is used in the reinforced concrete element to predict the failure of brittle materials in compression. If the compressive strength is exceeded in uniaxial, biaxial or triaxial compression, the material is assumed to crush. Crushing of the material results in complete deterioration of the structural integrity so that the material strength is assumed to have no contribution to the element stiffness at the corresponding integration point. A multiaxial stress state serves as the criterion for failure. It takes the general form

$$\frac{F}{f'_c} - S \geq 0 \tag{2.7}$$

where,

F= function of the principal stress state

S= failure surface defined by the principle stresses (σ_{xp}, σ_{yp}, σ_{zp}) and five input parameters (to be discussed)

f'_c= concrete cylinder compressive strength

The crushing capabilities are activated when all principal stresses are compressive; cracking occurs, when one of the prinicipal stresses is tensile. As mentioned earlier, five input parameters are required to define the failure surface and the ambient hydrostatic stress state

f_t= ultimate uniaxial tensile strength

f'_c= ultimate uniaxial compressive strength

f_{cb}= 1.2 f'_c= ultimate biaxial compressive strength (2.8)

f_1= 1.45 f'_c= ultimate compressive strength for a state of biaxial compression superimposed on hydrostatic stress state (2.9)

f_1= 1.725 f'_c= ultimate compressive strength for a state of uniaxial compression superimposed on hydrostatic stress state (2.10)

The presented equations for f_{cb}, f_1 and f_2 are defaults (Willam and Warnke, 1975) if the corresponding values are not explicitly defined. These defaults are valid in stress situations with a low hydrostatic stress component. In this project, the default values could be used.

To accurately predict the type of material failure, four domains of stress state situations are defined for the element (ANSYS Inc., 1996).

1. $0 \geq \sigma_1 \geq \sigma_2 \geq \sigma_3$ (compression-compression-compression)

2. $\sigma_1 \geq 0 \geq \sigma_2 \geq \sigma_3$ (tension-compression-compression)

3. $\sigma_1 \geq \sigma_2 \geq 0 \geq \sigma_3$ (tension-tension-compression)

4. $\sigma_1 \geq \sigma_2 \geq \sigma_3 \geq 0$ (tension-tension-tension)

where,

$$\sigma_1 = \max(\sigma_{xp}, \sigma_{yp}, \sigma_{zp}) \tag{2.11}$$

$$\sigma_2 = \min(\sigma_{xp}, \sigma_{yp}, \sigma_{zp}) \tag{2.12}$$

with $\sigma_1 \geq \sigma_2 \geq \sigma_3$

Each of the four domains is characterized by independent functions to describe the failure surface, S, and the function of the principle stress state, F. In the case of pure compression, the Willam-Warnke failure criterion (1975) is used. It defines a three-dimensional failure surface characterized by an octrahedral shape of the deviatoric stress tensor. The tensile and compressive meridians take the shape of quadratic parabolas (Fig. 2.3). If the failure criterion is met, the material is assumed to crush. In the tension-compression-compression regime the failure criterion initializes cracking in the plane perpendicular to principle stress σ_1 if satisfied. For the tension dominated domain ($\sigma_1 \geq \sigma_2 \geq 0 \geq \sigma_3$) cracking in two directions can result. If the failure criterion is satisfied for σ_1 and σ_2 cracking in the planes perpendicular to those principal stresses occurs. In case just σ_1 satisfies the failure function, cracking only occurs in the plane perpendicular to principal stress σ_1. The pure tension domain is

characterized by three possible cracking incidents. If all three principal stresses satisfy the failure criterion, cracks are assumed to form perpendicular to σ_1, σ_2 and σ_3. If the criterion is only satisfied in directions of σ_1 and σ_2, cracks occur only in the planes perpendicular to those stresses. If just the first principal stress, σ_1, exceeds the limit of the criterion, only the plane perpendicular to σ_1 is treated as cracked. Fig. 2.4 illustrates the failure surface in principal stress space σ_{zp} close to zero.

2.4 Numerical Formulations

The numerical formulations of the failure criteria for the different domains are adapted from the ANSYS Theory Manual (ANSYS Inc., 1996).

2.4.1 Domain $0 \geq \sigma_1 \geq \sigma_2 \geq \sigma_3$ (Compression-Compression-Compression)

Function of principal stress state:

$$F = F_1 = \frac{1}{\sqrt{15}}\left[(\sigma_1 - \sigma_2)^2 + (\sigma_2 - \sigma_3)^2 + (\sigma_3 - \sigma_1)^2 + \right]^{\frac{1}{2}} \tag{2.13}$$

Failure Surface:

$$S = S_1 = \frac{2r_2\left(r_2^2 - r_1^2\right)\cos\eta + r_2(2r_1 - r_2)\left[4\left(r_2^2 - r_1^2\right)\cos^2\eta + 5r_1^2 - 4r_1r_2\right]^{\frac{1}{2}}}{4\left(r_2^2 - r_1^2\right)\cos^2\eta + (r_2 - 2r_1)^2} \tag{2.14}$$

where,

$$\cos\eta = \frac{2\sigma_1 - \sigma_2 - \sigma_3}{\sqrt{2}\left[(\sigma_1 - \sigma_2)^2 + (\sigma_2 - \sigma_3)^2 + (\sigma_3 - \sigma_1)^2 + \right]^{\frac{1}{2}}} \tag{2.15}$$

η= angle of similarity (describes the relative magnitudes of σ_1, σ_2 and σ_3)

$\eta = 0°$ any stress state such that $\sigma_3 = \sigma_2 > \sigma_1$
(e.g. uniaxial compression, biaxial tension)

$\eta = 60°$ for any stress state where $\sigma_3 > \sigma_2 = \sigma_1$
(e.g. uniaxial tension, biaxial compression)

$0° \le \eta \le 60°$ in all other multiaxial stress states

$$r_1 = a_0 + a_1\xi + a_2\xi^2 \tag{2.16}$$

$$r_2 = b_0 + b_1\xi + b_2\xi^2 \tag{2.17}$$

$$\xi = \frac{\sigma_h}{f_c} \tag{2.18}$$

$$\sigma_h = \frac{1}{3}(\sigma_{xp} + \sigma_{yp} + \sigma_{zp}) = \text{hydrostatic stress state} \tag{2.19}$$

The function r_1 is calculated by adjusting a_0, a_1 and a_2 to satisfy the conditions

$$\begin{Bmatrix} \frac{F_1}{f_c}(\sigma_1 = f_t, \sigma_2 = \sigma_3 = 0) \\ \frac{F_1}{f_c}(\sigma_1 = 0, \sigma_2 = \sigma_3 = -f_{cb}) \\ \frac{F_1}{f_c}(\sigma_1 = -\sigma_h^a, \sigma_2 = \sigma_3 = -\sigma_h^a - f_1) \end{Bmatrix} = \begin{bmatrix} 1 & \xi_t & \xi_t^2 \\ 1 & \xi_{cb} & \xi_{cb}^2 \\ 1 & \xi_1 & \xi_1^2 \end{bmatrix} \begin{Bmatrix} a_0 \\ a_1 \\ a_2 \end{Bmatrix} \tag{2.20}$$

with,

$$\xi_t = \frac{f_t}{3f_c}, \xi_{cb} = -\frac{2f_{cb}}{3f_c}, \xi_1 = -\frac{\sigma_h^a}{f_c} - \frac{2f_1}{3f_c} \tag{2.21}$$

The function r_2 is calculated by adjusting b_0, b_1 and b_2 to satisfy the conditions

$$\begin{Bmatrix} \frac{F_1}{f_c}(\sigma_1 = \sigma_2 = 0, \sigma_3 = f) \\ \frac{F_1}{f_c}\left(\sigma_1 = \sigma_2 = -\sigma_h^a, \sigma_3 = -\sigma_h^a - \frac{f_2}{f_c}\right) \\ 0 \end{Bmatrix} = \begin{bmatrix} 1 & -\frac{1}{3} & \frac{1}{9} \\ 1 & \xi_2 & \xi_2^2 \\ 1 & \xi_0 & \xi_0^2 \end{bmatrix} \begin{Bmatrix} b_0 \\ b_1 \\ b_2 \end{Bmatrix} \tag{2.22}$$

with,

$$\xi_2 = -\frac{\sigma_h^a}{f_c} - \frac{f_2}{3f_c} \tag{2.23}$$

and ξ_0 is the positive root of the equation

$$r_2(\xi_0) = a_0 + a_1\xi_0 + a_2\xi_0^2 = 0 \tag{2.24}$$

(a_0, a_1, a_2 are determined by the function for r_1)

The failure surface is defined to be convex. Thus, the ratio of r_1/r_2 must fall in the range $0.5 < r_1/r_2 < 1.25$. For the coefficients a_0, a_1, a_2, b_0, b_1 and b_2 the following conditions must be satisfied

$$a_0 > 0,\ a_1 \le 0,\ a_2 \le 0 \tag{2.25}$$

$$b_0 > 0,\ b_1 \le 0,\ b_2 \le 0 \tag{2.26}$$

2.4.2 Domain $\sigma_1 \geq 0 \geq \sigma_2 \geq \sigma_3$ (Tension-Compression-Compression)

Function of principal stress state:

$$F = F_2 = \frac{1}{\sqrt{15}}\left[(\sigma_2 - \sigma_3)^2 + \sigma_2^2 + \sigma_3^2\right]^{\frac{1}{2}} \tag{2.27}$$

Failure Surface:

$$S = S_2 =$$

$$\left(1 - \frac{\sigma_1}{f_t}\right)\frac{2p_2\left(p_2^2 - p_1^2\right)\cos\eta + p_2(2p_1 - p_2)\left[4\left(p_2^2 - p_1^2\right)\cos^2\eta + 5p_1^2 - 4p_1p_2\right]^{\frac{1}{2}}}{4\left(p_2^2 - p_1^2\right)\cos^2\eta + (p_2 - 2p_1)^2}$$

with, (2.28)

$$p_1 = a_0 + a_1\chi + a_2\chi^2 \tag{2.29}$$

$$p_2 = b_0 + b_1\chi + b_2\chi^2 \tag{2.30}$$

$$\chi = \frac{1}{3}(\sigma_2 + \sigma_3) \tag{2.31}$$

where cos η and the coefficients a_0, a_1, a_2, b_0, b_1 and b_2 are determined as for the compression-compression-compression domain.

2.4.3 Domain $\sigma_1 \geq \sigma_2 \geq 0 \geq \sigma_3$ (Tension-Tension-Compression)

Function of principal stress state:

$$F = F_3 = \sigma_i;\ i = 1, 2 \tag{2.32}$$

Failure Surface:

$$S = S_3 = \frac{f_t}{f_c}\left(1 + \frac{\sigma_3}{S_2(\sigma_i, 0, \sigma_3)}\right);\ i = 1, 2 \tag{2.33}$$

2.4.4 Domain $\sigma_1 \geq \sigma_2 \geq \sigma_3 \geq 0$ (Tension-Tension-Tension)

Function of principal stress state:

$$F = F_4 = \sigma_I;\ i = 1, 2, 3 \tag{2.34}$$

Failure Surface:

$$S = S_3 = \frac{f_t}{f_c} \tag{2.35}$$

2.5 Reinforcing Steel

2.5.1 Manufacturing Processes

The effects of the material behavior of typical European reinforcing steel and American reinforcing bars on the overall performance of a one-way slab are evaluated in this study. Generally European reinforcing bars are manufactured in a weldable quality, which requires strict controls of its chemical constituents. The German DIN 488 (1984) code requirements for reinforcing steel, for example, limit the amounts of carbon, sulfur, phosphorus and nitrogen to insure quality. The bars may be manufactured using hot rolling techniques or processes where the steel is cold-worked. Most European reinforcing steels are hot rolled using the Tempcore process. This method provides added strength through heat treatment and without increases in carbon content. On the North American market the production standards differ somewhat for the different types of reinforcing bars. The reinforcing steel types A615 and A706 are manufactured in theory using either open-hearth, basic-oxygen or

electric furnace processes to produce the steel and the bars are processed from mold cast or strand cast steel in properly identified heats (ASTM, 1997). In reality in today's practice both the A706 and the standard A615 reinforcing steel are produced using recycled components, such as automobiles and appliances. The A615 steel does not require significant tests of its chemical composition, thus resulting in considerable variations in carbon content. Due to large amounts of carbon in the reinforcing bars, this steel is classified as non-weldable. An alternative choice for reinforcing steel is the A706 low-alloy steel, which is comparable to European reinforcement. It is characterized by higher quality standards. The chemical composition is closely monitored during the production process and limits for carbon sulfur, phosphorus and other elements are provided. A616 and A617, rail and axle steels, also are available, but are used in small quantities in North America. The A615 reinforcing steel represents over 90% of the tonnage rolled today, but A706 is gaining market share.

2.5.2 Constitutive Relationships

The different manufacturing methods of the reinforcing steel influence its material properties. Initially all reinforcement exhibits a linear elastic region up to the yield point of the material that is followed by a yield plateau. The length of the yield plateau varies with the strength of the steel and generally decreases as the steel strength increases. A study of the effects of explicitly defining or neglecting the yield plateau in the analysis is part of this project.

Post-yield behavior is significantly different for American and European reinforcing steel. North American steel is characterized by large amounts of work-

hardening or stress-stiffening on the order of at least $f_y/f_u = 1.25$ as defined by the ASTM standard for A706 steel (1997). Furthermore, the ultimate elongation covers a range from around 6 to 10% for A615 steel and 11-15% for A706 reinforcement. Typical European steels on the contrary exhibits little strain-hardening and its amount is in fact limited to no more than 10%. An upper bound for the ultimate elongation is defined around a maximum of 8%. Typical stress-strain curves for both steel categories are illustrated in Fig. 2.5.

The strain-hardening behavior of the reinforcing steel does affect the length of the plastic hinges in the test specimen. If the amounts of strain-hardening supported by the steel are large, more load can be carried by the bar, which allows the plastic hinge to form in a wider region in the concrete. It is believed that reinforcement with high ductility capacities could lead to structures with larger overall deformation capabilities.

Several models to represent this material behavior in a finite element analysis have been developed (Fig. 2.6). Typically the reinforcement is either modeled as elastic perfectly plastic material or as an elastic strain-hardening material. Since this study focuses on the effects of different reinforcing steel characteristics, a multilinear approximation to accurately model the stress-strain curves is used (Fig. 2.7).

Reinforcing steel is capable of carrying forces both parallel and perpendicular to its length in dowel action. The latter is activated when the bar crosses an open

crack. This ability to carry transverse shear is difficult to incorporate in a finite element model. The present study neglects the aspect of dowel action, since it is sufficient to assume uniaxial material behavior alone and dowel action here can be ignored (Darwin, 1993).

2.5.3 Modeling Considerations

To represent reinforcing steel in a finite element model, three distinct methods of modeling are applicable. These models treat the steel (a) as a uniaxial material distributed or 'smeared' throughout the finite element, (b) as a uniaxial element embedded in a larger finite element, or (c) as discrete bars connected to individual nodes of the finite element mesh.

In a distributed or 'smeared' representation, the uniaxial behavior of the reinforcing steel is incorporated in the material stiffness matrix of the finite element and the orientation of the bars has to be predefined. Typically a composite concrete-reinforcing constitutive relation is used to derive the material stiffness matrix. Thus, perfect bond conditions are represented. In many cases perfect bond is a correct assumption, however, there are situations where the bond may be far from perfect. The technique of an embedded steel model utilizes an intra-element representation for the reinforcing steel. The bar is modeled as an axial member built into a larger finite element. Thus, its displacements coincide with those of the surrounding element. Again, no provisions to allow for bond-slip are defined. The third option defines the reinforcing bars as separate structural entities connected to the surrounding concrete elements at the nodes. Standard axial force elements can be used to represent the

steel. If desired the bond-slip behavior can be simulated by defining special bond-link elements at the interface of the reinforcing steel with the concrete.

Discrete modeling of the reinforcing steel is used in this study. It allows for a more realistic model compared to the smeared representation and is easier to apply to the analysis than the embedded modeling approach. Furthermore, bond-slip behavior can be incorporated in the analysis process as discussed in the next paragraph. If perfect bond is desired, this behavior also could be accommodated in the analysis.

2.6 Bond-Slip Behavior

Bond between the reinforcing steel and the concrete is essential to insure compatibility between the strains in the two materials. Perfect bond between the two components exists only at low stress levels (early stages of loading). Once the load exceeds a certain level, slipping between the steel and the concrete occurs. The actual amount of slip is influenced by a variety of factors. The material properties of the concrete (e.g. strength, aggregate type and size), the reinforcing bar characteristics (e.g. rib pattern), the effective stiffness of the member, internal force distribution and location, and the spacing and width of cracks all have an effect on the bond-slip behavior. Hence, modeling of bond-slip is considered to be one of the most difficult aspects to be incorporated in a finite element analysis of reinforced concrete (ACI Committee 446, 1998).

When a certain load level is exceeded, the reinforcing bar starts to slip through the surrounding concrete parallel to the longitudinal axis of the steel. The counterpart

for the slip is provided by mechanical interlock, friction and adhesion of the concrete between the ribs of the reinforcing bar. Mechanical interlock takes place between the deformed surface of the steel and the aggregates in the concrete. Thus, plain bars resist the slip by friction and adhesion only. Obtaining the actual bond stress distribution along the bar is a difficult task. Experiments suggest that bond stresses are higher at the loaded end of the bar and diminish over distance. However, it is satisfactory to use a nominal average value for design purposes, except for high strength concrete where this assumption may be unconservative.

Current design provisions, such as the ACI 318-95 or the EC2, attempt to insure that a complete bond failure does not occur by basing the design criteria on other forms of failure (e.g. shear or flexural failure). Adequate anchorage of the reinforcing steel reduces the bond-slip. This effective insensitivity to bond strength causes some controversy in modeling bond-slip in a finite element analysis. Many previous researchers have totally ignored bond-slip behavior and have produced excellent analytical representations of experimental behavior. Recent experimental tests comparing the performance of epoxy-coated steel to uncoated reinforcement show that the load-deflection response of reinforced concrete members themselves is often insensitive to bond-slip (Darwin, 1993). However, bond-slip is considered in this project due to geometry considerations. The analyzed specimen is a relatively short member, so the relatively short anchorage zone could cause some sensitivity to the bond-slip phenomenon, as was the case in earlier studies (Chitipothu, 1997).

The interaction between the concrete and the steel can easily be incorporated in a model with a discrete representation of the steel. Instead of connecting the steel elements directly to the nodes of the concrete elements, so-called bond-link elements are used to create an interface between the two materials (Fig. 2.8). A bond-link element essentially consists of two orthogonal springs of zero length, which connect the nodes of the steel elements to those of the concrete elements. Normal and shear forces can be transferred by the bond-link element. A drawback of this method is that the steel-concrete interface is lumped at the connection points. A more accurate model would incorporate bond-interface elements, which connect the complete surface of the steel to the concrete. Because of the significantly increased modeling efforts and higher required computation time for the bond-interface elements, the connection between the steel and the concrete was modeled with bond-link elements.

The bond-slip response is treated as a material property for the axial component of the bond-link element. A bond-slip model from the 1990 CEB-FIP Model Code (Comité Euro-International du Béton, 1993a) was selected to be used in this study (Fig. 2.9). For monotonic loading the bond stresses between the steel and the concrete are determined by

$$\tau = \tau_{max}\left(\frac{s}{s_1}\right)^{0.4} \qquad \text{for } 0 \le s \le s_1 \tag{2.36}$$

$$\tau = \tau_{max} \qquad \text{for } s_1 < s \le s_2 \tag{2.37}$$

$$\tau = \tau_{max} - (\tau_{max} - \tau_f)\left(\frac{s - s_2}{s_3 - s_2}\right) \qquad \text{for } s_2 < s \le s_3 \tag{2.38}$$

$$\tau = \tau_f \qquad \text{for } s_3 < s \tag{2.39}$$

with,

$$\tau_{max} = 2.0\sqrt{f_{ck}} \quad \text{peak bond stress} \tag{2.40}$$

$$\tau_f = 0.15\,\tau_{max} \quad \text{frictional bond stress} \tag{2.41}$$

where,

f_{ck}= concrete cylinder compressive strength (5% fractile characteristic value)

$s_1 = s_2 = s_3$= characteristic slip values

(valid for unconfined concrete under good bond conditions)

For the finite element analysis a linear approximation for the initially parabolic slope of the stress-slip relationship was used.

2.7 Summary

To accurately model the behavior of reinforced concrete in a finite element analysis the complex material behavior needs to be incorporated in the numerical model. Four nonlineariaties critical to the structrual behavior of reinforced concrete are accounted for in this study. In that manner cracking and compressive failure of the concrete, post-yield behavior of the reinforcement and the interaction between the steel and the concrete in form of bond-slip are represented.

The development of the finite element grid and adequate solution techniques for a nonlinear analysis are presented in the next chapter. Moreover, the issue of calibrating the finite element model is disscussed.

CHAPTER 3

FINITE ELEMENT ANALYSIS – GEOMETRY MODEL CONSIDERATIONS AND NUMERICAL PROCEDURES

3.1 General

The motivation behind this study is to analytically inquire the influence of varying reinforcing steel characteristics on the performance of a one-way slab in three point bending. It is of special interest to evaluate American steel compared to European reinforcement and to capture the influences of changes in the effective reinforcing ratio on the structural performance. Also, the influences of a variation of the concrete strength at a highly reinforced specimen are examined.

In order to obtain a finite element model that is able to accurately predict the behavior of reinforced concrete, a series of preliminary studies was carried out. The general performance of the reinforced concrete finite element was verified in simple compression and tension tests; the quantification of the shear retention factors for open and closed cracks was determined. Moreover, effects of element size, load step increment and convergence criteria were investigated prior to analyzing the actual analysis cases.

3.2 Analyzed Structure

The analyzed structure is a one-way slab spanning in one direction over a simple span. Thus, the cross-section could be represented as a beam segment with a width of 1000mm. The specimen was designed with single tensile reinforcement at equal spacing. No additional confinement through stirrups and no compression reinforcement were considered. The layout of the cross-section is illustrated below in Fig. 3.1.

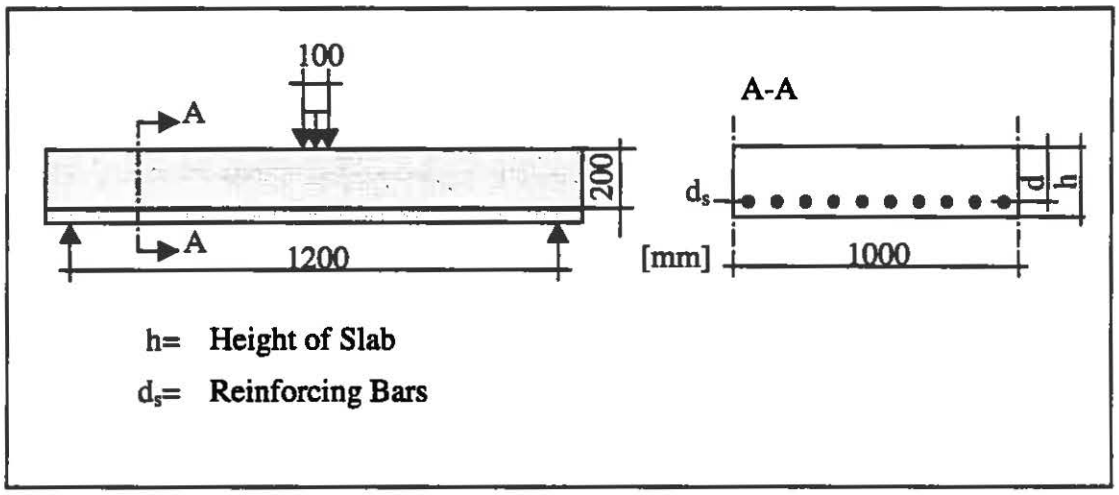

Figure 3.1 Slab Cross Section

The effective depth was kept constant for all analysis cases. However, changes of the total height of the slab, h, due to changes in the effective reinforcing ratio were considered. Loading in form of displacements was imposed over a load application area covering the width of the slab and one-half the effective depth over the length of the slab.

For the finite element modeling process symmetry considerations were used to keep the model as compact as possible to obtain reasonable computing times. The actual finite element grid modeled half the structure in length and is 100mm wide incorporating one reinforcing bar (Fig. 3.2).

3.3 Loading

Monotonic loading was imposed to the structural system using a displacement control approach. This technique has the advantage that descending branches in the load-displacement history can be monitored whereas methods, which apply forces to the system, are not able to capture these effects and, therefore, terminate the solution as soon as a local maximum of force is reached. Since the material models for the concrete and the steel assumed the material stiffness to be zero once the ultimate material capacity was exceeded, actual limit loads could be captured with the model.

3.4 Modeling Reinforcement

The one-way slab investigated in this study was reinforced with unidirectional longitudinal steel bars only. As discussed in Section 2.6, the reinforcement was considered a structural entity and was represented by discrete bars. To insure inter-element displacement compatibility between the steel and the concrete, two-node three-dimensional rod elements were used. The element length of a steel element equaled the longitudinal edge length of a concrete element. To account for possible

bond-slip behavior at the interface between the two materials, the steel and concrete elements were connected with two orthogonal one-dimensional springs as illustrated in Fig. 2.8. Since the nodes of the reinforcing bar and the concrete coincided, the spring elements were of zero length. One spring connected the two materials in vertical direction and, by using a large stiffness for the spring, the two nodes essentially acted as a unit. In the longitudinal direction a nonlinear spring that used the bond-slip behavior incorporated as a material variable was required.

3.5 Preliminary Studies

3.5.1 Verification of Reinforced Concrete Element Behavior

This study utilized a finite element capable of cracking and crushing provided by the analysis software ANSYS. Since this was an attempt to incorporate an element with a predefined concrete behavior pattern, simple compression and tension analyses were performed to verify the failure criteria and to become familiar with the element features. A specimen of 2x2x4 elements with perfectly shaped elements was created and analyzed under uniaxial tension and compression. The effects of cracking and crushing could be shown and the analyses precisely resembled the predicted cracking and crushing response of the material.

3.5.2 Mesh Considerations

In a smeared crack modeling representation mesh size effects can significantly influence the analytical solution (Bazant, 1976; Chitipothu, 1997). If the finite element mesh is too coarse the measured response tends to be more insensitive to localized cracking, which leads to predictions of a higher load capacity and larger deflections. One might think that using a very dense mesh would be the solution to the meshing considerations. However, with increasing mesh density the computational time involved increases by the order of a cubic function for the number of elements involved. Moreover, fine meshes have the drawback of being sensitive to the crack band phenomenon (Bazant and Cedolin, 1979 and 1980; Bazant and Oh, 1983, Rots et al., 1984, Darwin 1985). To determine an adequate mesh density, three mesh configurations were developed and compared to each other. Since the shape of the elements also can influence the results, especially when the shapes of an element are non-proportional, it was imperative to use elements of essentially equal size and with good proportions. The first mesh type used 4 elements over the height of the beam, 2 through its thickness and 12 over the length (Fig. 3.3a). The denser model was comprised of twice the amount of elements in all three directions (Fig. 3.3b). The third model presented a very fine mesh over the height of the beam. It incorporated 16 elements over the height of the member with the other two directions being partitioned in the same way as the second mesh (Fig. 3.3c). The idea behind this model was to provide for more accuracy in determining compression and tension zones under bending conditions.

The structural response due to imposed displacements was monitored for the three models and load-displacement graphs were generated (Fig. 3.4). As predicted, the coarse model displayed significant insensitivity to cracking and crushing and exhibited a high ultimate capacity and enormous plastic deformation. The two denser models predicted little plastic deformation and their ultimate loads were in the same vicinity. A decision to use the model with perfectly cubic elements was made as an effort to minimize the computation time involved, yet obtaining as accurate a set of results as possible.

3.5.3 Local Element Instabilities

In the preliminary modeling phase many of the analyzed models displayed a localized element failure of the elements at the support (Fig 3.5a). The supports were modeled by constraining the nodes on the edge of the beam. This posed numerical problems for the analysis. To avoid localized failure at the support region the material model for the elements at the support and one element into the slab was assumed to be linear elastic (Fig. 3.5b). This assumption represented the effects of local confining reinforcement that would be present in a real structure and allowed for a higher local stiffness, but did not affect the overall behavior of the structure (Fig 3.5c).

3.5.4 Shear Retention Factors

The element formulation for the behavior after cracking occurs (Section 2.3) incorporates shear transfer coefficients to account for residual load transfer at an open crack face, β_t, and for a reduced shear capacity in case of a closed crack, β_c. A variety

of combinations for β_c and β_t were studied and the effects on the overall structural behavior were monitored (Fig. 3.6). In most cases the structural response displayed a similar behavior. Upper and lower bound estimates for the coefficients also were analyzed to investigate the possible extremes. Both significantly underestimated the maximum carrying capacity of the member. In the case of the lower bound estimate ($\beta_c = \beta_t = 0.1$), the virtual absence of closed crack shear transfer caused the structure to fail at a low load level. The upper bound estimate assumed unrealistic shear transfer coefficients of $\beta_c = \beta_t = 1$ and exhibited crushing failure at early loading stages. A combination of $\beta_c = 0.8$ and $\beta_t = 0.6$ predicted a structural response closest to experimental data (Walraven, 1978) and was, therefore, selected to be used in the finite element analyses.

3.6 Solution Techniques

A finite element analysis of reinforced concrete incorporates materials that behave in a nonlinear manner. These material nonlinearities can be evaluated using an iterative nonlinear solution method to solve a series of successive linear approximations with corrections to approximate the structural response. Typically loading is imposed in small increments and the structural response is obtained at every load-step, thus approximating the actual solution. In a pure incremental solution the structural stiffness matrix is adjusted at the end of every load increment and, if no additional measures are taken, an error is accumulated with every load increment

(Fig. 3.7a). The finite element software ANSYS utilizes the Newton-Raphson approach to minimize that error. This method enhances the solution accuracy by performing equilibrium iterations for each load increment (Fig. 3.7b). The solution is considered converged, once the solution lies within a predefined tolerance. At the beginning of each load increment the out-of-balance load vector (difference between the load corresponding to the element stresses and the applied loads) is determined and the stiffness matrix updated. The out-of-balance load vector is used to obtain a linear solution, which is then checked for convergence. The process starts over if the convergence criterion is not met.

3.6.1 Load-Step Size

The size of the load increments has an effect on the overall solution because of the path dependent nature of a nonlinear analysis. Generally, the size of a load increment should neither be too large nor too small. If the increments are large, fine variations in the actual structural behavior may remain undetected and the solutions tend to become inaccurate. In case very small steps are used, local convergence difficulties may be encountered. ANSYS provides an option of automatically adjusting the step size if needed. This possibility of optimizing the substep size was considered, but preliminary analyses revealed, that the automatic stepping option does not necessarily choose adequate substep intervals. Instead the load was applied in multiple load steps with varying substep increments. The substep sizes for each step were determined from evaluation of numerous preliminary analysis cases. Two basic step sizes were used in the study. Initially the substeps were defined to 0.1mm/step

for a range of stable structural behavior (no significant influence of concrete cracking or crushing or steel yielding). This range covered a deflection of up to 2.5mm selected from the results of numerous test analyses. A length of 0.02mm/step was selected for additional substeps. This significant size change enabled the program to accurately capture the structural behavior in the deflection range where the material nonlinearities governed the overall behavior of the system. However, for the lightly reinforced specimen the step-size was adjusted back to 0.1mm/step after the concrete cracked and the structural behavior became dependent solely on the strain-hardening of the steel.

3.6.2 Convergence

The iterative solution process for each load increment was executed until convergence was achieved or a predefined number of equilibrium iterations were exceeded. If the latter was the case, the program terminated the analysis and the load increment could be adjusted or the convergence criterion altered.

Convergence criteria can be based on forces, moments, displacements or rotations or combinations of those items and each criterion can be characterized by a predefined tolerance and convergence norm. Force (moment) convergence displays an absolute measure of convergence and takes the form

$$\|\{R\}\| < \varepsilon_R R_{ref} \tag{3.1}$$

where,

$$\{R\} = \{F_a\} - \{F_{nr}\} = \text{residual load vector} \tag{3.2}$$

Displacement (rotation) convergence on the other hand only provides a relative measure of apparent convergence to verify

$$\|\{\Delta u_i\}\| < \varepsilon_u u_{ref} \tag{3.3}$$

Thus, force based convergence checks were performed in the study.

The vector norm for both cases may be defined as any of the following three forms. It can be characterized as (a) the maximum value in the vector (also referred to as infinite norm), (b) the sum of the absolute value of the terms and, (c) as the square root of the sum of the squares (Euclidian Norm). Their mathematical formulations are as follows

(a) $$\|\{R\}\| = \max|R_i| \tag{3.4}$$

(b) $$\|\{R\}\| = \sum |R_i| \tag{3.5}$$

(c) $$\|\{R\}\| = \left(\sum |R^2{}_i|\right)^{\frac{1}{2}} \tag{3.6}$$

As discussed, the Euclidian Norm calculates an average of the values in the vector and, therefore, presents a realistic way to monitor the convergence. Thus, the Euclidian Norm (option (c)) was selected to define the vector norm in this project.

The speed of convergence and the accuracy of the results also are influenced by the fault tolerance of the convergence norm. Excessively tight fault tolerances lead to extreme computation requirements and sometimes predict non-convergence, sign reversal of the incremental loads at each iteration or even diverging behavior of the

equilibrium iteration. On the contrary, if the limits are loose, accuracy and correct convergence suffers and the results become questionable. From preliminary studies, a force convergence tolerance of 0.5% was found to yield reasonable results while keeping the computational efforts within an acceptable time frame. Using an increased fault tolerance for a small number of substeps was used to treat instances during the course of an analysis where convergence difficulties were encountered. This method proved to maintain good accuracy of the overall analysis and did not increase the computation time as much as decreasing the substep size.

Another option to improve the convergence speed is to influence the stiffness matrix during the equilibrium process. The adaptive descent technique switches to a 'stiffer' matrix if convergence difficulties are encountered and uses the full tangent matrix as the solution converges. Numerically this method is described as

$$[K_{T,i}] = \xi [K_S] + (1-\xi)[K_T] \tag{3.7}$$

where,

$[K_T]$= tangent matrix

$[K_S]$= most stable matrix (secant matrix)

ξ= descent parameter

Each substep is initialized using the tangent matrix. During the iterative solution process changes in the residual norm $\|\{R\}\|$ are monitored. An increasing residual is interpreted as a possibly diverging solution. The current solution is then removed and the iteration is redone with the descent parameter set to $\xi = 1$ (if $\xi = 1$ already, the iteration is continued). In case the residual norm decreases (indicating a converging solution) the descent parameter is adjusted in one of the three ways outlined below.

1. If $\xi = 1$ and $\|\{R\}\|$ has been decreasing for three iterations in a row, ξ is decreased by 0.25 and the iteration is continued.
2. If ξ was increased to 1 during the iteration (divergence indicated) and $\|\{R\}\|$ has been decreasing for two iterations in a row, ξ is decreased by 0.25 and the iteration is continued.
3. If $\xi < 1$, the descent parameter is again decreased by 0.25 and the iteration is continued.

When the value of the descent parameter decreases below 0.0156, ξ is set to 0, and thus, the tangent matrix is used for further equilibrium iterations. In case an ill-conditioned matrix is detected (negative main diagonal), the current solution is stopped, ξ is set to 1 and the iteration is redone with the secant matrix. If the descent parameter already equals 1 upon detection of the ill-conditioned matrix the execution of the program is terminated (ANSYS Inc., 1996). The adaptive descent option was utilized to enhance solution convergence of the analyses in this research project.

3.7 Calibration Model

Analyzing reinforced concrete structures is dependent on numerous material model considerations and oftentimes sensitive to many aspects of the finite element model. Although every influencing factor may be tested separately, it is the right combination of all discussed entities, which makes a model function properly. To evaluate the overall performance of the obtained finite element model, experimental data from Walraven (1978) served as a calibration tool for the analyses. The predictions of the numerical analyses were found to be within a 5% margin of the results from experimental testing (Fig. 3.8).

3.8 Summary

The structure investigated in this study is introduced and the process of obtaining the finite element model is described. The issues of general element behavior, mesh size effects, local stability problems and shear retention factors are discussed in detail and the loading and solution techniques involved in the analysis process are presented. To monitor the accuracy of the finite element model, experimental test data (Walraven, 1978) is used as a calibration tool.

The following chapter describes the analysis series and the results obtained from the different analyses.

CHAPTER 4

FINITE ELEMENT ANALYSIS – RESULTS

4.1 General

A parametric study of a simply supported one-way slab in three point bending was conducted, incorporating the modeling procedures and solution techniques introduced in Chapters 2 and 3. The investigated structural system, described in detail in Section 3.2, was kept constant throughout the study. The effects of changes in the ductility characteristics of the reinforcing steel and the effective reinforcing ratio were investigated. A series of analyses also was carried out to monitor the effects of high strength concrete (C70/80) in case of a highly reinforced slab. In the following the analysis cases investigated in this study are introduced and the results are discussed.

4.2 Analysis Parameters

The parameters incorporated in the analysis process, namely changes in the material behavior of the steel, changes of the effective reinforcing ratio and a variation of the concrete strength, are introduced.

4.2.1 Reinforcing Steel – Ductility Characteristics

Eight steel types were analyzed to investigate the influence of varying stress-strain curves on the structural behavior. Four material models represented the behavior of typical European reinforcing steel according to the steel ductility classes in the 1990 CEB-FIP Model Code (1993a), the EC2 (1991) and the EC8 (1988), two of which explicitly incorporated a yield plateau. Of the remaining cases, two followed the minimum requirements of stress-strain behavior defined by the American Society for Testing and Materials for billet steel conforming to A615/A615M–96a grade60 and low-alloy steel conforming to A706/A706M–96b (ASTM, 1997). The other two represented an upper bound of the requirements for these steels. Tables 4.1 and 4.2 contain the main characteristics of each material type.

Table 4.1 European Reinforcing Steel Characteristics

Type	Code	f_{ym} [MPa]	f_{tm} [MPa]	e_{sh} [%]	e_{su} [%]	Remarks
1	B	550	578	-	2.5	
2	A1	550	594	-	5	
3	S2	550	632	2	6	yield plateau
4	C2	550	632	2	8	yield plateau

where,

f_{ym}= Yield Strength (Mean Value)
f_{tm}= Tensile Strength (Mean Value)
ε_{sh}= Strain at Onset of Strain Hardening
ε_{su}= Ultimate Strain

Table 4.2 American Reinforcing Steel Characteristics

Type	Code	f_{ym} [MPa]	f_{tm} [MPa]	ε_{sh} [%]	ε_{su} [%]	Remarks
5	A615/grade60	420	620	-	4.9	min. requirements
6	A615/grade60	483	690	-	6.2	upper bound values
7	A706/grade60	420	550	-	7.4	min. requirements
8	A706/grade60	540	707	-	9.3	upper bound values

where,

f_{ym}= Yield Strength (Mean Value)
f_{tm}= Tensile Strength (Mean Value)
ε_{sh}= Strain at Onset of Strain Hardening
ε_{su}= Ultimate Strain

All reinforcing steels were assumed to have a modulus of elasticity of E_s= 200000MPa and a Poisson's ratio of ν= 0.3. The mean values of the steel strength, f_{ym}, rather than the characteristic values, f_{yk}, were used to account for the actual material properties. The strain value at the onset of the strain-hardening zone for steels with a yield plateau was arbitrary selected to e_{sh}= 2%.

To account for strength variations due to manufacturing inconsistencies, an upper bound estimate for the ductility behavior of A615/grade60 reinforcing steel was obtained by a 25% increase of the minimum yield strength specified by ASTM. The ultimate strength and elongation at failure were scaled accordingly to represent typical variations in the overall material behavior. The ASTM standards for A706 bars provide a target range for the yield strength, thus ultimate strength and

elongation at failure were derived accordingly to represent this 'window' for changes of the material behavior in the finite element analysis.

The stress-strain properties were implemented into the analysis process using a multilinear approximation model (Fig. 2.7). Until the yield strength of the steel was reached the material strength monotonically increased. A yield plateau, if defined, was modeled by a zone with zero slope in the stress-strain diagram. The following strain-hardening region was then linearly approximated. The behavior after the ultimate strength was reached was represented differently for European and American reinforcing bars. Typically European steel exhibits little gain in elongation after the ultimate strength is exceeded. Thus, additional elongation of 10% without softening was defined as the ultimate elongation (Fig. 2.7b). On the contrary, American steels are characterized by a significant elongation gain after exceeding the ultimate strength. To capture this material behavior, a downward branch was introduced in the stress-strain curve (Fig. 2.7a).

4.2.2 Effective Reinforcing Ratio

The influence of the effective reinforcing ratio also was assessed and, therefore, analyses at three different reinforcing levels to cover a range of members with low to large amounts of steel were carried out. The effective mechanical percentage of tensile reinforcement, ω_{eff}, is defined as

$$\omega_{eff} = \frac{A_s f_{ym}}{b\, d\, f_{cm}} \tag{4.1}$$

where,

A_s= cross-sectional area of reinforcement

f_{ym}= yield strength of steel (mean value)

f_{cm}= concrete compressive strength (cylinder, mean value)

b= member width

d= effective member depth

and values for the analysis parameter ω_{eff} were selected to 0.03, 0.10 and 0.25, respectively. The term ω_{eff} is equal to ρ (f_{ym}/f_{cm}) and accounts for variations in the steel reinforcing ratio, ρ, as well as strength variations in the steel and the concrete.

4.2.3 Concrete Strength

Throughout the study concrete with a mean compressive strength of f_{cm}= 43MPa (C30/40) was used. The mean value of the compressive strength was selected because the actual behavior of the structure was investigated. The effects of changes in concrete strength on the structural behavior were examined at a high effective reinforcing ratio. In that case a concrete strength of f_{cm}= 83MPa (C70/80) was applied to the analysis. Material characteristics for these two concrete types are listed in Table 4.3.

Table 4.3 Concrete Characteristics

Type	Code	f_{cm} [MPa]	f_{cck} [MPa]	f_{ck} [MPa]	f_{ctm} [MPa]	$f_{ctk0.05}$ [MPa]	$f_{ctk0.95}$ [MPa]
1	C30/40	43	43.5	35	3.2	2.2	4.2
2	C70/80	83	85	75	5.3	3.6	7.1

where,

f_{cm}= Compressive Strength (Cylinder, Mean Value)
f_{cck}= Compressive Strength (Cube, 5% Fractile Characteristic Value)
f_{ck}= Compressive Strength (Cylinder, 5% Fractile Characteristic Value)
f_{tm}= Tensile Strength (mean value)
$f_{ctk0.05}$= Tensile Strength (5% Fractile Characteristic Value)
$f_{ctk0.95}$= Tensile Strength (95% Fractile Characteristic Value)

Both types of concrete utilized a Poisson's ratio of $\nu = 0.15$ and the modulus of elasticity E_c was calculated using

$$E_c = 4700\sqrt{f'_c} \quad \text{[MPa]} \tag{4.2}$$

with,

f'_c= concrete cylinder compressive strength

according to ACI 318-95 (1995) provisions.

4.3 Analysis Cases

This section introduces the analysis cases evaluated in this study and illustrates the combinations of parameters investigated. Reference numbers were assigned to each analysis to be used in the subsequent discussion. At all three

effective reinforcing ratios, the influence of the eight steel types and their ductility characteristics on the rotation capacity was analyzed. In addition, the performance of high strength concrete in a highly reinforced slab was tested with all eight reinforcing steels. Table 4.4 includes a listing of the parameter settings for all 32 finite element analyses.

Table 4.4 Analysis Cases

Ref. Number	Steel Code	Concrete Code	Eff. Reinf. Ratio	Ref. Number	Steel Code	Concrete Code	Eff. Reinf. Ratio
Series 1 Low Effective Reinforcing Ratio				**Series 2 Moderate Effective Reinforcing Ratio**			
1-1	B	C30/40	0.03	2-1	B	C30/40	0.10
1-2	A1	C30/40	0.03	2-2	A1	C30/40	0.10
1-3	S2	C30/40	0.03	2-3	S2	C30/40	0.10
1-4	C2	C30/40	0.03	2-4	C2	C30/40	0.10
1-5	A615 min	C30/40	0.03	2-5	A615 min	C30/40	0.10
1-6	A615 max	C30/40	0.03	2-6	A615 max	C30/40	0.10
1-7	A706 min	C30/40	0.03	2-7	A706 min	C30/40	0.10
1-8	A706 max	C30/40	0.03	2-8	A706 max	C30/40	0.10
Series 3 High Effective Reinforcing Ratio				**Series 4 High Effective Reinforcing Ratio, High Strength Concrete**			
3-1	B	C30/40	0.25	4-1	B	C70/80	0.25
3-2	A1	C30/40	0.25	4-2	A1	C70/80	0.25
3-3	S2	C30/40	0.25	4-3	S2	C70/80	0.25
3-4	C2	C30/40	0.25	4-4	C2	C70/80	0.25
3-5	A615 min	C30/40	0.25	4-5	A615 min	C70/80	0.25
3-6	A615 max	C30/40	0.25	4-6	A615 max	C70/80	0.25
3-7	A706 min	C30/40	0.25	4-7	A706 min	C70/80	0.25
3-8	A706 max	C30/40	0.25	4-8	A706 max	C70/80	0.25

For each series of analyses, the capacity of the slab was calculated using ACI provisions to be compared with the analysis results. The nominal strength of the slab was used here rather than the design strength, which incorporates a strength reduction factor, because the actual structural behavior was monitored in the study. The nominal moment capacity, M_n, was calculated as follows

$$M_n = A_s f_{ym}\left(d - \frac{a}{2}\right) \qquad [kNm] \tag{4.3}$$

with,

$$a = \frac{A_s f_{ym}}{0.85 f_{cm} b} \qquad [mm] \tag{4.4}$$

where,

M_n= nominal strength of the member

A_s= cross-sectional area of reinforcement

f_{ym}= yield strength of steel (mean value)

d= distance from extreme compression fiber to centroid of reinforcement

a= depth of equivalent rectangular stress block

f_{cm}= concrete compressive strength (cylinder, mean value)

b= member width

With that the ultimate load for the slab was calculated as

$$P_u = \frac{4M_n}{l} \qquad [kN] \tag{4.5}$$

where,

l= member length

Thus, the ACI predictions for the structural capacity of the four analysis series were calculated to be

Analysis Series 1: P_u= 169 [kN]

Analysis Series 2: P_u= 540 [kN]

Analysis Series 3: P_u= 1223 [kN]

Analysis Series 4: P_u= 2360 [kN]

In addition to the nominal strength of the slab, the shear resistance of the specimen can become an important factor in the analysis. When large amounts of reinforcement are employed the load capacity of the slab is increased and, thus, the demands on the carrying capacity of the compression strut could exceed the available shear resistance. The EC2 Building Code explicitly includes provisions to verify the shear capacity of the compression strut. For the design of structures that do not require reinforcement with stirrups, two criteria, V_{Rd1}, and V_{Rd2}, need to be evaluated. The actual shear force needs to be less then the lower value of these equations. The equations take the form

$$V_{Rd1} = [\tau_{Rd}\, k(1.2 + 40\rho_l)]\, b_w\, d \qquad [kN] \qquad (4.6)$$

with,

$$\rho_l = \frac{A_{sl}}{b_w\, d} \leq 0.02 \qquad (4.7)$$

where,

τ_{Rd}= basic shear strength (values tabulated in EC2)

k= 1 for members where more then 50% of bottom reinforcement is curtailed
$1.6 - d \geq 1$ in all other cases

b_w= minimum width of the section over the effective depth

d= effective depth

A_{sl}= area of tension reinforcement

and

$$V_{Rd2} = 0.5\, \upsilon\, f_{cd}\, b_w\, 0.9\, d \qquad [kN] \qquad (4.8)$$

with,

$$\upsilon = 0.7 - \frac{f_{ck}}{200} \geq 0.5 \qquad (4.9)$$

where,

f_{ck}= concrete cylinder compressive strength (5% fractile characteristic value)

f_{cd}= concrete cylinder compressive strength (design value)

Since the issue of shear strength is of importance in cases where large amounts of reinforcement are employed, the shear resitance was calculted and evaluated in analysis series 3 and 4. The EC2 predictions turned out to be

Analysis Series 3:	V_{Rd1}=	51 [kN]	V_{Rd2}=	110 [kN]
Analysis Series 4:	V_{Rd1}=	60 [kN]	V_{Rd2}=	146 [kN]

In case the graphical analysis output suggested that the shear strength was exceeded, the actual shear capacity of the specimen was obtained by summing up the vertical nodal stresses, σ_y, from the finite element analysis at the cross-section of the specimen where element failure was detected.

4.4 Analysis Results

Results and failure characteristics at different effective reinforcing ratios turned out different for the four analysis series. The results are discussed separately for each series of analyses. A set of typical input files for the ANSYS finite element analysis can be observed in Appendix B.

In general the cases with low amounts of reinforcement were governed by the ductility behavior of the steel. The concrete failed early in tension, so the load was carried by a compression zone in the upper portion of the slab and by tensile forces in the steel at the bottom. Cases with moderate amounts of reinforcement exhibited failure due to crushing of the compression zone of the concrete except for one case, where the steel characteristics controlled the structural behavior. The two analysis series with high effective reinforcing ratios were governed by the shear capacity. All specimens showed a failure of the compression strut (Fig. 4.1), most often close to the support, and had an overall load capacity significantly lower than the capacity calculated with the ACI design equations.

4.4.1 Low Effective Reinforcing Ratio

All cases with a low effective reinforcing ratio (ω_1= 0.03) investigated in this study were governed by the steel ductility characteristics and the ultimate capacity for each case was found to be greater than the ACI prediction (169kN). Initial tension cracking occurred in the early stages of loading and the load-displacement diagrams exhibit a sudden drop indicating that the tensile capacity of the concrete was exceeded, and the reinforcing steel took over carrying the tensile forces in the structure. Upon yielding of the steel, the load-displacement curves exhibit a secondary slope which essentially follow the stress-strain properties of each reinforcing steel. Therefore, the carrying capacity of the slab depended on the ultimate capacity of the reinforcement and the ultimate elongation of the steel determined the overall ductility of the structure, which can be seen in Fig. 4.2 on the next page.

The specimens that employed European reinforcing bars with little strain-hardening (#1-1, #1-2) failed at deflections of 8mm and 16mm, respectively (Fig 4.3). The two slabs that incorporated reinforcing bars with a yield plateau (#1-3, #1-4) led to load-displacement plots that reflect the yield plateau of the steel with a region with no increase in carrying capacity for the overall structure (Fig. 4.4). The ultimate structural capacity was essentially the same for both cases (207kN), which could be expected, because the ultimate strength of the reinforcing bars was the same. The difference in structural deflection at failure (#1-3: 21mm, #1-4: 26.5mm) is due to the difference in ultimate elongation of the reinforcing steel (6% versus 8%).

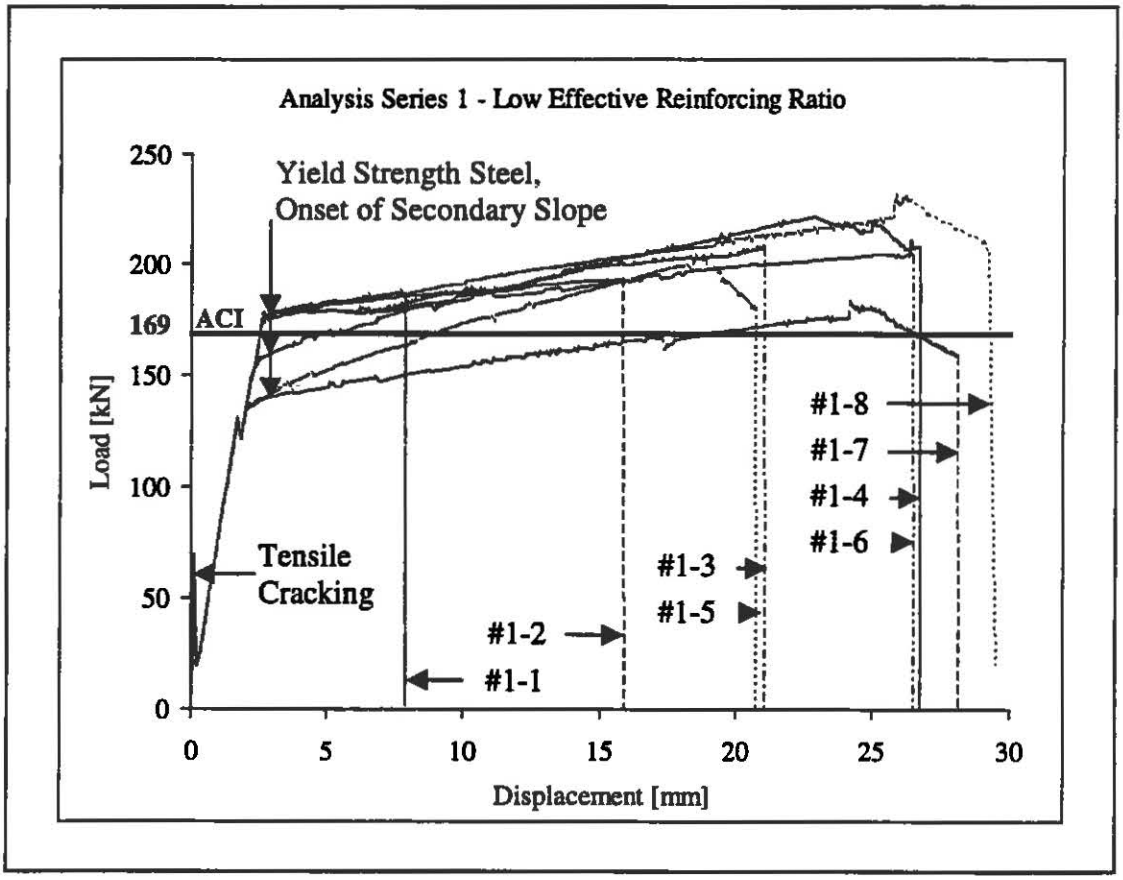

Figure 4.2 Analysis Series 1 - Overview Results

The tolerances in the steel characteristics of American reinforcing bars led to significantly different behavior of the overall structure (Figs. 4.5 and 4.6). Specimens that employed reinforcing steel produced according to the ASTM requirements reached the onset of the secondary slope of the load-displacement plot at a lower load level, due to the lower yield capacity of the reinforcing steel. Thus, the carrying capacity predicted by the ACI Building Code approach was met at larger deflections of the overall structure. Analyses with A615/grade60 billet reinforcing steel resulted in ultimate load capacities of 203kN for the specimen using reinforcement with the minimum strength requirements (#1-5), and 220kN for the analysis where steel with the upper bound strength requirements was employed (#1-6). The ultimate deflections of the slabs incorporating A615/grade60 billet steel differed by as much as 5mm for the tolerances in material strength and ultimate elongation allowed by the ASTM requirements (#1-5: 21mm, #1-6: 26.5mm). The findings for the structures reinforced with steel representing the lower- and upper bound requirements for low-alloy A706 steel qualitatively matched the results for variations in strength of A615/grade60 reinforcement (Fig. 4.6). The increased yield strength in case the maximum requirements of ASTM were employed moved the onset of the strain-hardening region to a higher load level, and the carrying capacity calculated with ACI equations was exceeded before the reinforcing steel exhibited strain-hardening behavior. The ultimate capacities were calculated to be 180kN (#1-7) and 230kN (#1-8) and the specimens failed at 28mm and 29.5mm, respectively. The load-displacement curves for the American reinforcing bars all are characterized by a sudden jump in capacity

right before a downward drop in structural carrying capacity, indicating that the steel had exceeded its ultimate capacity. This behavior is not a structural characteristic, but rather due to convergence issues as the ultimate strength of the reinforcement was exceeded and the stress-strain curve of the steel takes a downward slope. To investigate the structural behavior past this point, the fault tolerance for the convergence criterion was set to a higher value. Thus, the analyses locally predicted a higher overall capacity of the structure. The trend of the load-displacement plot is no doubt downward, however, the exact values are open to question.

4.4.2 Moderate Effective Reinforcing Ratio

Up to a deflection of about 2.5mm, all analyses with an effective reinforcing ratio of ω_2= 0.10 exhibited identical structural behavior. Tensile cracking occurred shortly after initial loading, which led to a drop in the overall capacity of the slab. The load was then carried as a tensile force in the steel only and as a compressive force in the upper portion of the concrete slab in an arch-like manner. Between 2.5mm and 3.0mm, at a corresponding load level of around 380kN to 420kN, all specimens exhibited crushing failure of some concrete elements of the top finite element layer. Thus, the overall capacity of the slab dropped locally. Internal load redistribution allowed the structure to regain capacity up to a load level at which the reinforcing steel reached its yield capacity, and a secondary slope is introduced in the load-displacement plot. The strain-hardening characteristics of the reinforcement influenced the ductility behavior of the structure differently for the different analysis cases, therefore, playing an important role for the ultimate deflections of the analysis

specimens. The load-displacement plots presented in Fig. 4.7 provide an overview of the analysis results for this analysis series and the main characteristics of the results are pointed out.

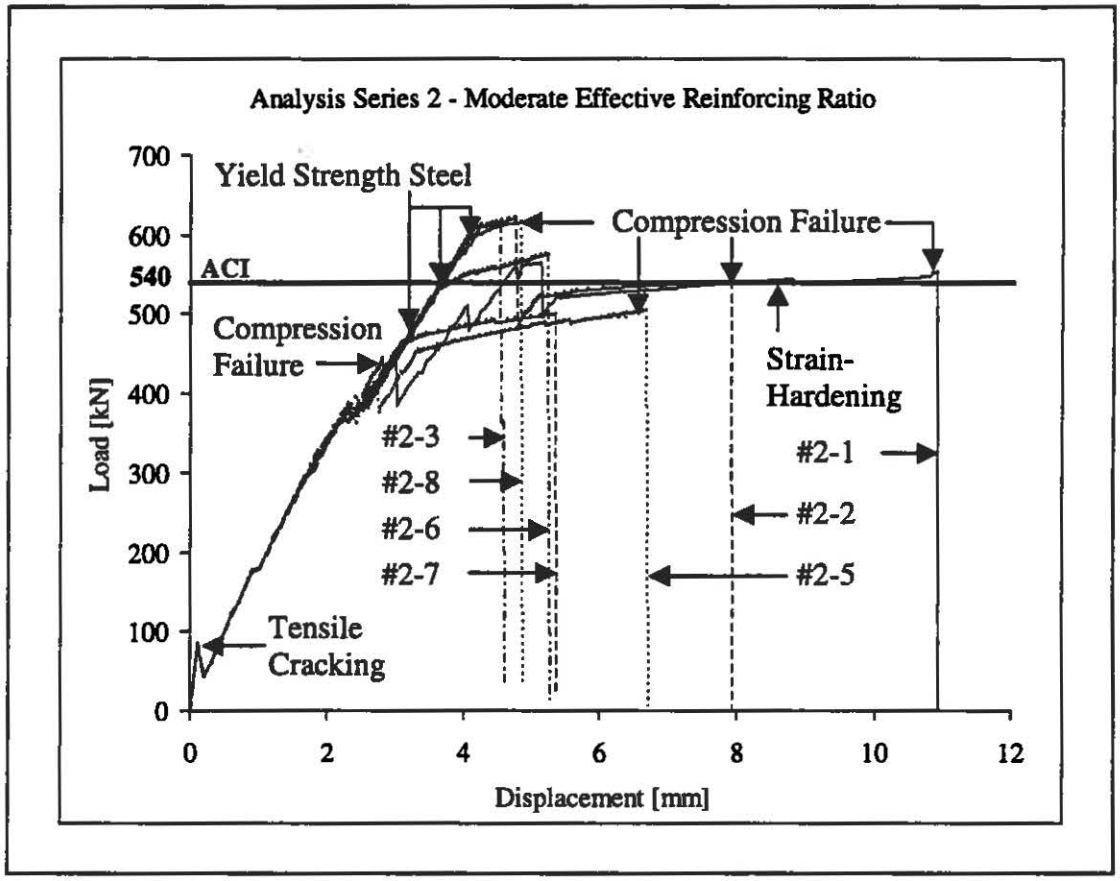

Figure 4.7 Analysis Series 2 - Overview Results

All European reinforcing steels caused the structure to gain a maximum capacity over the value predicted using the ACI approach to determine the carrying capacity (540kN). After the peak capacity was reached more finite elements failed in compression, leading to a sudden loss of structural capacity. The two specimens reinforced with steels without a yield plateau regained strength around the predicted

capacity, but failed in compression at 8mm (#2-2) and 11mm (#2-1), respectively (Fig. 4.8). The two structures reinforced with steels incorporating a yield plateau performed significantly different (Fig. 4.9). Using the steel with the lower ductility (#2-3), the slab exhibited a widespread failure of compression elements and lost its structural integrity after a peak capacity of 613kN at 4.5mm was reached. The more ductile reinforcing steel (#2-4) led to a structure that also exhibited compressive failure at a displacement of 4.7mm, but maintained a load level of around 480kN. The steel characteristics governed the structural behavior from then on resulting in a flat load-displacement curve. The specimen failed as the ultimate elongation of the steel was reached at 39.3mm.

The analysis cases in which American reinforcing bars were used produced significant differences in capacity between the minimum requirements and the upper bound estimates for the reinforcing bar (Fig. 4.10). Both specimens reinforced with the steels meeting the minimum strength requirements resulted in an ultimate capacity lower than the predicted structural capacity (#2-5: 505kN, #2-7: 500kN). However, the ductility of these specimens was larger than that of slabs reinforced with their upper bound counterparts. Both cases where the upper bound estimate for the steel strength was used showed capacities over the predicted carrying capacity. The specimen with A615/grade60 steel reinforcement (#2-6) reached its ultimate capacity at a deflection of 5.2mm with 576kN carrying capacity and the slab with A706 steel (#2-8) reached 617kN at 4.8mm before both failed due to crushing of the concrete in the compression zone of the slab.

4.4.3 High Effective Reinforcing Ratio

The structural response for the highly reinforced specimens (ω_3= 0.25) was characterized by brittle failure of the compression strut (Fig. 4.1) at low structural deflections. The maximum compressive strength of some finite elements in the compression strut was exceeded at various locations in the different specimens (Table 4.5). A representative selection with plots of this failure mode can be observed in Fig. 4.11. However, in all eight cases the compressive strength of the concrete was exhausted before the steel reached its yield strength. Therefore, the overall structural performance was similar in all eight cases, and the true nonlinear steel characteristics were not activated. The ultimate capacity of the structure turned out to be less than 75% of the predicted capacity using the ACI equations (1223kN). In three cases (#3-3, #3-6, #3-8) the analyzed specimen completely failed in compression after reaching an ultimate carrying capacity of around 900kN. The other analyses were characterized by a drop in capacity at a load level between 800kN and 900kN due to partial failure of some finite elements in the compression strut. With load redistribution within the structure, the overall capacity increased again up to a similar load level, before more finite elements failed in compression leading to a widespread deterioration of the structure. This load redistribution added some additional ductility to the structural response. Nevertheless the deflections upon failure were found to be between 3.5mm and 5mm for all analyses, so generally all specimens behaved in a brittle manner. The main characteristics of this analysis series can be seen in Fig. 4.12.

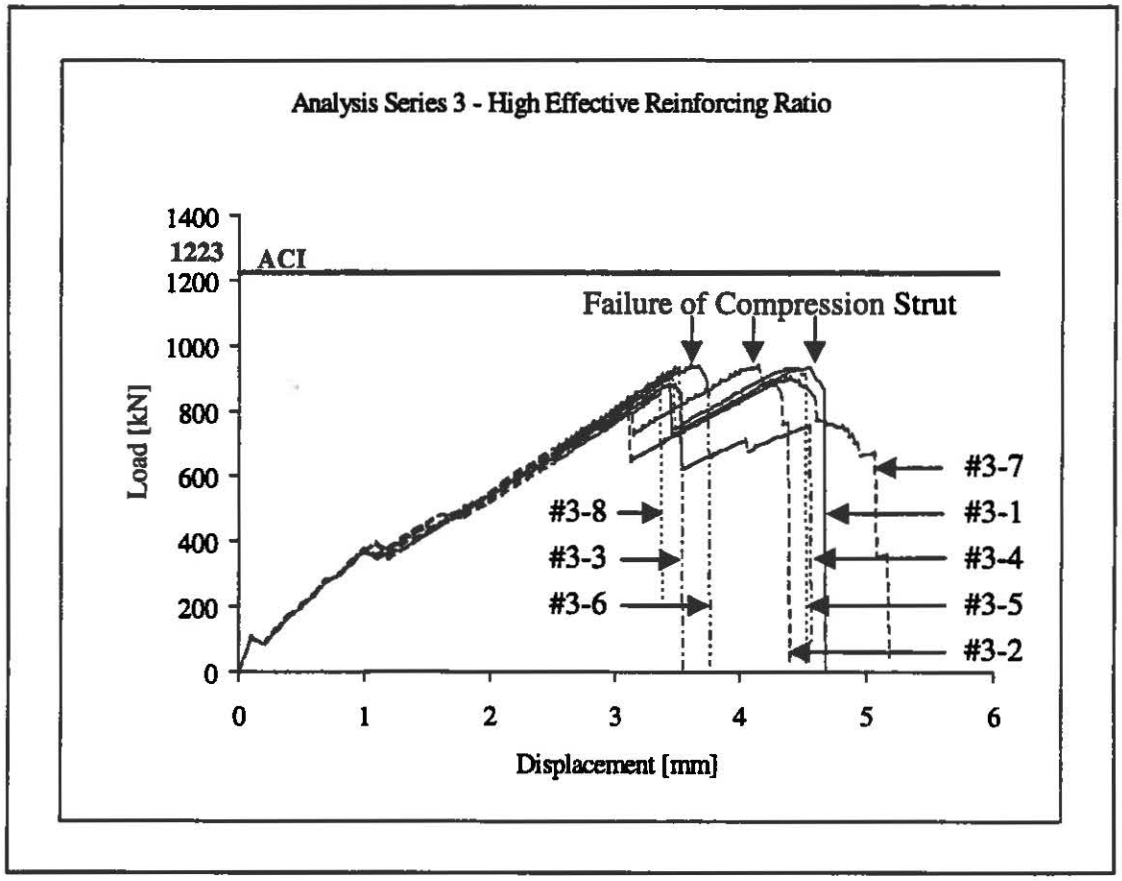

Figure 4.12 Analysis Series 3 - Overview Results

4.4.4 High Effective Reinforcing Ratio with High Strength Concrete

This series of analyses was performed to investigate the influence of the concrete strength (f_{cm}= 83MPa) on the structural behavior of a highly reinforced slab (ω_3= 0.25). As described in Section 4.4.3, structures with large amounts of reinforcement tend to exhibit a sudden failure governed by crushing of finite elements in the compression strut caused by compressive stresses that are beyond the material strength (Table 4.6). Figure 4.11 provides a representative display of this failure mode with results from the study. Initially all analysis specimens were characterized

by a similar gain in capacity until a load level in the vicinity of 1500kN was reached, which was 35% below the capacity predicted by the ACI approach (2360kN). For all investigated cases, the capacity obtained at this deflection (about. 4mm) represented the maximum capacity of the structure. After this peak load was exceeded, all specimens exhibited partial element failure in the compression strut and, thus, the overall load carrying capacity dropped. Redistribution of the loads in the structure caused the specimens to regain some load carrying capacity and protected the structural integrity. This process of localized compressive failure of finite elements in the compression strut followed by internal load redistribution took place repetitively in the different analyses leading to ultimate deflections of 6mm, 8-8.5mm and 14-15mm, as can be seen in Fig. 4.13 on the next page.

It is important to note that the ultimate deflections should be treated with great caution. It is questionable whether or not the structural integrity can be maintained if partial crushing of the compression strut occurs. Even though the results suggest a considerable amount of rotation capacity does exist, compared to the analysis series using C30/40 concrete, the structural behavior must be characterized as brittle because the failure of the concrete ultimately represents the failure mode of the overall structure.

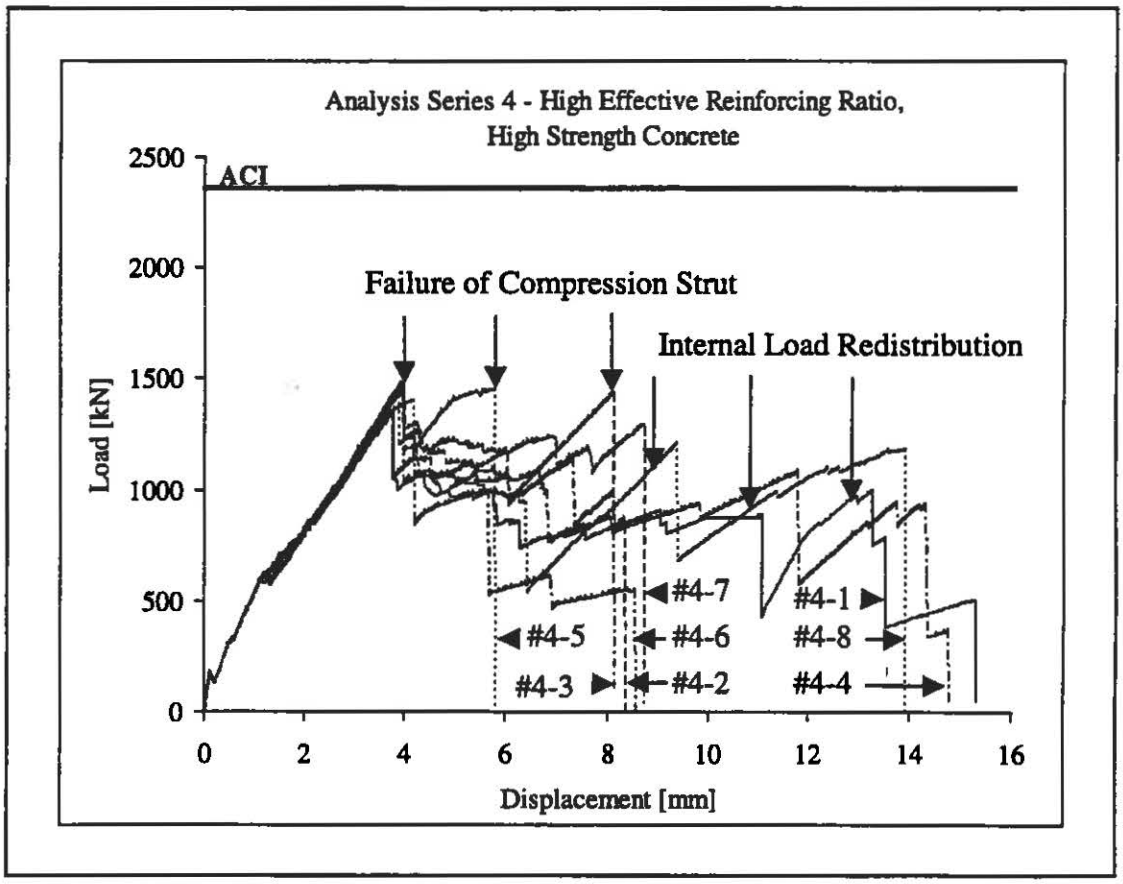

Figure 4.13 Analysis Series 4 - Overview Results

4.5 Failure Modes

As revealed in the preceding section, the failure modes of the structure were observed to be significantly influenced by the effective reinforcing ratio of the specimen. The structural performance of each reinforcing steel under the four analysis settings is graphically compared in Figs. 4.14 through 4.21. The variations in the overall structural ductility due to changes in the amount of steel employed in the structure can be observed and differences in the influence of the material properties of the steel type on the structural behavior can be seen.

At a low reinforcing level, the load carrying capacity was low and the structural behavior was governed by the ductility characteristics of the steel, resulting in ductile behavior of the overall structure. Different material characteristics, such as variations in yield strength, a yield plateau, or a downward slope after exceeding the ultimate capacity, could be identified in the load-displacement plots of the structural response. Hence, the use of reinforcement with different ductility characteristics did affect the overall rotation capacity. Structures that incorporated moderate amounts of reinforcing steel exhibited a behavior comprised partially of the steel ductility characteristics and the carrying capacity of the compression zone in the upper portion of the slab. All steels reached their yield strength, thereby introducing a secondary slope to the load-displacement plots. The ultimate deflection, in all but one case, was then determined by the failure mode of the compression zone in the upper portion of the slab. In one case the steel ductility governed the overall structural behavior and the specimen failed as the ultimate steel capacity was exceeded. This result indicates that the choice of the reinforcing steel could be crucial to the overall structural behavior. As the amounts of reinforcement were further increased, the structural response shifted to a brittle failure mode. The reinforcing steel no longer reached its yield strength and the compressive strength of the compression strut in the slab was exceeded, thus causing the structure to collapse at low deflections and at a load level below the prediction according to ACI. In the cases where high strength concrete was used in highly reinforced specimens, the failure mode was again governed by the compressive capacity of the compression strut. Although the analyses suggested that

internal load redistribution provided a larger ductility to the structure than in the analysis series with normal strength concrete, the structures failed in a brittle manner. In both series of analyses with large amounts of reinforcement, the choice of reinforcing steel and its stress-strain properties did not have a significant effect on the overall structural performance since the stresses in the steel were below the yield strength of the material. Thus, the overall structural behavior was governed by the concrete characteristics alone.

4.6 Summary

The analysis series investigated in this study are introduced and its analysis parameters are identified. Four test series at different effective reinforcing ratios and concrete strengths were carried out, each incorporating analyses of eight reinforcing steels with different ductility characteristics. The results for each series of analyses are described and significant differences in structural behavior were found. The failure modes of the structures were influenced by the effective reinforcing ratio employed. In structures with low amounts of reinforcement, the structural behavior was governed by the ductility characteristics of the steel, resulting in notable amounts of rotation capacity of the overall structure. As the effective reinforcing ratio was increased, the influence of the steel ductility characteristics gradually diminished. In case moderate amounts of reinforcement were employed, the reaction of the structure was partially influenced by the concrete and the steel characteristics, implying that the choice of reinforcement could shift the overall structural behavior from a brittle to

a ductile failure mode. For highly reinforced specimens the structural behavior was governed solely by the concrete characteristics and the reinforcing steel did not reach its yield strength. Therefore, the choice of reinforcement did not have an effect on the overall structural performance.

The bond strength at the interface from the steel to the concrete was not exceeded in any of the analysis cases, hence slipping of the reinforcing bars did not occur. Therefore, the specimens in this study were found to be insensitive to the effects of bond-slip on the structural behavior. This indicates that the steel was sufficiently developed in all slabs investigated in this project.

The following chapter summarizes the work of the project and concludes the study.

CHAPTER 5

SUMMARY AND CONCLUSIONS

5.1 Summary

This study analytically investigated the influence of material parameters on the rotation capacity of a one-way slab subjected to three point bending using the Finite Element Method. The influence of different stress-strain behavior of the reinforcing steel was of special interest and the performance of eight different reinforcing steel types from Europe and the United States was analyzed. Finite element analyses at three different effective reinforcing ratios were carried out to assess the behavior of specimens incorporating low to large amounts of reinforcing steel. In addition to that, the structural behavior of a highly reinforced slab with high strength concrete was investigated.

The finite element model used for this project was developed in three-dimensional space and incorporated four different types of finite elements. The concrete component was represented by three-dimensional eight node isoparametric elements. The smeared crack modeling approach (Rashid, 1968) was adapted in this study to approximate the tensile concrete behavior and was, therefore, used to model flexure and shear cracks in the concrete. The Willam-Warnke compression-softening model (1975) was utilized to predict the behavior of concrete in compression and its failure. Reinforcement was introduced into the finite element model with two-node

three-dimensional rod elements, which were capable of incorporating the nonlinear material properties of the steel. The two materials were connected with bond-link elements in the form of one-dimensional linear and nonlinear spring elements. Vertical linear springs with a large stiffness were used to assure a stiff connection between the two materials and vertical displacement compatibility. In the longitudinal direction the steel-concrete interface was modeled using nonlinear spring elements to allow for relative movement at the interface to the reinforcing steel in case the bond strength was exceeded.

In the nonlinear analysis process, load-displacement plots were obtained to monitor the structural behavior of each specimen. The maximum values of the carrying capacity were compared to the predictions obtained with calculations using ACI 318-95 (1995) provisions. The structural performance of the different reinforcing steels was evaluated by comparing the findings at each reinforcing level. The results showed that the influence of the ductility characteristics of the reinforcing steel on the rotation capacity of the structure was profoundly affected by the effective reinforcing ratio of the specimen. Structures with low amounts of reinforcement were governed by the ductility characteristics of the steel, thus the amount of deflection at failure depended on the ultimate elongation of the steel. With an increase of the reinforcing percentage the compressive strength of the concrete became a factor for the structural behavior. At moderate reinforcing levels the choice of the reinforcing steel determined whether the structural behavior was governed by the steel characteristics or the concrete behavior, resulting in ductile or progressively more brittle overall

behavior. As the amounts of reinforcing steel were further increased, the concrete characteristics completely determined the structural behavior. Generally, all specimens with high effective reinforcing ratios exhibited a failure of the compression strut in the concrete - a brittle failure mode – while the steel did not even reach its yield capacity. The carrying capacity for all analysis cases with large amounts of reinforcement was found to be significantly lower than the capacity obtained by using standard ACI design philosophy. In none of the cases did the bond stress exceed the stress level necessary to cause slippage and, therefore, all investigated specimens proved to be insensitive to bond-slip, which indicates that the reinforcement was sufficiently developed in all cases.

5.2 Conclusions and Recommendations

The results of the finite element analyses discussed in this study support the following conclusions.

1. The ultimate structural rotation capacity strongly depends on the amount of steel employed in the specimen. If a large ductility is desired, low to moderate effective reinforcing ratios should be used.
2. Structures using low effective reinforcing ratios generally exhibit the largest deflections upon failure and are the most ductile, since the structural behavior is governed by the ductility characteristics of the reinforcement.

3. When the amount of reinforcement in the structure is moderate, the choice of the reinforcing steel could be crucial to the structural response because the influence of both the steel and the concrete characteristics on the rotation capacity are equally important. Thus, finding the right combination of steel characteristics to match the concrete behavior is the key to a large overall structural ductility.

4. Great care should be taken when large amounts of reinforcement are used because the structures do not reach the load carrying capacities predicted by standard design provisions. Moreover, highly reinforced structures exhibit brittle failure modes due to failure of the compression strut and, thus, do not provide significant amounts of ductility.

5. The behavior of concrete in compression is crucial to the plastic deformation behavior of the analysis specimens, especially for highly reinforced specimens. Thus, accurate models, such as the Willam-Warnke compression-softening model (1975) need to be incorporated in a finite element analysis to accurately predict the concrete behavior.

6. The simply supported one-way slab evaluated in this study proved to be insensitive to bond-slip. The reason being that the reinforcement was adequately anchored in the concrete.

5.3 Future Research Needs

The structural behavior of reinforced concrete structures is a complex matter influenced by the material properties of the concrete and the steel and geometry considerations. This study explicitly focussed on the influence of the ductility characteristics of the reinforcement and the amounts of steel employed in the structure. The influence of concrete strength also was assessed.

Future investigations should consider parametric studies with several steel characteristics and assess the effects of changes in the geometry of the structure. Thus, the effects of inclined shear cracking and size dependence can be monitored. Another area of interest is the influence of compression reinforcement on the rotation capacity and increased ductility. The effect of confining reinforcement in form of stirrups also is an area that should be studied since there is a strong interaction between shear and flexural demands. Finite element studies also could be extrapolated to investigate the influence of changes in the material properties of the reinforcing steel on the overall structural behavior of reinforced concrete frames and incorporate different loading patterns (i.e. earthquake loading).

Currently there is no code guidance for the appropriate use of reinforcing steel with different ductility characteristics. Ideally, the research efforts described here could lead to recommendations for improved ductile design by defining relations between the ductility characteristics of the steel and the rotation capacity of the structure. The work by Task Group II/2 of the Comité Euro-International du Béton is especially focussed on providing guidance into this important area.

APPENDIX A

COMPARISON OF BUILDING CODE DEFINITIONS

A.1 Comparison of the Concrete Strength Definitions in ACI 318-95 and EC2

The ACI 318-95 (1995) Building Code utilizes the concrete cylinder compressive strength, f'_c, in its design provisions. The value is derived from experimental testing and has to satisfy two criteria

1. No individual strength test result (the average of a pair of cylinder tests) falls below the required f'_c by more than 500psi
2. Every arithmetic average of any three consecutive strength tests equals or exceeds f'_c

which are defined in the ASTM C172 (1998) and ASTM C31 (1998) standards.

In the European EC2 Building Code (1991) three values for the concrete strength are defined. The mean value of the concrete strength, f_{cm}, is generally not used for design purposes. However, this study utilizes this feature of the concrete strength because the structural performance at the limit state of the material is investigated. Usually the 5% fractile value of the concrete cylinder compressive strength, f_{ck}, and the design concrete strength, f_{cd}, are used for design purposes.

The characteristic compressive concrete strength, f_{ck}, is defined as that value of strength below which 5% of all possible strength test results for the specified

concrete may be expected to fall. The value of the design concrete strength is derived from f_{ck} and takes the form

$$f_{cd} = \frac{f_{ck}}{\gamma_c} \qquad [MPa] \qquad (A\text{-}1)$$

where,

γ_c= partial factor (favorable or unfavorable actions)

The partial factor incorporated in the design strength of the concrete reflects the safety concept of the EC2 Building Code. In contrast to the ACI 318-95 Building Code, where safety factors are considered for the calculations of the required strength of the structure in form of factored load combinations and an overall reduction of the design strength, the EC2 design philosophy incorporates reduction factors imposed on the loads applied to the structure and on the material property values of the steel and the concrete to calculate the design strength of the member.

APPENDIX B

INPUT FILES COMPUTER ANALYSIS

This appendix contains typical input files with instructions for the finite element analysis with ANSYS. The complete analysis process is comprised of a pre-processing and solution part as well as a post-processing section. To represent different analysis specimens the parameters in the 'input' portion of each file need to be adjusted.

B.1 Typical Analysis Input File

```
/BATCH
/COM,ANSYS REVISION  5.3                34    18:20:30    01/31/1998
/FILNAM,slab,db
/TITLE,Concrete slab loaded in three point bending
/PREP7
!Notes:         reinforced concrete slab - imposed displacements
!               models half the geometry
!               a crossection w/ one rebar (b=100mm) is analyzed
!               solid 65 elements are used throughout the beam
!               includes bond slip behavior
!               substep length is initialized to 1 step/0.1mm
!               solution will be saved at every 2nd substep

!               if changes in the model are made, manual changes have
!               to be made to nodes where displ. is applied, the
!               elements which model the steel and the bond-slip FE

!--------------------------------INPUT-------------------------------!
!GEOMETRY
xs1=   0.0          ! startpoint
xs2= 600.0          ! effective length of slab (x direction)
yt=   235           ! dist. to top of slab (y direction)
y1=   3*yt/4        ! dist to top of tensile elements
y2=   yt/8          ! dist to centroid of rebar layer (-> d=200mm)
yb=   0.0           ! bottom of slab
z1=  50             ! half width of slab (z direction)
z2= -z1             ! half width of slab
```

```
!MESH
divx= 24! elements over length, x dir. (element length= 50mm)

divy= 2 ! elements over height of compression section  (y dir.)
divy_b=5! elements over height of tension section (between reinf.
        ! and start of comp. zone)
divy_r=1! elements between bottom and reinforcement layer

divz= 4 ! elements over width of beam, z dir.(element length= 25mm)


!LOADING
!imposed displacement over whole width and d/2
!(100mm for d=20, 300mm for d=600) in x direction

imp_uy= -2.5          ! imposed displacement in mm (NEGATIV)


!MATERIAL PROPERTIES
!steel
!note: yield strain and shear modulus are calculated by the program

fym= 550              ! yield strength
fum= 578              ! ultimate strentgh
ffm= 578              ! strength at failure
e_u= 0.025            ! ultimate strain
e_f= 0.028            ! strain at failure

ex_s= 200000          ! modulus of elasticity, MPa
dens_s= 7.85e-5       ! density N/mm^3
nu_s= 0.3             ! poisson's ratio

a_s=156.4             ! Area of rebar, single bar

!concrete
!note: modulus of elasticity and shear modulus are calculated by the
program

fcm= 43               ! crushing strength in MPa
ftm= 3.2              ! tensile strength in MPa
dens_c= 2.4E-5        ! density N/mm^3
nu_c= 0.15            ! poisson's ratio


!INFORMATION FOR ANALYSIS PROCESS
! number of substeps is set to one step per 0.1 mm

equilib=300           ! maximum number of equilibrium iterations
tol=0.005             ! tolerance for force convergence

!------------------------------END INPUT-----------------------------!
```

```
!----------------------------PREPROCESSOR-------------------------!

!----CALCULATED VARIABLES

!steel
e_y= fym/ex_s            ! yield strain
g_s= ex_s/(2*(1+nu_s))   ! shear modulus

!concrete
ex_c= 4700*sqrt(fcm)     ! modulus of elasticity, MPa
g_c= ex_c/(2*(1+nu_c))   ! shear modulus

!other
prs= -imp_uy        !sets the displ. value = total time of load step
subst=prs*10        !initializes the number of substeps to 0.1mm/step

!----END CALCULATED VARIABLES


KEYW,PR_SET,1
KEYW,PR_STRUC,1
KEYW,PR_THERM,0 ansys
KEYW,PR_ELMAG,0
KEYW,PR_FLUID,0
KEYW,PR_MULTI,0
KEYW,PR_CFD,0


!----ELEMENTS
ET,1,SOLID45        !for elastic portion at support
ET,2,SOLID65        !entire model (concrete)
ET,3,LINK8          !for reinforcement

! THE FOLLOWING ELEMENT DON'T NEED MATERIAL
ET,4,COMBIN14       !for y-fixation of steel to concrete
ET,5,COMBIN39       !to model bond slip behavior in x direction


!----KEYOPTIONS
!solid45
KEYOPT,1,5,1        !solution at every integration point
KEYOPT,1,6,3        !print solution at each integration point

!solid65
KEYOPT,2,5,1        !solution at every integration point
KEYOPT,2,6,3        !print solution at each integration point
KEYOPT,2,7,1        !include tensile stress relaxation after cracking
                    !to help convergence

!link8 (Element#3) doesn't have keyoptions
```

```
!combine 14 (y-fixation, Element#4)
KEYOPT,4,1,0      !linear solution
KEYOPT,4,2,2      !1-d longitudinal spring-damper, y direction

!combine39 (bond slip in x direction, Element#5)
KEYOPT,5,1,1      !unload on loading path parallel to original slope
                  !(un-conservative approach)
KEYOPT,5,2,0      !compr. loading follows defined comp. curve
                  !(or reflect tensile curve if not defined)
KEYOPT,5,3,1      !1-d nonlinear sprint, x direction
KEYOPT,5,4,0      !use keyoption 3 (element just has 1 DOF)
KEYOPT,5,6,1      !prints load-displ curve at first iteration


!----REAL CONSTANTS
! solid65 (concrete element)
R,2,2,0, , , , ,
RMORE, , , , , , ,
RMORE, ,

!link8 (rebar)
R,3,a_s, , , , , ,

!combin14 (y-fixation)
R,4,1e10,0,0          !spring const., damping coeff., damping coeff.

!combin39 (bond slip in x-direction)
!values for force/displ. curve
pi=3.14159265359      !defines pi
radi=sqrt(a_s/pi)     !calculates radius of steel from given

steel area
b_area= xs2*pi*radi/(divx)     !area for bondslip

!good bond conditions -> CEB-FIP model code 1990, p.83
s1= 0.6               !displacement @ max. bond stress
s2= 0.6               !displacement @ end of max bond stress plateau
s3= 1.0               !displacement @ low level bond stress
s4= 100               !arbitrary diplacement

tau_max=2*sqrt(fcm)   !maximum bond-stress
tau_f=0.15*tau_max    !low level bond stress

f_max=b_area*tau_max  !maximum force for load-displ diagram
f_f=b_area*tau_f      !low level force for load-displ diagram

R,5,s1,f_max,s3,f_f,s4,f_f
```

```
!----MATERIAL PROPERTIES
!steel
UIMP,1,EX, , ,ex_s,
UIMP,1,DENS, , ,dens_s,
UIMP,1,ALPX, , ,,
UIMP,1,REFT, , , ,
UIMP,1,NUXY, , ,nu_s,
UIMP,1,GXY, , ,g_s,
UIMP,1,MU, , , ,
UIMP,1,DAMP, , , ,
UIMP,1,KXX, , , ,
UIMP,1,C, , , ,
UIMP,1,ENTH, , , ,
UIMP,1,HF, , , ,
UIMP,1,EMIS, , ,1,
UIMP,1,QRATE, , , ,
UIMP,1,MURX, , , ,
UIMP,1,MGXX, , , ,
UIMP,1,RSVX, , , ,
UIMP,1,PERX, , , ,
UIMP,1,VISC, , , ,
UIMP,1,SONC, , , ,

!concrete
UIMP,2,EX, , ,ex_c,
UIMP,2,DENS, , ,dens_c,
UIMP,2,ALPX, , ,,
UIMP,2,REFT, , , ,
UIMP,2,NUXY, , ,nu_c,
UIMP,2,GXY, , ,g_c,
UIMP,2,MU, , , ,
UIMP,2,DAMP, , , ,
UIMP,2,KXX, , , ,
UIMP,2,C, , , ,
UIMP,2,ENTH, , , ,
UIMP,2,HF, , , ,
UIMP,2,EMIS, , ,1,
UIMP,2,QRATE, , , ,
UIMP,2,MURX, , , ,
UIMP,2,MGXX, , , ,
UIMP,2,RSVX, , , ,
UIMP,2,PERX, , , ,
UIMP,2,VISC, , , ,
UIMP,2,SONC, , , ,
```

```
!elastic zone (at support)
UIMP,4,EX, , ,ex_c,
UIMP,4,DENS, , ,dens_c,
UIMP,4,ALPX, , ,,
UIMP,4,REFT, , , ,
UIMP,4,NUXY, , ,nu_c,
UIMP,4,GXY, , ,g_c,
UIMP,4,MU, , , ,
UIMP,4,DAMP, , , ,
UIMP,4,KXX, , , ,
UIMP,4,C, , , ,
UIMP,4,ENTH, , , ,
UIMP,4,HF, , , ,
UIMP,4,EMIS, , ,1,
UIMP,4,QRATE, , , ,
UIMP,4,MURX, , , ,
UIMP,4,MGXX, , , ,
UIMP,4,RSVX, , , ,
UIMP,4,PERX, , , ,
UIMP,4,VISC, , , ,
UIMP,4,SONC, , , ,

!'dummy' material for combine elements -> no content
UIMP,7,EX, , ,,
UIMP,7,DENS, , ,,
UIMP,7,ALPX, , ,,
UIMP,7,REFT, , , ,
UIMP,7,NUXY, , ,,
UIMP,7,GXY, , ,
UIMP,7,MU, , , ,
UIMP,7,DAMP, , , ,
UIMP,7,KXX, , , ,
UIMP,7,C, , , ,
UIMP,7,ENTH, , , ,
UIMP,7,HF, , , ,
UIMP,7,EMIS, , ,1,
UIMP,7,QRATE, , , ,
UIMP,7,MURX, , , ,
UIMP,7,MGXX, , , ,
UIMP,7,RSVX, , , ,
UIMP,7,PERX, , , ,
UIMP,7,VISC, , , ,
UIMP,7,SONC, , , ,
```

```
!----DATA TABLES
!Nonlinear Material Properties

! Steel
!multilinear kinematic behavior
TB,MKIN,1, , ,0
TBMODIF,1,2,e_y              !yield strain
TBMODIF,1,3,e_u              !yield @ fum
TBMODIF,1,4,e_f              !yield @ failure
TBMODIF,1,5,e_f+0.0001       !yield @ stress=0

TBMODIF,2,2,fym              !yield strength
TBMODIF,2,3,fum              !ultimate strength
TBMODIF,2,4,ffm              !failure strength
TBMODIF,2,5,0                !after failure
TBPLOT,MKIN,1,               !plots stress - strain diagram

! Concrete
TB,CONCR,2, , ,0
TBDATA,1,0.6                 ! Shear transf. at open crack
TBDATA,2,0.8                 ! shear transf. at closed crack
TBDATA,3,ftm                 ! cracking strength
TBDATA,4,fcm                 ! crushing strength
TBLIST


!----ASSEMBLING THE MODEL
!create Keypoints

K,1,xs1,yb,z1                !left support, bottom layer
K,2,xs1,yb,0
K,3,xs1,yb,z2

K,4,xs1,y2,z1                !left support, rebar layer
K,5,xs1,y2,0
K,6,xs1,y2,z2

K,7,xs1,y1,z1                !left support, top of tension layer
K,8,xs1,y1,0
K,9,xs1,y1,z2

K,10,xs1,yt,z1               !left support, top layer
K,11,xs1,yt,0
K,12,xs1,yt,z2


K,13,2*(xs2/divx),yb,z1      !end left elastic zone, bottom layer
K,14,2*(xs2/divx),yb,0
K,15,2*(xs2/divx),yb,z2

K,16,2*(xs2/divx),y2,z1      !end left elastic zone, rebar layer
K,17,2*(xs2/divx),y2,0
K,18,2*(xs2/divx),y2,z2
```

```
K,19,2*(xs2/divx),y1,z1      !end left el. zone, top of tension Layer
K,20,2*(xs2/divx),y1,0
K,21,2*(xs2/divx),y1,z2

K,22,2*(xs2/divx),yt,z1      !end left elastic zone, top layer
K,23,2*(xs2/divx),yt,0
K,24,2*(xs2/divx),yt,z2


K,25,xs2-2*(xs2/divx),yb,z1 !start right elastic zone, bottom layer
K,26,xs2-2*(xs2/divx),yb,0
K,27,xs2-2*(xs2/divx),yb,z2

K,28,xs2-2*(xs2/divx),y2,z1 !start right elastic zone, rebar layer
K,29,xs2-2*(xs2/divx),y2,0
K,30,xs2-2*(xs2/divx),y2,z2

K,31,xs2-2*(xs2/divx),y1,z1 !start right elastic zone, top of
K,32,xs2-2*(xs2/divx),y1,0  !tension layer
K,33,xs2-2*(xs2/divx),y1,z2

K,34,xs2-2*(xs2/divx),yt,z1 !start right elastic zone, top layer
K,35,xs2-2*(xs2/divx),yt,0
K,36,xs2-2*(xs2/divx),yt,z2


K,37,xs2,yb,z1               !right support, bottom layer
K,38,xs2,yb,0
K,39,xs2,yb,z2

K,40,xs2,y2,z1               !right support, rebar layer
K,41,xs2,y2,0
K,42,xs2,y2,z2

K,43,xs2,y1,z1               !right support, top of tension layer
K,44,xs2,y1,0
K,45,xs2,y1,z2

K,46,xs2,yt,z1               !right support, top layer
K,47,xs2,yt,0
K,48,xs2,yt,z2

kplot                        !plots keypoints on screen


! create lines
! (x-direction)

*do,i,1,12                   !creates lines 1 through 12
      L,i,i+12,2
*enddo
```

```
*do,i,13,24
      L,i,i+12,divx-4          !creates lines 13 through 24
*enddo

*do,i,25,36
      L,i,i+12,2               !creates lines 25 through 32
*enddo


! (y-direction)

*do,i,1,3                      !creates lines 33 through 36
      L,i,i+3,divy_r
*enddo

*do,i,4,6                      !creates lines 37 through 39
      L,i,i+3,divy_b
*enddo

*do,i,7,9                      !creates lines 40 through 43
      L,i,i+3,divy
*enddo


*do,i,13,15                    !creates lines 44 through 46
      L,i,i+3,divy_r
*enddo

*do,i,16,18                    !creates lines 47 through 50
      L,i,i+3,divy_b
*enddo

*do,i,19,21                    !creates lines 51 through 54
      L,i,i+3,divy
*enddo


*do,i,25,30                    !creates lines 55 through 57
      L,i,i+3,divy_r
*enddo

*do,i,28,30                    !creates lines 58 through 61
      L,i,i+3,divy_b
*enddo

*do,i,31,33                    !creates lines 62 through 65
      L,i,i+3,divy
*enddo


*do,i,37,39                    !creates lines 66 through 68
      L,i,i+3,divy_r
*enddo
```

```
*do,i,40,42                    !creates lines 69 through 72
      L,i,i+3,divy_b
*enddo

*do,i,43,45                    !creates lines 73 through 76
      L,i,i+3,divy
*enddo


! (z-direction)

*do,j,1,16
    *if,j,eq,1,then
     n=1
    *elseif,j,gt,1
     n=n+3
    *endif
  *do,i,n,n+1                  !creates lines 74 through 106
     L,i,i+1,divz/2
  *enddo
*enddo


! Set screen view to Isometric
/VIEW, 1 ,1,1,1
/ANG, 1
/REP
lplot


!create volumes

*do,j,1,3                      !creates volumes 1 through 6
    *if,j,eq,1,then
        n=1
    *elseif,j,gt,1
        n=n+3
    *endif
  *do,i,n,n+1
         V,i,i+12,i+13,i+1,i+3,i+15,i+16,i+4
  *enddo
*enddo

*do,j,1,3                      !creates volumes 7 through 12
    *if,j,eq,1,then
        n=13
    *elseif,j,gt,1
        n=n+3
    *endif
  *do,i,n,n+1
         V,i,i+12,i+13,i+1,i+3,i+15,i+16,i+4
  *enddo
*enddo
```

```
*do,j,1,3              !creates volumes 13 through 18
    *if,j,eq,1,then
        n=25
    *elseif,j,gt,1
        n=n+3
    *endif
  *do,i,n,n+1
         V,i,i+12,i+13,i+1,i+3,i+15,i+16,i+4
  *enddo
*enddo

vplot                  !displays volumens on screen

!----Mesh volumes (concrete)

!lower level
VATT,4,0,1,0,          !left section
vmesh,1                !lower volume, left
VATT,4,0,1,0,
vmesh,2                !lower volume, right

VATT,2,2,2,0,          !middle section
vmesh,7                !lower volume, left
VATT,2,2,2,0,
vmesh,8                !lower volume, right

VATT,2,2,2,0,          !right section
vmesh,13               !lower volume, left
VATT,2,2,2,0,
vmesh,14               !lower volume, right


!middle level
VATT,2,2,2,0,          !left section
vmesh,3                !middle volume, left
VATT,2,2,2,0,
vmesh,4                !middle volume, right

VATT,2,2,2,0,          !middle section
vmesh,9                !middle volume, left
VATT,2,2,2,0,
vmesh,10               !middle volume, right

VATT,2,2,2,0,          !right section
vmesh,15               !middle volume, left
VATT,2,2,2,0,
vmesh,16               !middle volume, right


!top level
VATT,2,2,2,0
vmesh,5                !upper volume, left
VATT,2,2,2,0,
vmesh,6                !upper volume, right
```

```
VATT,2,2,2,0,          !middle section
vmesh,11               !upper volume, left
VATT,2,2,2,0,
vmesh,12               !upper volume, left


VATT,2,2,2,0,          !right section
vmesh,17               !upper volume, left
VATT,2,2,2,0,
vmesh,18               !upper volume, right

eplot                  !displays all elements


!create nodes for rebar
!manual input of existing node numbers at reinf. level needed

!first nodes and last five nodes have to be created manually
n,10001,xs1,y2,0
n,10002,xs1+xs2/(divx),y2,0
n,10003,xs1+2*(xs2/(divx)),y2,0

n,10023,xs2-2*(xs2/(divx)),y2,0
n,10024,xs2-1*(xs2/(divx)),y2,0
n,10025,xs2,y2,0

*do,j,1,divx+1-6
      n,10003+j,xs1+(2+j)*(xs2/(divx)),y2,0
*enddo


!create elements for y-fixation
type,4       !sets element type (COMBIN14)
real,4
mat,7

e,15,10001
e,16,10002
e,13,10003

*do,i,1,divx+1-6
       e,112+i,10003+i
*enddo

e,111,10023
e,241,10024
e,239,10025
```

```
!create elements for bond slip in x direction
type,5      !sets element type (COMBIN39)
real,5
mat,7

e,15,10001
e,16,10002
e,13,10003

*do,i,1,divx+1-6
       e,112+i,10003+i
*enddo

e,111,10023
e,241,10024
e,239,10025

!create rebar elements
type,3      !sets element type (LINK8)
real,3
mat,1

*do,i,1,divx
       e,10000+i,10001+i
*enddo


!----CREATE CONSTRAINTS, APPLY LOADS

! Support @ x=0
! Set Min and Max Ranges for this support

NSEL,S,LOC,X,xs1
NSEL,R,LOC,Y,yb

nplot

D,ALL,UY
D,ALL,UZ

! Support @ x=length
! Set Min and Max Ranges for this support

NSEL,S,LOC,X,xs2

nplot
D,ALL,UX
D,ALL,UZ

NSEL,ALL
eplot
```

```
! Boundary conditions at the side of the slab

NSEL, S, LOC,Z,z1
NSEL, A, LOC,Z,z2
nplot

D,ALL,UZ

NSEL,ALL
eplot


! Show the BC's on the screen
!*
/PSF,DEFA, ,1
/PBF,DEFA, ,1
/PSYMB,CS,0
/PSYMB,NDIR,0
/PSYMB,ESYS,0
/PSYMB,LDIR,0
/PSYMB,LAYR,0
!*
/PBC,ALL,,1
/PBC,NFOR,,0
/PBC,NMOM,,0
/PBC,RFOR,,0
/PBC,RMOM,,0
/REPLOT
!*

! applies displacement to nodes at 1250mm from support off each side
nsel,s,node,,906
nsel,a,node,,948
nsel,a,node,,946
nsel,a,node,,1026
nsel,a,node,,1028

*do,i,1,10
     nsel,a,node,,1104+2*i
*enddo

d,all,uy,imp_uy

nsel,all

!----SETTINGS FOR SOLVER
NLGEOM,OFF       !suppresses geom. nonlinear behavior
SSTIF,0
NROPT,AUTO, ,    !full newton raphson method and adaptive descent
                 !Program chosen newton raphson method
PSTRES,0
LUMPM,0
EQSLV,FRONT
TOFFST,0,
```

```
!----SETTINGS FOR NONLINEAR ANALYSIS

!define time and substepsize
TIME, prs            !duration of loadstep (= value applied pressure)
NSUBST, subst, , ,   !# of substeps as specified in input section
CNVTOL,f,,tol,2, ,   !sets tolerance value, force convergence and
                     !square root of the squares check
KBC,0                !use ramped loads for substeps

! set number of equilibrium iterations
neqit,equilib        !number of equilibrium iterations as specified
                     !in input section
OUTPR,BASIC,5,
LSWRITE,0,
LSSOLVE,0,0,1,
SAVE                 !saves slab.db
FINISH

!--------------------------END PREPROCESSOR-----------------------!


!-----------------------------SOLUTION-----------------------------!

/SOLU
OUTRES,ALL,1,    !output for all results for every second substep
/STAT,SOLU
SOLVE
SAVE             !needed for subsequent restart of analysis
FINISH

!--------------------------END SOLUTION--------------------------!


!-------------------------POSTPROCESSING-------------------------!

!TIME HISTORY PROCESSOR - to list uy

/POST26
NUMVAR,50        !number of variables allowed

!select nodes
RFORCE,2,906,f,y
RFORCE,3,948,F,Y
RFORCE,4,946,F,Y
RFORCE,5,1028,F,Y
RFORCE,6,1026,F,Y

*do,i,1,10
     rforce,i+6,1104+2*i,f,y
*enddo
```

```
!procedure to calculate mean value of loads at left displ.
!sum of all loads
ADD,27,3,2

*do,i,1,13
      ADD,27,3+i,27  !#27 is the sum of all displ. at left displ
*enddo

QUOT,28,2,2           !initializes #28 to 1
!calculate #29 as #27*20/(#28*-1000)-> total load for 1000mm in kN
QUOT,29,27,28, ,total_l , , ,20,-1000

!list load - displacement values
!save the load displacement values to 'load-displ.out'
/OUTPUT,load-disp-av,out
PRVAR,29              !lists substep, load and mean values of displ.
/OUTPUT

FINISH
!-------------------------END POSTPROCESSING----------------------!
```

B.2 Analysis Restart File – Adjusts Analysis Parameters

```
/FILNAME,slab,db
RESUME
/SOLU
ANTYPE,STATIC,REST  !restarts the static analyis w/ filename slab.db

!notes:
!       adds loadsteps
!       rename slab.osav to slab.esav before if unconverged solution


!------------------------------INPUT-----------------------------!
!changes loading (add displacements to existing)
!initial displacement prs=2.5 [mm]
imp_uy1=-2.5
imp_uy= -32.5     ! imposed displacement in mm (NEGATIV)
                  ! REPLACES existing value

!number of substeps
!first run with 0.1mm per step
!factor 10 -> 0.01mm per step
!factor 5 -> 0.02mm per step
!factor 2 -> 0.05mm per step
fac= 5

!tolerance of convergence criteria
!start/default: 0.005
tol=0.005

!change number of max. equilibrium iterations
!first run started w/ 100 iterations
NEQIT, 300

!frequency for saving results
!started with every second step -> 1
!for output of results at every step -> 1
quant=1
!----------------------------END INPUT---------------------------!


!--------------------------PREPROCESSOR-------------------------!

!----define values for variables
prs= -imp_uy            !set displ. value = tot. time of load step
subst=(prs+imp_uy1)*10 !initializes the # of substeps to 0.02mm/step
TIME, prs               !duration of loadstep (= applied pressure)
NSUBST, subst*fac, ,    !sets number of substeps
CNVTOL,f,,tol,2, ,      !sets tolerance value
KBC,0                   !use ramped loads for substeps
```

```
!----- applies displacement to nodes at midspan
nsel,s,node,,906
nsel,a,node,,948
nsel,a,node,,946
nsel,a,node,,1026
nsel,a,node,,1028

*do,i,1,10
     nsel,a,node,,1104+2*i
*enddo

d,all,uy,imp_uy
nsel,all


!display model on screen
ESEL,ALL
EPLOT
/PBC,U, , 1          !displays constraints
/PBC,PRES, ,1        !displays pressures
/REPLOT

OUTRES,ALL,quant,  !output for all results for every 'quant' substep

SAVE
SOLVE                !starts solution
SAVE                 !needed for possible subsequent restart
FINISH

!-------------------------END PREPROCESSOR-----------------------!


!-------------------------POSTPROCESSING-------------------------!

!TIME HISTORY PROCESSOR - to list uy

/POST26
NUMVAR,50            !number of variables allowed

!select nodes
RFORCE,2,906,f,y
RFORCE,3,948,F,Y
RFORCE,4,946,F,Y
RFORCE,5,1028,F,Y
RFORCE,6,1026,F,Y
*do,i,1,10
     rforce,i+6,1104+2*i,f,y
*enddo
```

```
!procedure to calculate mean value of loads at left displ
!sum of all loads
ADD,27,3,2

*do,i,1,13
      ADD,27,3+i,27    ! #27 is the sum of all displacements at left
displ
*enddo

QUOT,28,2,2            !initializes #28 to 1
!calculate #29 as #27*20/(#28*-1000)-> total load for 1000mm in kN
QUOT,29,27,28, ,total_l , , ,20,-1000


!list load - displacement values
!save the load displacement values to 'load-displ.out'
/OUTPUT,load-disp-av,out
PRVAR,29               !lists substep, load and mean values of displ.
/OUTPUT

FINISH

!-------------------------END POSTPROCESSING-----------------------!
```

B.3 Post-Processing Input File - Plots

```
!note: load appropriate time/load step via the GUI
!      select all entities
!      rename output file for different cases

!-------------------------------INPUT-------------------------------!

!load step (time)
l_time=3

!-----------------------------END INPUT-----------------------------!

/POST1
SET, , ,1, ,l_time, , !loads the results for the time increment
                      !specified in input section
!/SHOW,TERM !directs plots to screen (in case it was to file before)

!sets frontal view
/VIEW, 1 ,,,1
/ANG, 1
/REP

!select all entities for display
VSEL,ALL
ASEL,ALL
LSEL,ALL
KSEL,ALL
ESEL,ALL
NSEL,ALL

!define etable for steel results
etable,saxl,ls,1        !longitudinal stress
etable,epel,lepel,1     !longitudinal elastic strain
etable,eppl,leppl,1     !longitudinal plastic strain

!plot results to graphic files
!concrete results
/show,results,grph      !defines the name for the output file
/gfile,600              !resolution in pixel
plnsol,s,x              !plots x-stress in concrete
plnsol,s,y              !plots y-stress (shear stress) in concrete
plnsol,epel,x           !plots x elastic strain in concrete
plnsol,epel,y           !plots y elastic strain in concrete
plnsol,eppl,x           !plots x plastic strain in concrete
plnsol,epto,x           !plots x total strain in concrete

!steel results
ESEL,S,MAT,,1           !selects steel elements for printout
pletable,saxl,noav      !plots x-stress in steel
pletable,epel,noav      !plots x elastic strain in steel
pletable,eppl,noav      !plots x plastic strain in steel

FINISH
```

B.4 Post-Processing Input File – Shear Data

```
!note:
!       the node numbers need to be changed if a different failure
!       cross section is evaluated
!       node numbers can be obtained from model plots

!--------------------------------INPUT-------------------------------!
!load step (time)
l_time=15.28
!-----------------------------END INPUT-----------------------------!


/POST1

SET, , ,1, ,l_time, , !loads the results for the time increment
                      !specified in input section
!/SHOW,TERM !directs plots to screen (in case it was to file before)

!select all entities for display
VSEL,ALL
ASEL,ALL
LSEL,ALL
KSEL,ALL
ESEL,ALL
NSEL,ALL

!select all nodes at the evaluated cross section
nsel,s,node,,876
nsel,a,node,,884
nsel,a,node,,882
nsel,a,node,,896
nsel,a,node,,894

nsel,a,node,,877
nsel,a,node,,885
nsel,a,node,,883
nsel,a,node,,897
nsel,a,node,,895

nsel,a,node,,251
nsel,a,node,,271
nsel,a,node,,266
nsel,a,node,,301
nsel,a,node,,296

nsel,a,node,,255
nsel,a,node,,275
nsel,a,node,,270
nsel,a,node,,305
nsel,a,node,,300
```

```
nsel,a,node,,254
nsel,a,node,,274
nsel,a,node,,269
nsel,a,node,,304
nsel,a,node,,299

nsel,a,node,,253
nsel,a,node,,273
nsel,a,node,,268
nsel,a,node,,303
nsel,a,node,,298

nsel,a,node,,272
nsel,a,node,,252
nsel,a,node,,272
nsel,a,node,,267
nsel,a,node,,302
nsel,a,node,,297

nsel,a,node,,10
nsel,a,node,,14
nsel,a,node,,13
nsel,a,node,,26
nsel,a,node,,25

nsel,a,node,,2
nsel,a,node,,5
nsel,a,node,,4
nsel,a,node,,20
nsel,a,node,,19


!save shear data to file 'shear1528.out'
/OUTPUT,shear1528,out
prnsol,s,comp
/OUTPUT

nsel,all

FINISH
```

REFERENCES

ACI Committee 318, 1995, *Building Code Requirements for Reinforced Concrete (ACI 318-M95) and Commentary (ACI 318RM-95) – Metric Version*, Farmington Hills, MI

ACI Committee 446, 1998 "Finite Element Analysis of Fracture in Concrete Structures: State-of-the-Art", *ACI 446.3R-97*, American Concrete Institute, Farmington Hills, MI

ANSYS Inc., 1996, *ANSYS 5.3 Analysis Guides Set*, 1st Edition, Houston, PA

ASTM, 1997, *Annual Book of ASTM Standards*, Vol. 4.02, Philadelphia, PA, November

ASTM, 1998, *Annual Book of ASTM Standards*, Vol. 1.04, West Conshohocken, PA, February

Barsoum, R. S., 1976 "On the Use of Isoparametric Finite Elements in Linear Fracture Mechanics", *Int. J. Num. Meth. In Engrg.*, Vol. 10, pp. 25-37

Bazant, Z. P., 1976 "Instability, Ductility and Size Effect in Strain-Softening Concrete", *J. Engrg. Mech. Div.*, ASCE, Vol. 102, No. EM2, April, pp. 331-344

Bazant, Z. P.; Cedolin, L, 1979 "Blunt Crack Band Propagation in Finite Element Analysis", *J. Engrg. Mech.*, ASCE, Vol. 105, No. 2, February, pp. 297-315

Bazant, Z. P.; Cedolin, L, 1980 "Fracture Mechanics of Reinforced Concrete", *J. Engrg. Mech. Div.*, ASCE, Vol. 106, No. 6, December, pp. 1287-1306

Bazant, Z. P.; Oh, B. H., 1983 "Crack Band Theory for Fracture of Concrete", *Mater. Struct.*, RILEM, Paris, France, Vol. 16, February, pp. 155-177

Bazant, Z. P.; Tabbara, M. R.; Kazemi, M. T.; Pijaudier-Cabot, G., 1990 "Random Particle Model for Fracture of Aggregate or Fiber Composites", *J. Engrg. Mech. Div.*, ASCE, Vol. 116, No. 8, August, pp. 1686-1705

CEB-Comité Euro-International du Béton, 1993a "CEB-FIP Model Code 1990", *Bulletin d'Information No. 213-214*, Lausanne, Switzerland, May

CEB-Comité Euro-International du Béton, 1993b "Ductility Reinforcement", *Bulletin d'Information No. 218*, Lausanne, Switzerland

Chen, W. F; Han, D. J., 1988, *Plasticity for Structural Engineers*, Springer-Verlag, New York

Chen, W.F., 1982, *Plasticity in Reinforced Concrete*, McGraw-Hill, New York

Chitipothu, Radhika, 1997, *Evaluation of Factors Affecting the Shear Strength of Reinforced Concrete Beams using Nonlinear Finite Element Analysis and Fracture Mechanics Principles*, Masters Thesis, Dept. of Civil and Env. Engrg., University of Kansas, Lawrence, KS

Clough, R. W., 1962 "The Stress Distribution of Norfolk Dam", *Series 100*, Issue 19, Institute of Engineering Research, University of California, Berkeley, CA, August

Darwin, D., 1985 "Concrete Crack Propagation-Study of Model Parameters", *Finite Element Analysis of Reinforced Concrete Structures*, edited by C. Meyer and H. Okamura, ASCE, New York, pp. 184-203

Darwin, D., 1993 "Reinforced Concrete", Chapter 4, *Finite Element Analysis of Reinforced Concrete Structures II*, edited by Isenberg, J., American Society of Civil Engineers, pp.203-232

DIN 488 T1, 1984, *Betonstahl: Sorten, Eigenschaften, Werkkennzeichen*, Beuth Verlag, Berlin, September

Dodds, R.H.; Darwin, D.; Leibengood, L. D., 1984 "Stress Controlled Smeared Cracking in R/C Beams" *J. Struct. Engrg. Div.*, ASCE, Vol. 110, No. 9, Sep., pp. 1959-1976

ENV 1992-1-1, 1991, *Eurocode 2: Design of Concrete Structures*, Beuth Verlag, Berlin, December

ENV 1998-1-1, 1988, *Eurocode 8: Earthquake Resistant Design of Structures*, Beuth Verlag, Berlin, March

Gerstle, W. H., 1982, *The Fracture Mechanics of bond in Reinforced Concrete*, Ph.D. Thesis, Dept. of Struct. Engrg., Cornell University, Ithaca, NY

Gerstle, W. H., 1986, *Finite and Boundary Element Modeling of Crack Propagation in Two- and Three-Dimensions Using Interactive Computer Graphics*, Dept. of Struct. Engrg., Cornell University, Ithaca, NY

Hellen, T. K., 1975 "On the Method of Virtual Crack Extensions", *Int. J. Num. Meth. In Engrg.*, Vol. 9, pp. 187-207

Hillerborg, A.; Modéer, M; Petersson, P.-E., 1976 "Analysis of Crack Formation and Crack Growth in Concrete by Means of Fracture Mechanics and Finite Elements" *Cement and Concrete Research*, Vol. 6, No. 6, November, pp.773-782

Ingraffea, A. R., 1977, *Discrete Fracture Propagation in Rock: Laboratory Tests and Finite Element Analysis*, Ph.D. Dissertation, University of Colorado, Boulder, CO

Ingraffea, A. R; Manu, C., 1980 "Stress-Intensity Factor Computation in Three Dimensions with Quarter-Point Elements", *Int. J. Num. Meth. In Engrg.*, Vol. 15, pp. 1427-1445

Ma, T., Niwa, J., McCabe, S.L., 1991, *Nonlinear Finite Element Evaluation of Shear Behavior of Reinforced Concrete Beams Using Fracture Mechanics Principals*, Master of Science Project, Dept. of Civil and Env. Engrg, University of Kansas, Lawrence, KS

Ma, T., Niwa, J., McCabe, S.L., 1992 "Evaluation of the Shear Behavior of Reinforced Concrete Beams – A Comparism of Code and Fracture Mechanics Predictions", *Fracture Mechanics of Concrete Structures*, Proceedings of the First International Conference on Fracture Mechanics of Concrete Structures, Breckenridge, CO, June

Ngo, D.; Scordelis, A. C., 1967 "Finite Element Analysis of Reinforced Concrete Beam", *ACI Journal*, Proceedings, Vol. 64, No. 3, March, pp. 152 – 163

Nilson, A. H., 1967, *Finite Element Analysis of Reinforced Concrete*, Ph.D. Thesis, Dept. of Civil Engineering, University of California, Berkeley, CA

Nilson, A. H., 1968 "Nonlinear Analysis of Reinforced Concrete by Finite Element Method", *ACI Journal*, Proceedings, Vol. 65, No. 9, September, pp. 757–766

Parks, D. M., 1974 "A Stiffness Derivative Finite Element Technique for Determination of Crack Tip Stress Intensity Factors", *Int. J. of Fract.*, Vol. 10, No. 4, pp. 487-502

Rashid, Y. R., 1968 "Ultimate Strength Analysis of Prestressed Concrete Pressure Vessels", *Nuclear Engineering and Design*, Vol. 7, pp. 334-344

Rots, J. G.; Kusters, G. M. A.; Blaawendraad, J., 1984 "The Need for Fracture Mechanics Options in Finite Element Models for Concrete Structures", *Computer-Aided Analysis and Design of Concrete Structures*, part I, pp. 19-32

Saouma, V. E., 1981, *Interactive Finite Element Analysis of Reinforced Concrete: A Fracture Mechanics Approach*, Ph.D. Thesis, Dept. of Struct. Engrg., Cornell University, Ithaca, NY

Swenson, D. V.; Ingraffea, A. R., 1988 "Modeling Mixed-Mode Dynamic Crack Propagation Using Finite Elements: Theory and Applications", *Comput. Mech.*, Vol. 3, pp. 381-397

Tong, P.; Pian, T. H. H.; Lasry S. J., 1973 "A Hybrid Element Approach to Crack Problems in Plane Elasticity", *Int. J. Num. Meth. In Engrg.*, Vol. 7, pp. 293-308

Tracey, D. M., 1971 "Finite Elements for the Determination of Crack Tip Elastic Stress Intensity Factors", *Engrg. Fract. Mech.*, Vol. 3, pp. 245-265

Walraven, 1978 "The influence of depth on the shear strength of lightweight concrete beams without shear reinforcement" *Report 5-78-4*, Stevin Laboratory, Delft University of Technology

Wawrzynek, P. A.; Ingraffea, A. R., 1986 "Local Remeshing around a Propagating Crack Tip Using Interactive Computer Graphics", *Finite Element Method, Modeling and New Applications*, E. M. Patten et al., eds., ASME CED-1, PVP-101, pp. 33-38

Westergaard, H. M., 1934 "Stresses at a Crack, Size of the Crack, and the Bending of Reinforced Concrete", *ACI Journal*, Proceedings Vol. 30, pp.93-102

Willam, K.J.; Warnke, E.D., 1975 "Constitutive Model for the Triaxial Behavior of Concrete", *Proceedings, International Association for Bridge and Structural Engineering*, Vol. 19, ISMES, Bergamo, Italy, p. 174

Wilson, W. K., 1969, *On Combined Mode Fracture Mechanics*, Ph.D. Dissertation, University of Pittsburgh, Pittsburgh, PA

TABLES

Table 4.1 European Reinforcing Steel Characteristics

Type	Code	f_{ym} [MPa]	f_{tm} [MPa]	e_{sh} [%]	e_{su} [%]	Remarks
1	B	550	578	-	2.5	
2	A1	550	594	-	5	
3	S2	550	632	2	6	yield plateau
4	C2	550	632	2	8	yield plateau

where,

f_{ym}= Yield Strength (Mean Value)
f_{tm}= Tensile Strength (Mean Value)
ε_{sh}= Strain at Onset of Strain Hardening
ε_{su}= Ultimate Strain

Table 4.2 American Reinforcing Steel Characteristics

Type	Code	f_{ym} [MPa]	f_{tm} [MPa]	ε_{sh} [%]	ε_{su} [%]	Remarks
5	A615/grade60	420	620	-	4.9	min. requirements
6	A615/grade60	483	690	-	6.2	upper bound values
7	A706/grade60	420	550	-	7.4	min. requirements
8	A706/grade60	540	707	-	9.3	upper bound values

where,

f_{ym}= Yield Strength (Mean Value)
f_{tm}= Tensile Strength (Mean Value)
ε_{sh}= Strain at Onset of Strain Hardening
ε_{su}= Ultimate Strain

Table 4.3 Concrete Characteristics

Type	Code	f_{cm} [MPa]	f_{cck} [MPa]	f_{ck} [MPa]	f_{ctm} [MPa]	$f_{ctk0.05}$ [MPa]	$f_{ctk0.95}$ [MPa]
1	C30/40	43	43.5	35	3.2	2.2	4.2
2	C70/80	83	85	75	5.3	3.6	7.1

where,

f_{cm}= Compressive Strength (Cylinder, Mean Value)
f_{cck}= Compressive Strength (Cube, 5% Fractile Characteristic Value)
f_{ck}= Compressive Strength (Cylinder, 5% Fractile Characteristic Value)
f_{tm}= Tensile Strength (mean value)
$f_{ctk0.05}$= Tensile Strength (5% Fractile Characteristic Value)
$f_{ctk0.95}$= Tensile Strength (95% Fractile Characteristic Value)

Table 4.4 Analysis Cases

Ref. Number	Steel Code	Concrete Code	Eff.Reinf. Ratio	Ref. Number	Steel Code	Concrete Code	Eff.Reinf. Ratio
Series 1 Low Effective Reinforcing Ratio				**Series 2 Moderate Effective Reinforcing Ratio**			
1-1	B	C30/40	0.03	2-1	B	C30/40	0.10
1-2	A1	C30/40	0.03	2-2	A1	C30/40	0.10
1-3	S2	C30/40	0.03	2-3	S2	C30/40	0.10
1-4	C2	C30/40	0.03	2-4	C2	C30/40	0.10
1-5	A615 min	C30/40	0.03	2-5	A615 min	C30/40	0.10
1-6	A615 max	C30/40	0.03	2-6	A615 max	C30/40	0.10
1-7	A706 min	C30/40	0.03	2-7	A706 min	C30/40	0.10
1-8	A706 max	C30/40	0.03	2-8	A706 max	C30/40	0.10
Series 3 High Effective Reinforcing Ratio				**Series 4 High Effective Reinforcing Ratio, High Strength Concrete**			
3-1	B	C30/40	0.25	4-1	B	C70/80	0.25
3-2	A1	C30/40	0.25	4-2	A1	C70/80	0.25
3-3	S2	C30/40	0.25	4-3	S2	C70/80	0.25
3-4	C2	C30/40	0.25	4-4	C2	C70/80	0.25
3-5	A615 min	C30/40	0.25	4-5	A615 min	C70/80	0.25
3-6	A615 max	C30/40	0.25	4-6	A615 max	C70/80	0.25
3-7	A706 min	C30/40	0.25	4-7	A706 min	C70/80	0.25
3-8	A706 max	C30/40	0.25	4-8	A706 max	C70/80	0.25

Table 4.5 Capacity Compression Strut – Analysis Series 3

Ref. Number	FEM Result [kN]	V_{Rd1} [kN]	V_{Rd2} [kN]
3-1	50	51	110
3-2	59	51	110
3-3	55	51	110
3-4	62	51	110
3-5	79	51	110
3-6	55	51	110
3-7	49	51	110
3-8	50	51	110

Table 4.6 Capacity Compression Strut – Analysis Series 4

Ref. Number	FEM Result [kN]	V_{Rd1} [kN]	V_{Rd2} [kN]
4-1	77	60	146
4-2	67	60	146
4-3	63	60	146
4-4	61	60	146
4-5	57	60	146
4-6	59	60	146
4-7	55	60	146
4-8	61	60	146

FIGURES

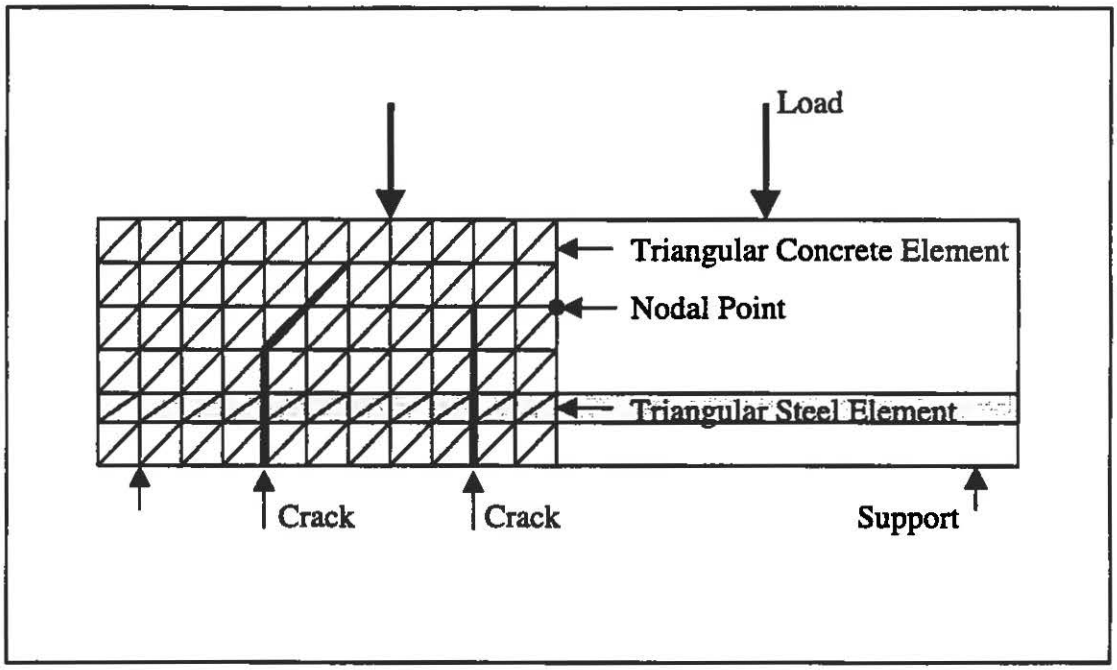

Figure 1.1 The First Finite Element Model of a Concrete Beam (Ngo and Scordelis, 1967)

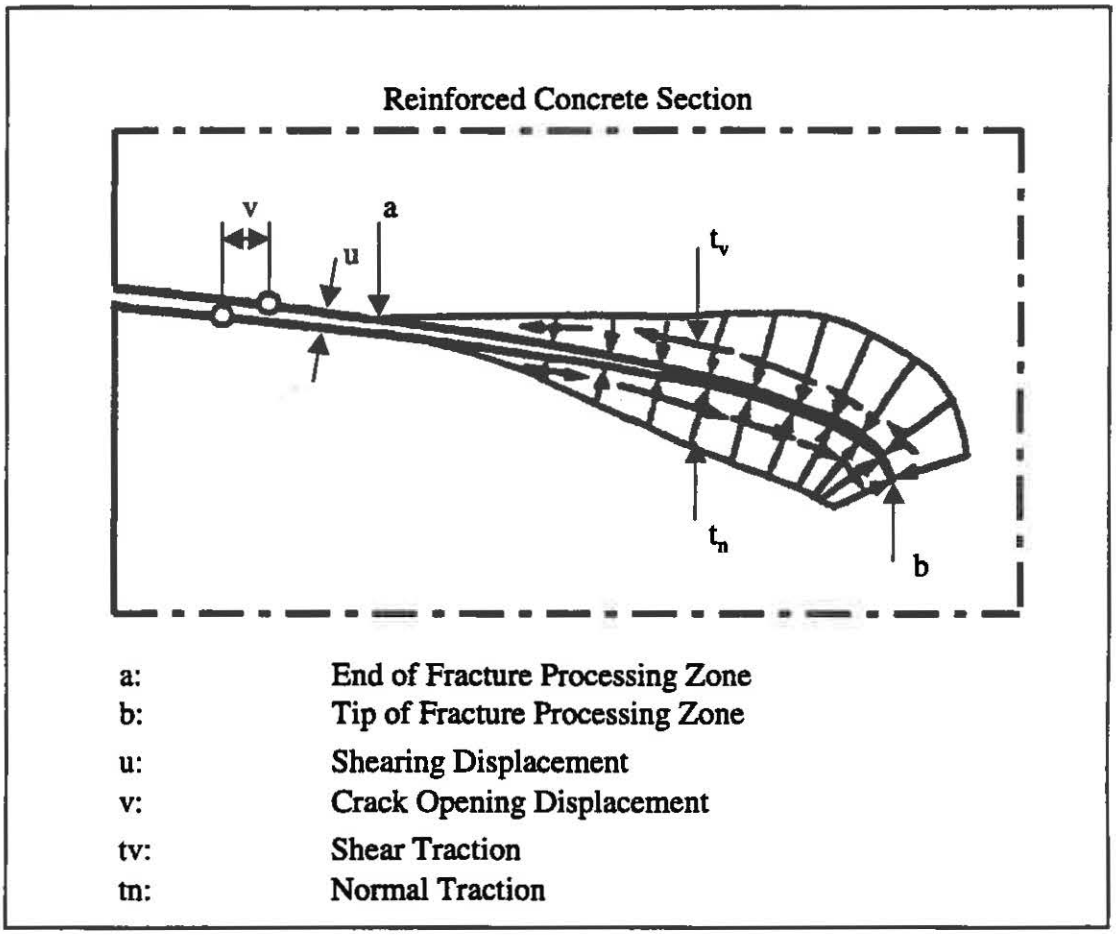

Figure 1.2 Fictitious Crack Model - Terminology (Hillerborg et al., 1976)

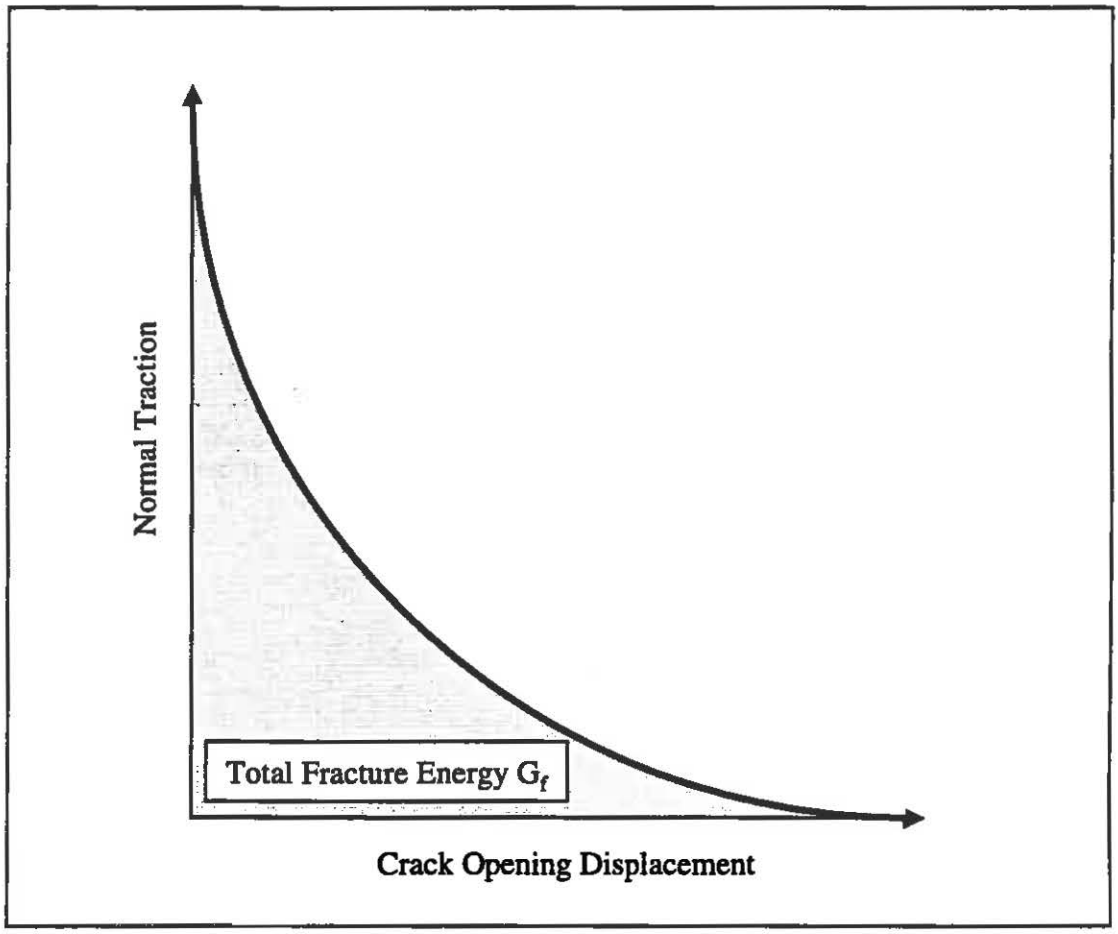

Figure 1.3 Fictitious Crack Model - Concept
(Hillerborg et al., 1976)

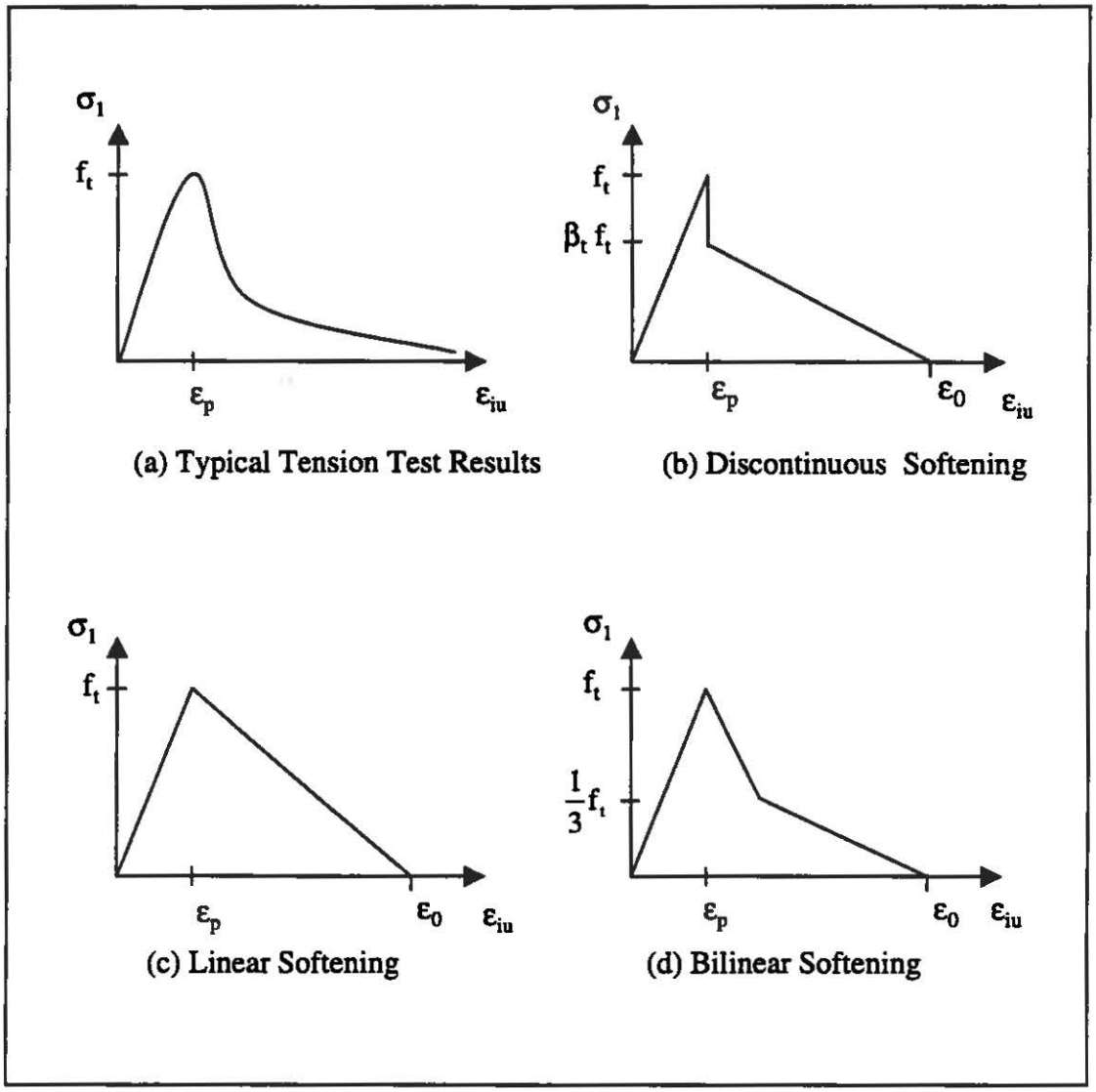

Figure 1.4 Tensile Behavior of Concrete - Typical Test Results (a) and Common Approximations for Finite Element Analyses (b), (c), (d)

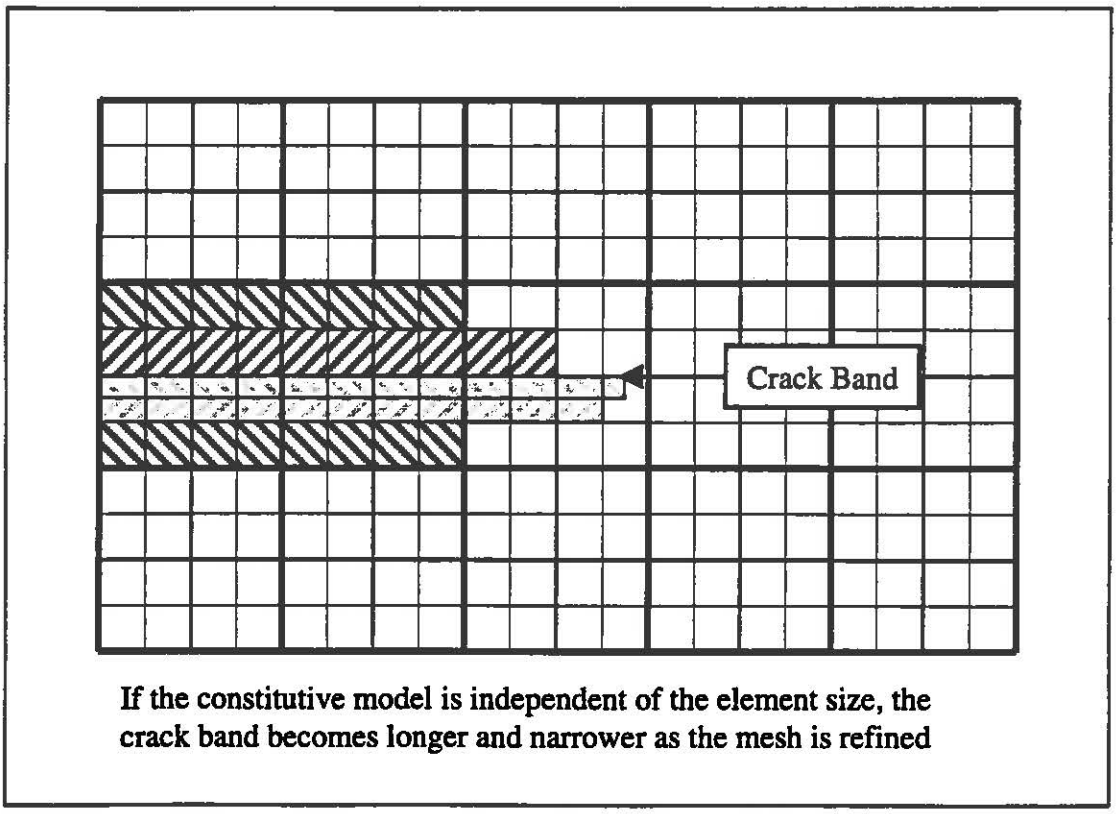

Figure 1.5 Crack Band Phenomenon
(ACI Committee 446, 1998)

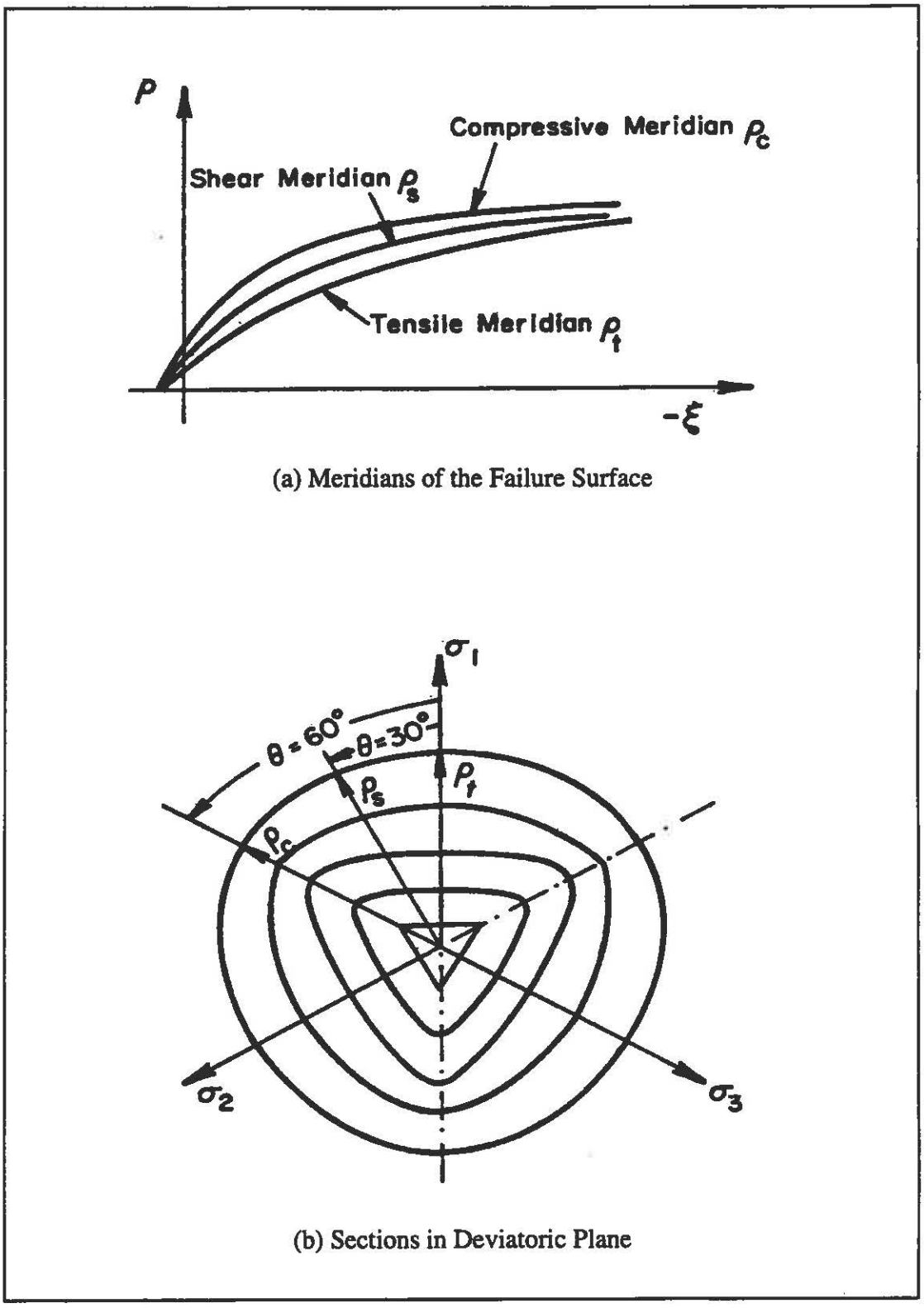

Figure 2.1 Basic Features of the Failure Surface of Concrete in Compression (Chen and Han, 1988)

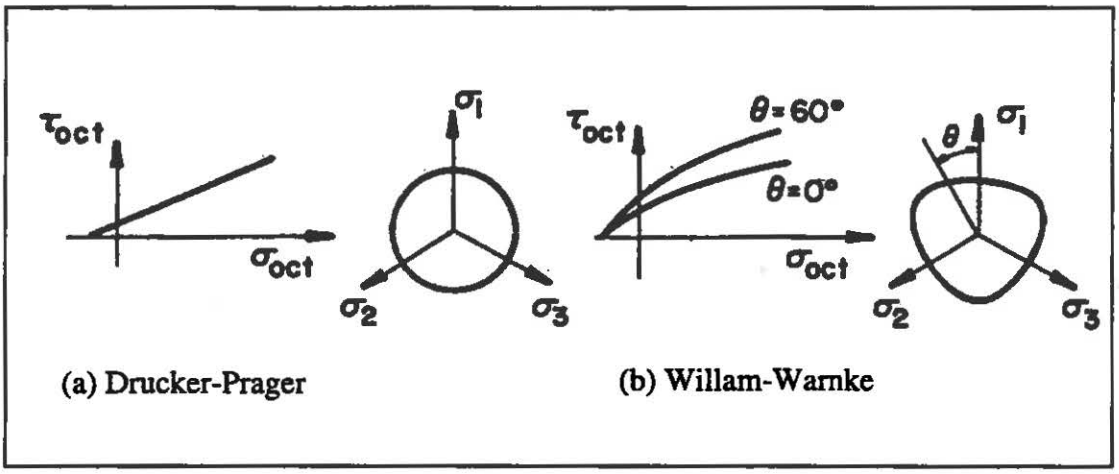

Figure 2.2 Common Concrete Failure Models (Chen and Han, 1988)

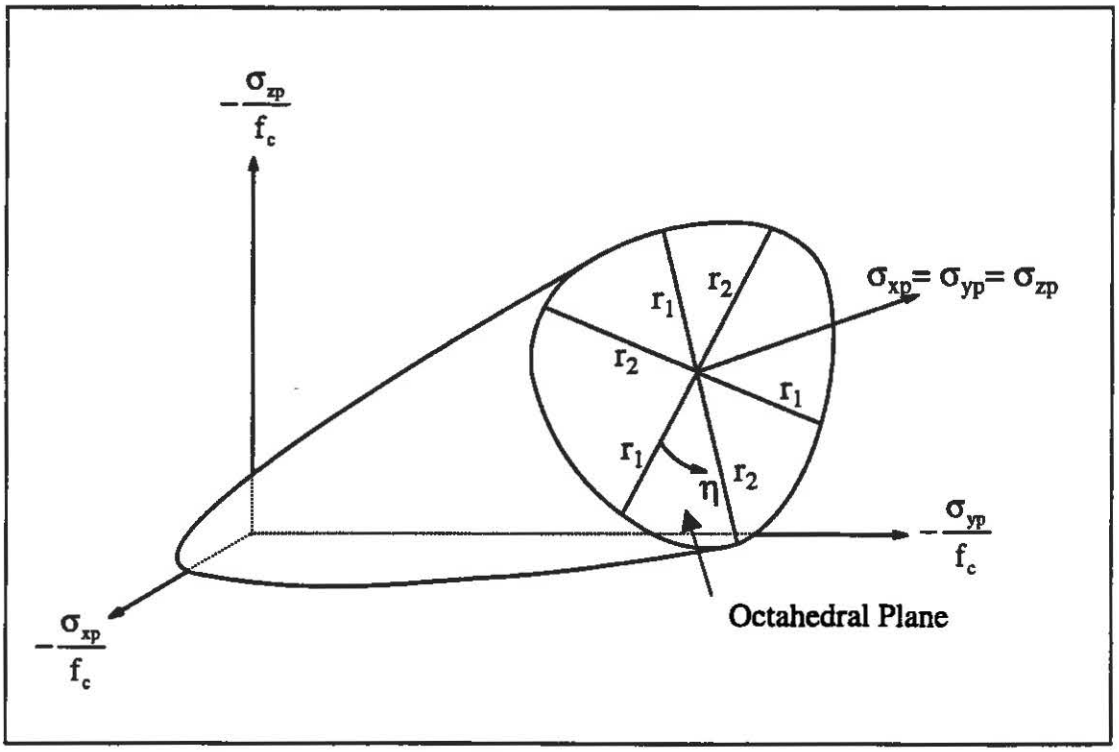

Figure 2.3 3-D Failure Surface in Principal Stress Space (ANSYS Inc.,1996)

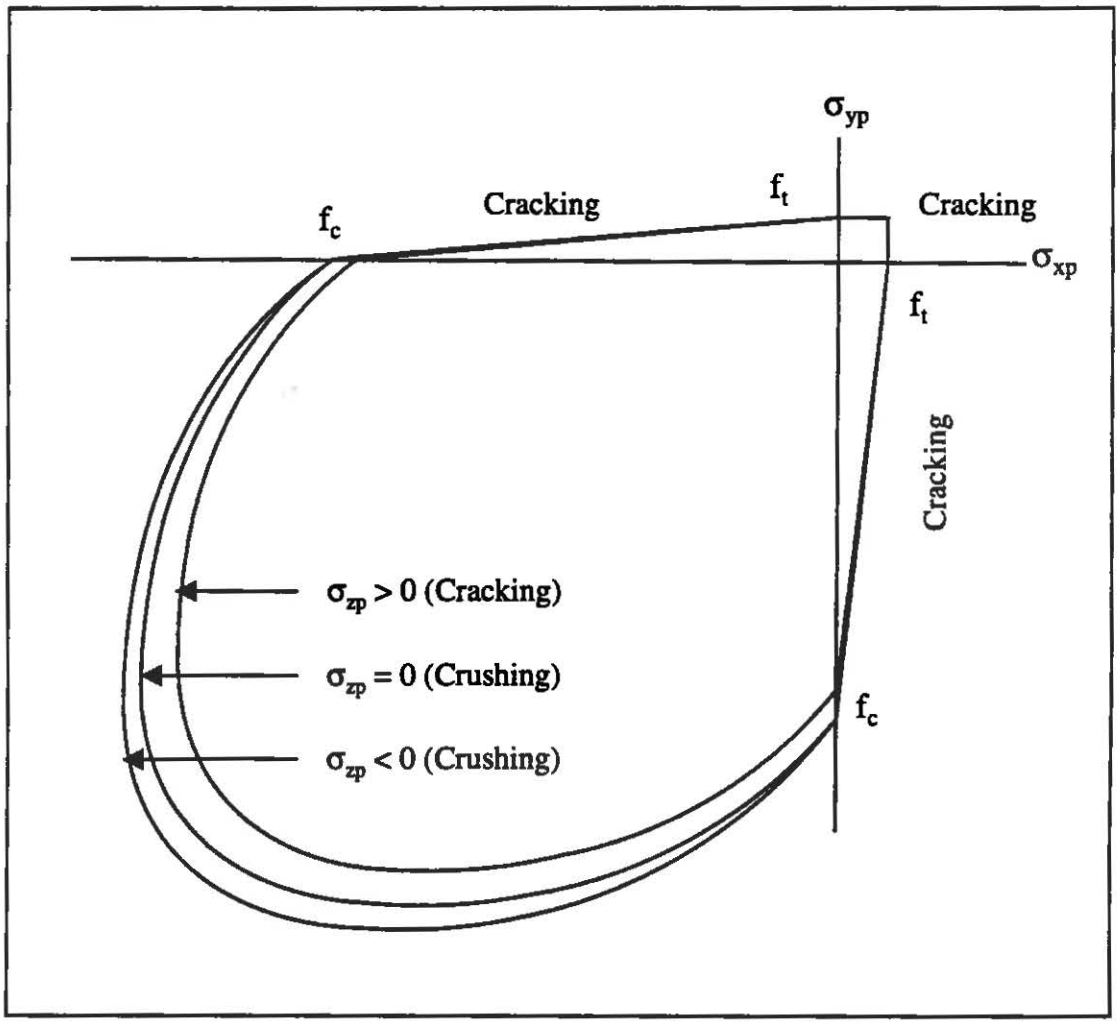

Figure 2.4 Failure Surface in Principal Stress Space σ_{zp} close to Zero (ANSYS Inc.,1996)

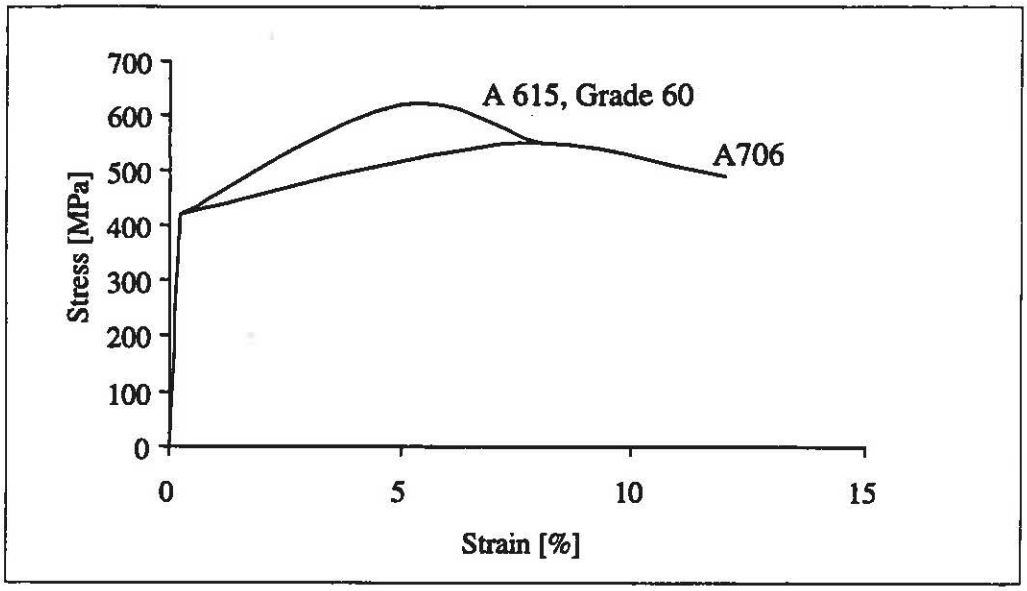

(a) American Reinforcing Steel

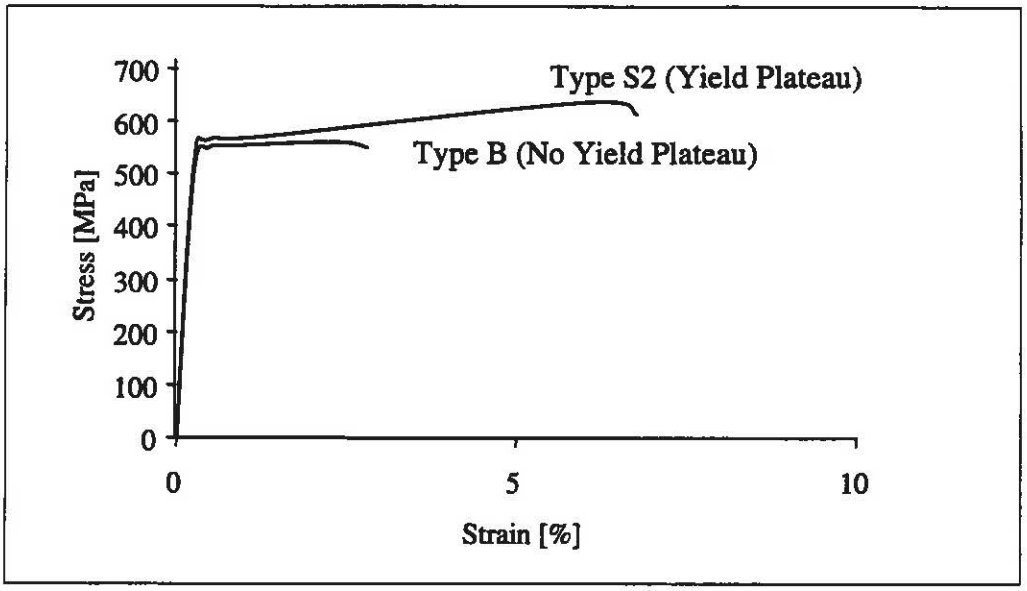

(b) European Reinforcing Steel

Figure 2.5 Typical Stress-Strain Curves for Reinforcing Steel

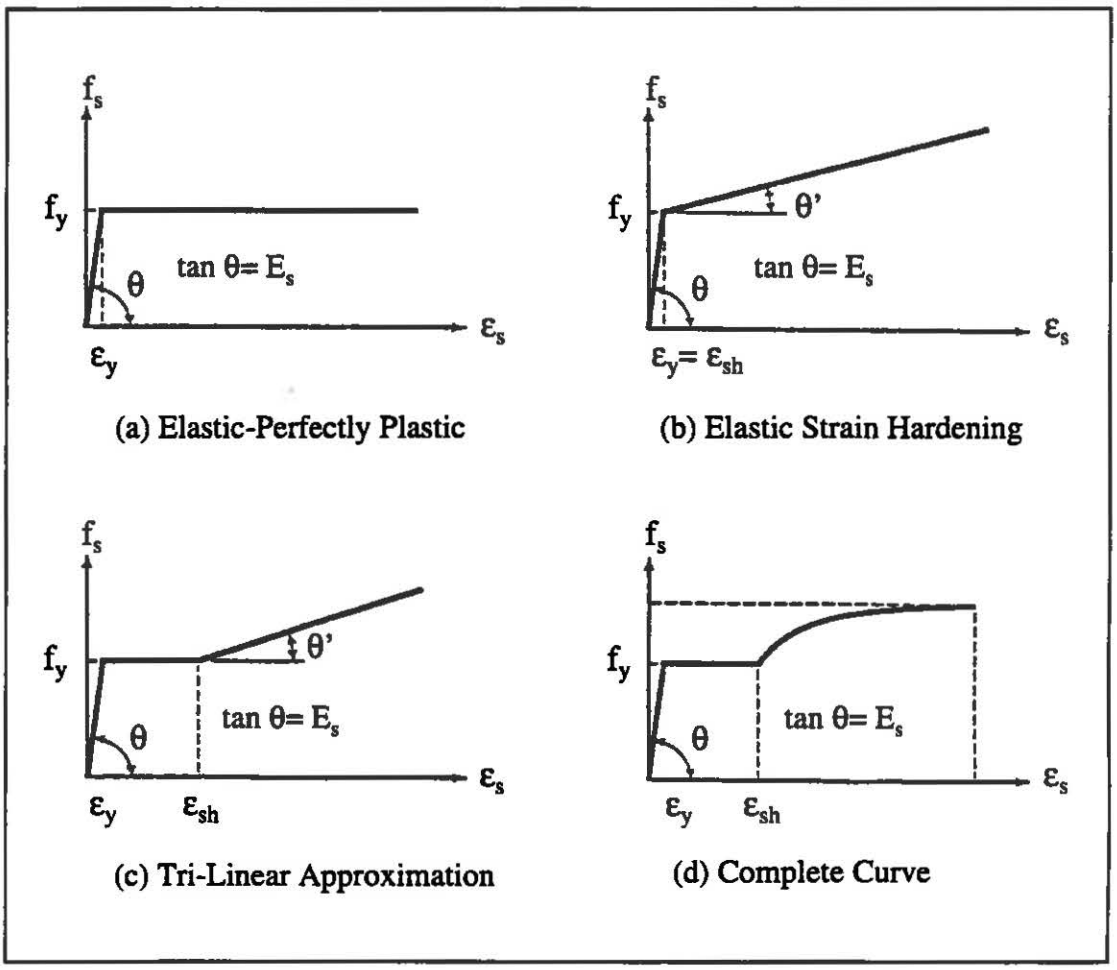

Figure 2.6 Common Idealizations of Stress-Strain Behavior for Finite Element Analyses (Darwin, 1993)

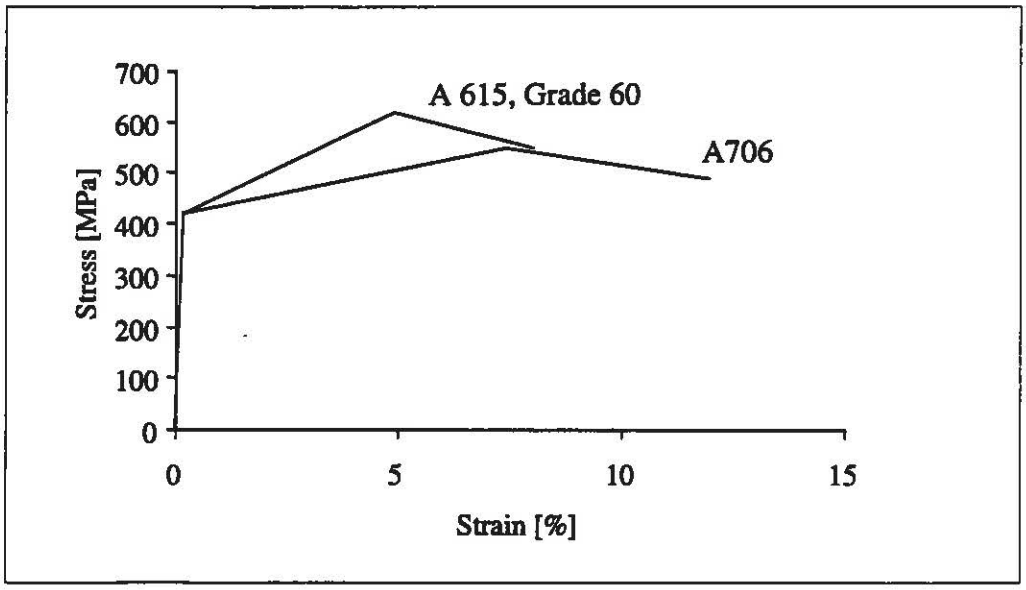

(a) American Reinforcing Steel

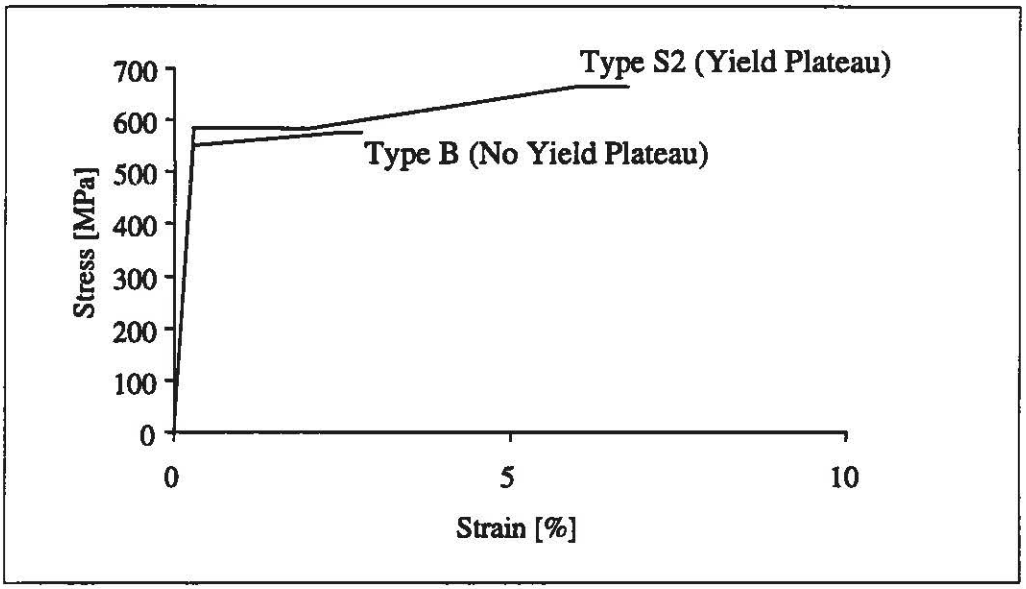

(b) European Reinforcing Steel

Figure 2.7 Idealized Stress-Strain Curves for Finite Element Analyses

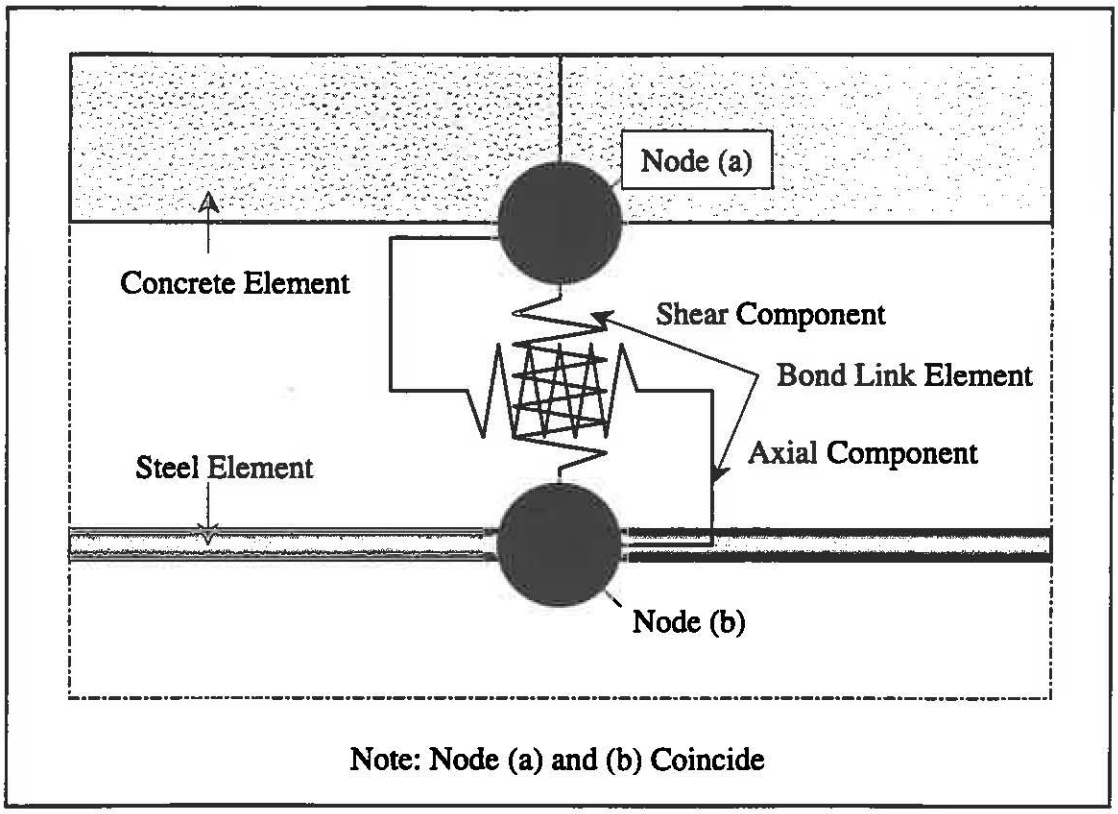

Figure 2.8 Schematic Illustration of the Bond-Link Finite Elements at the Steel-Concrete Interface

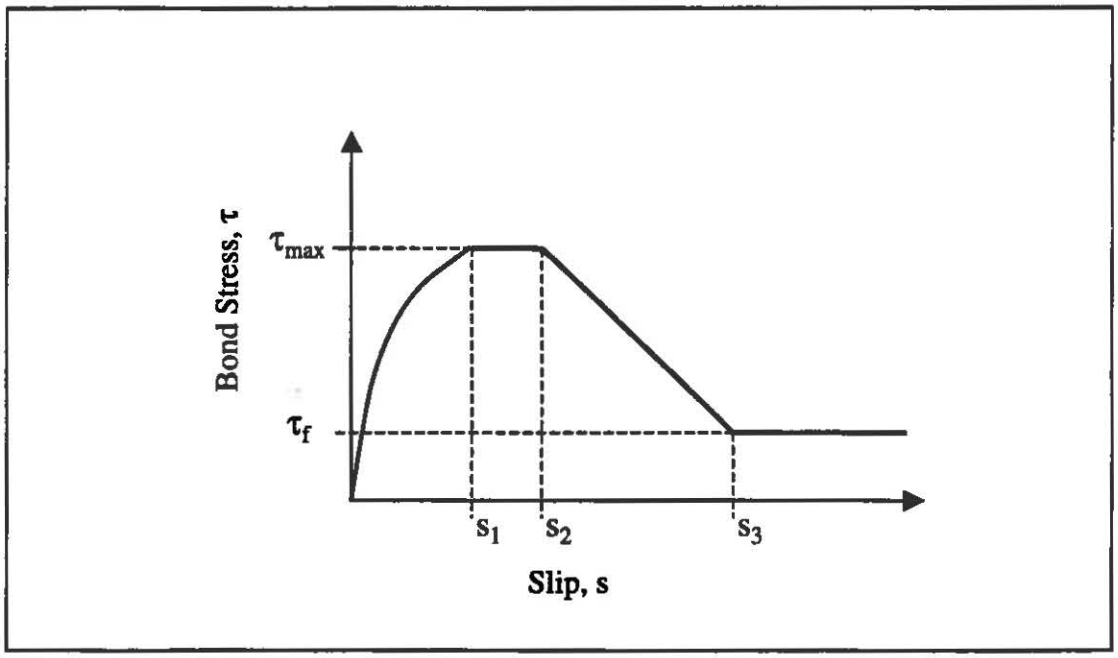

Figure 2.9 Analytical Bond Stress-Slip Relationship (Comité Euro-International du Béton, 1993a)

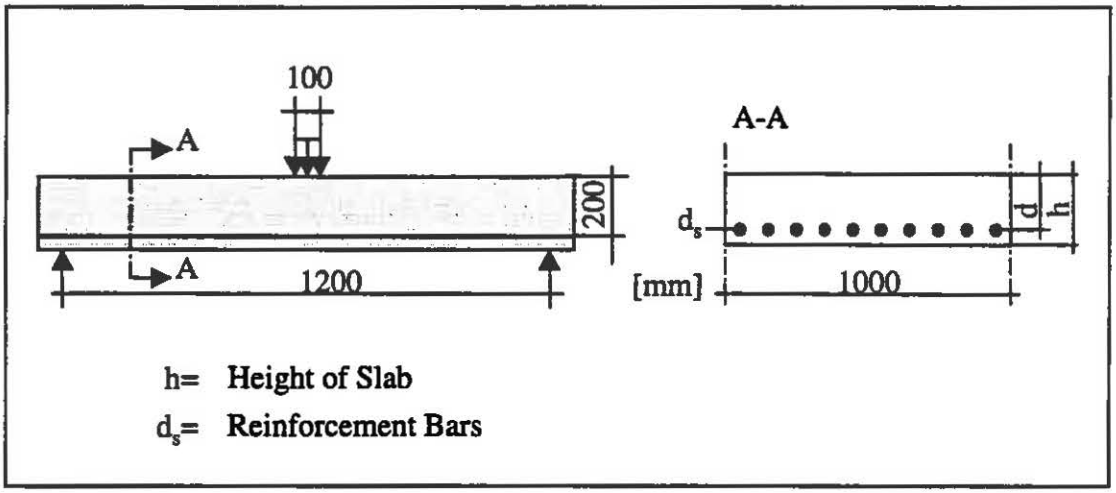

Figure 3.1 Slab Cross Section

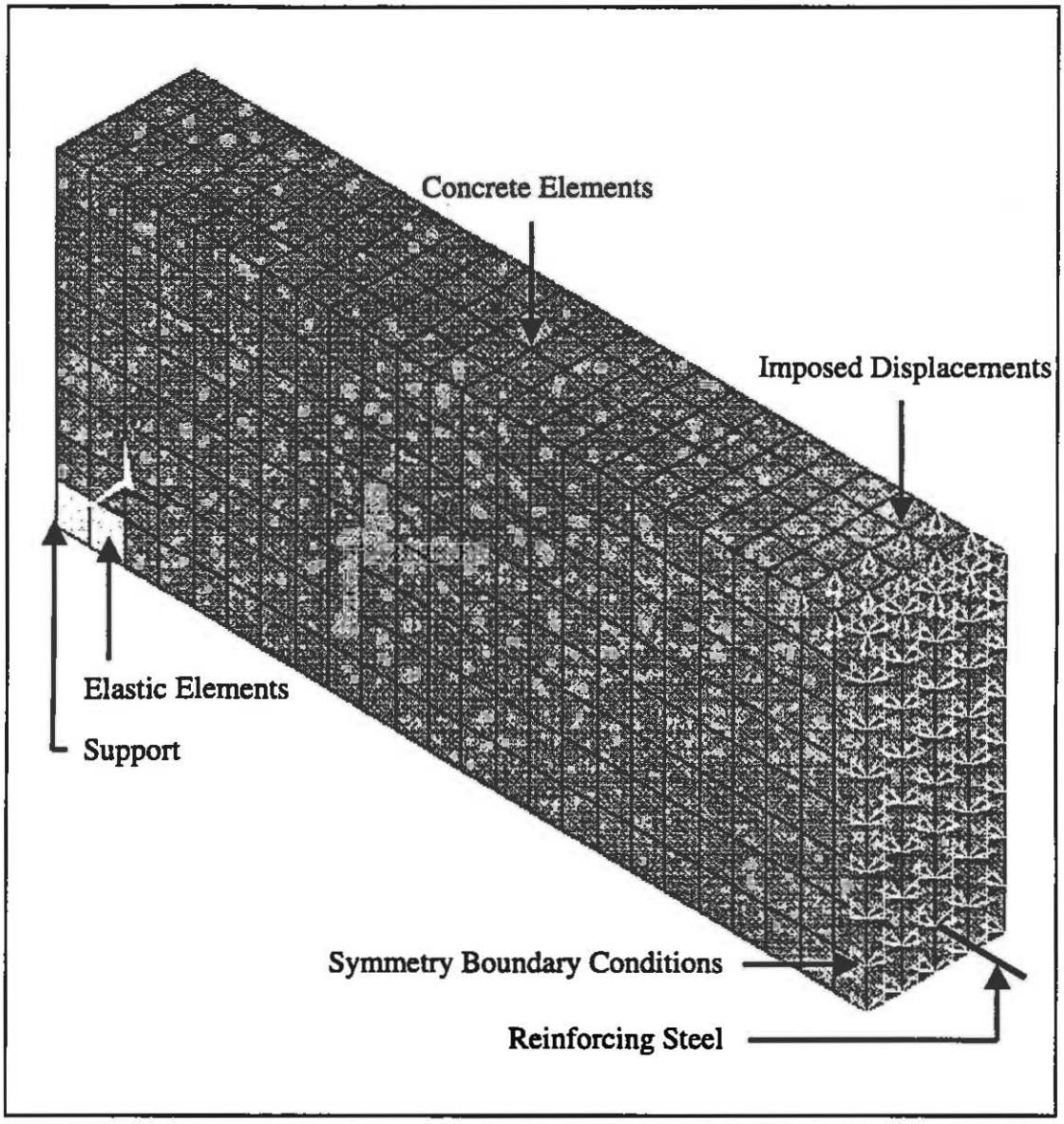

Figure 3.2 Finite Element Mesh Used in the Study

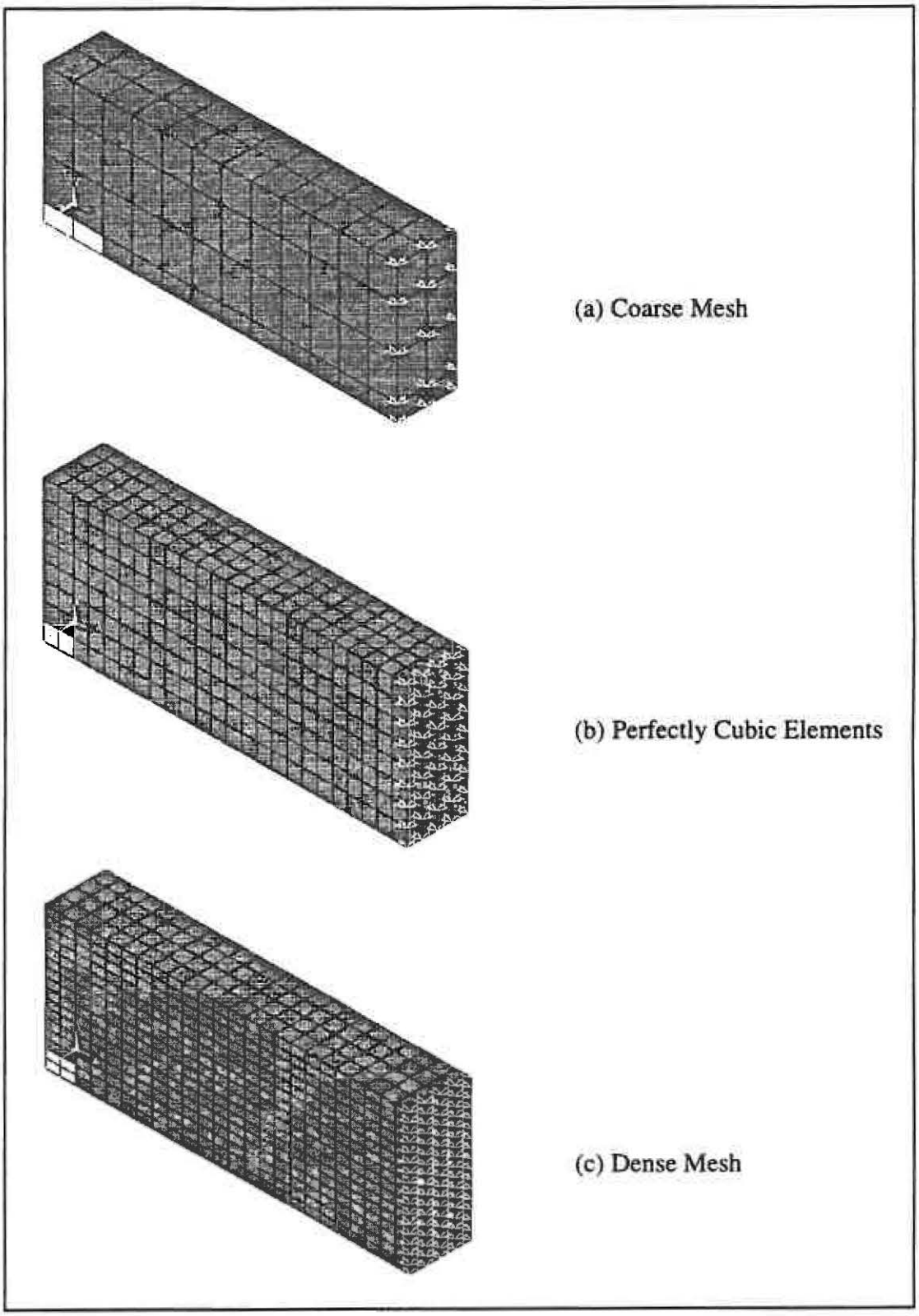

Figure 3.3 **Mesh Configurations Considered in Preliminary Studies**

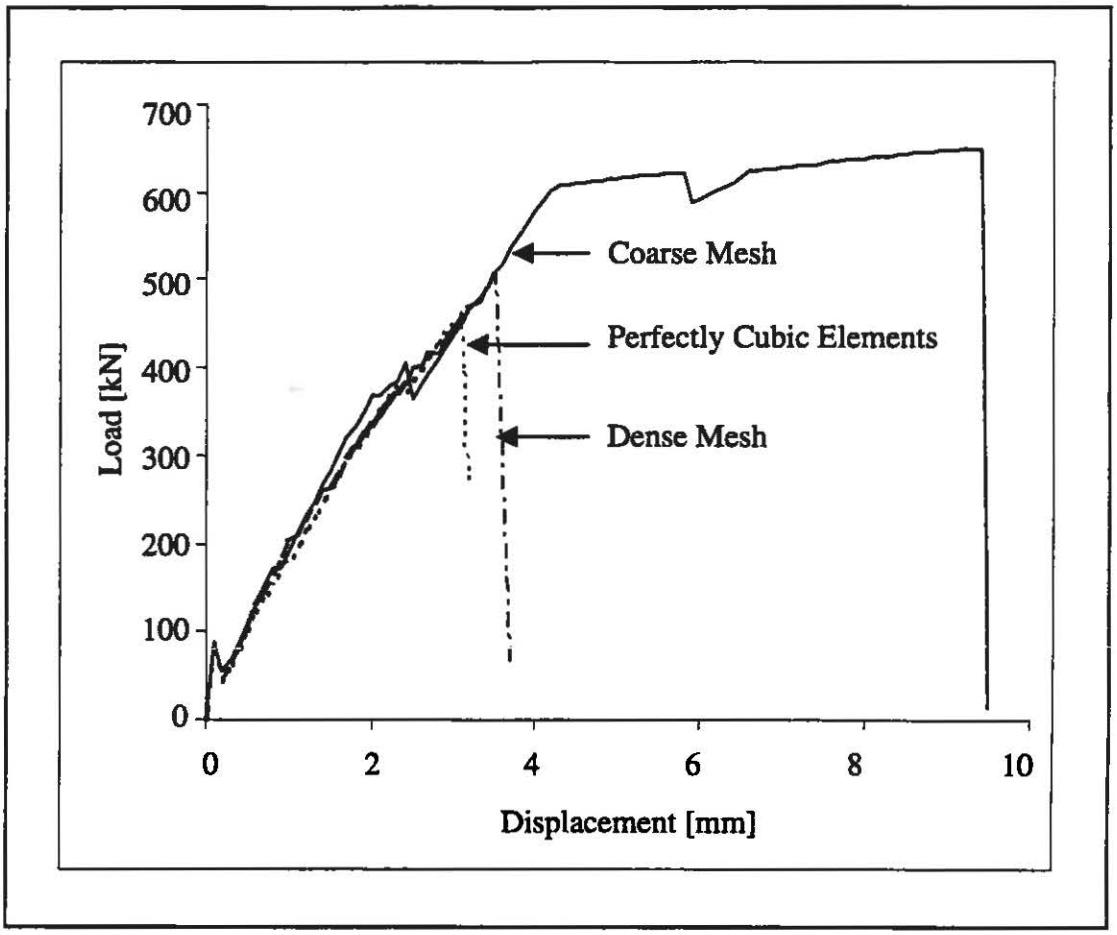

Figure 3.4 Influence of Element Size on Analysis Results

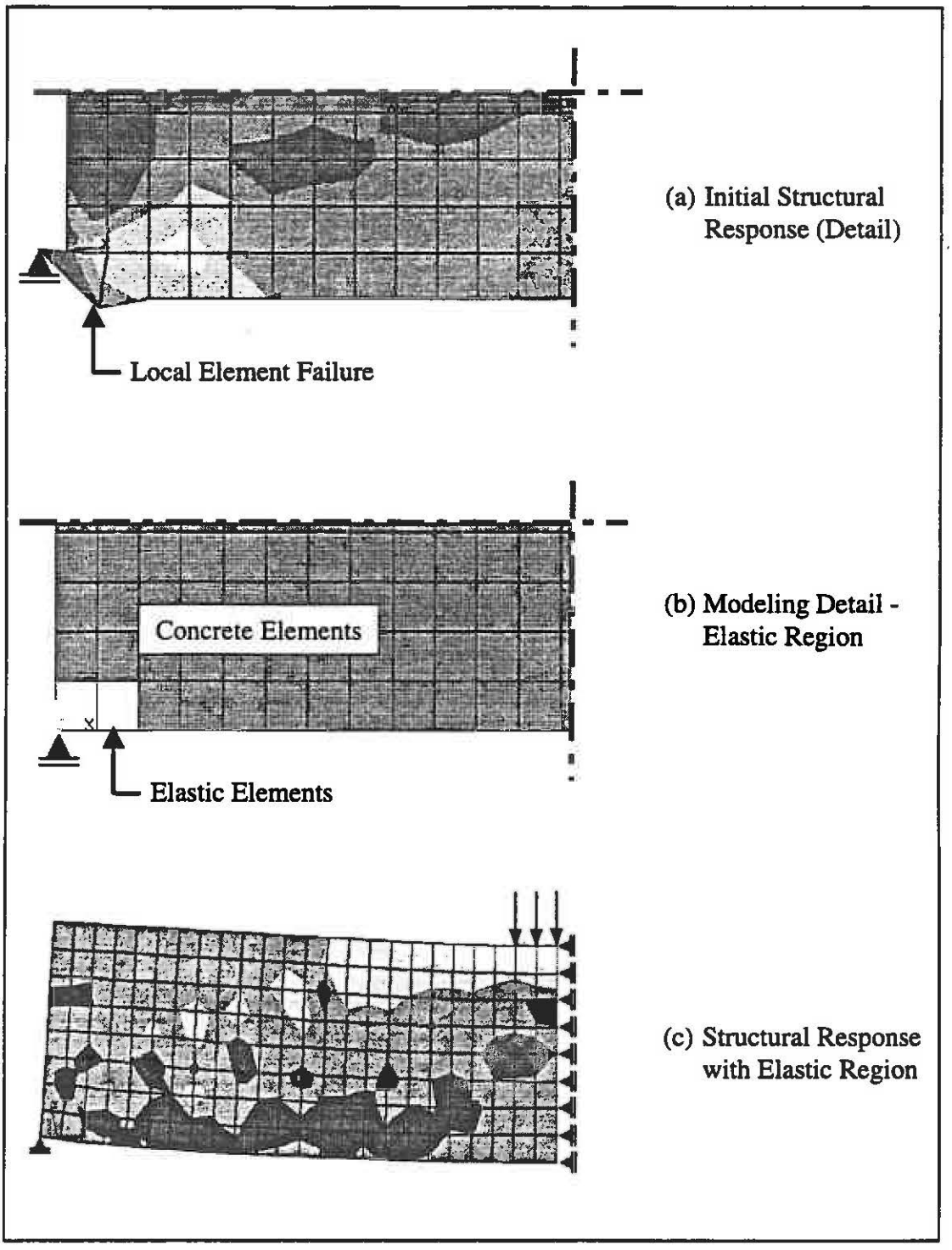

Figure 3.5 Local System Instability and Countermeasure

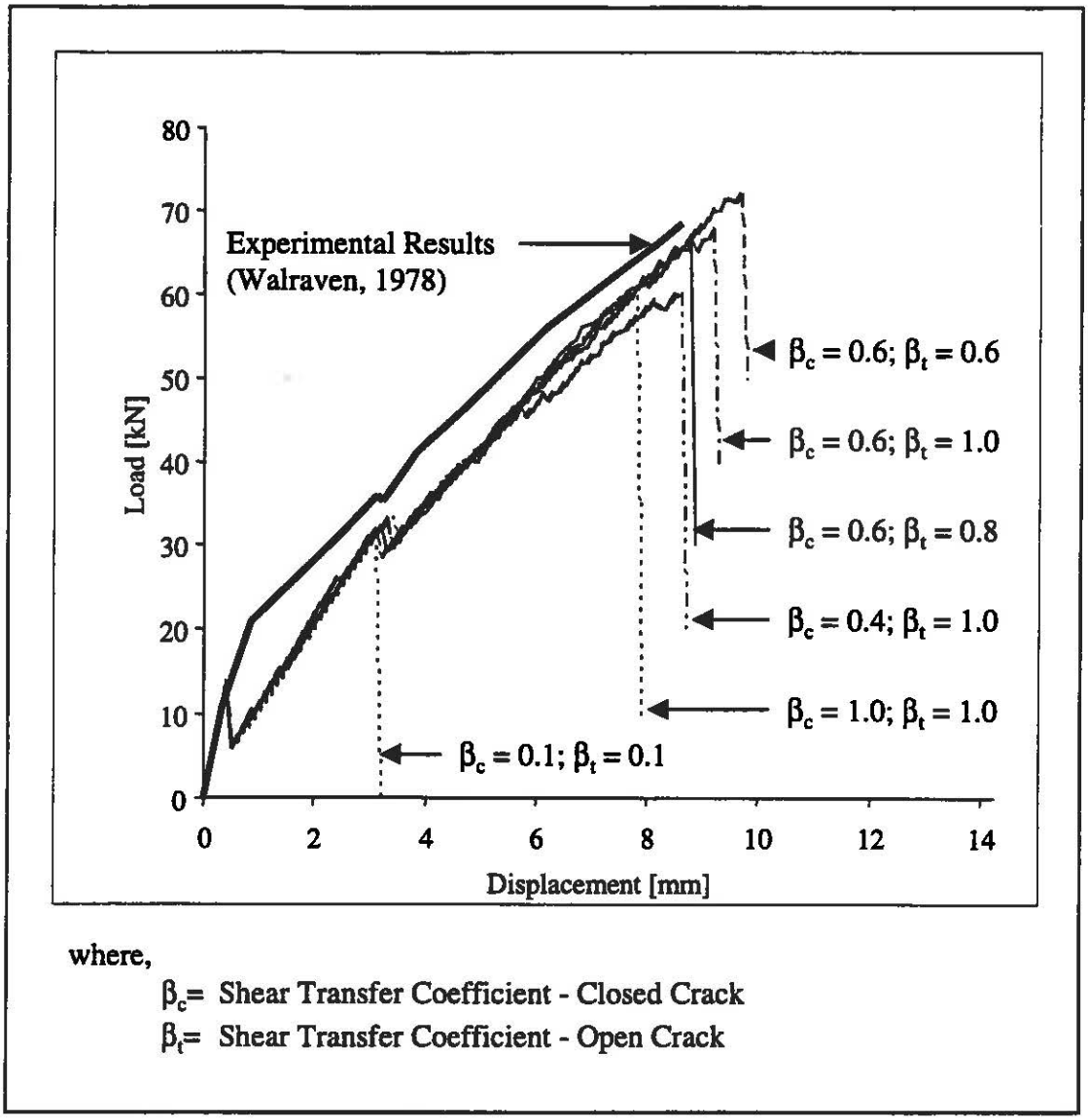

Figure 3.6 Influence of Changes in Shear Transfer Capability

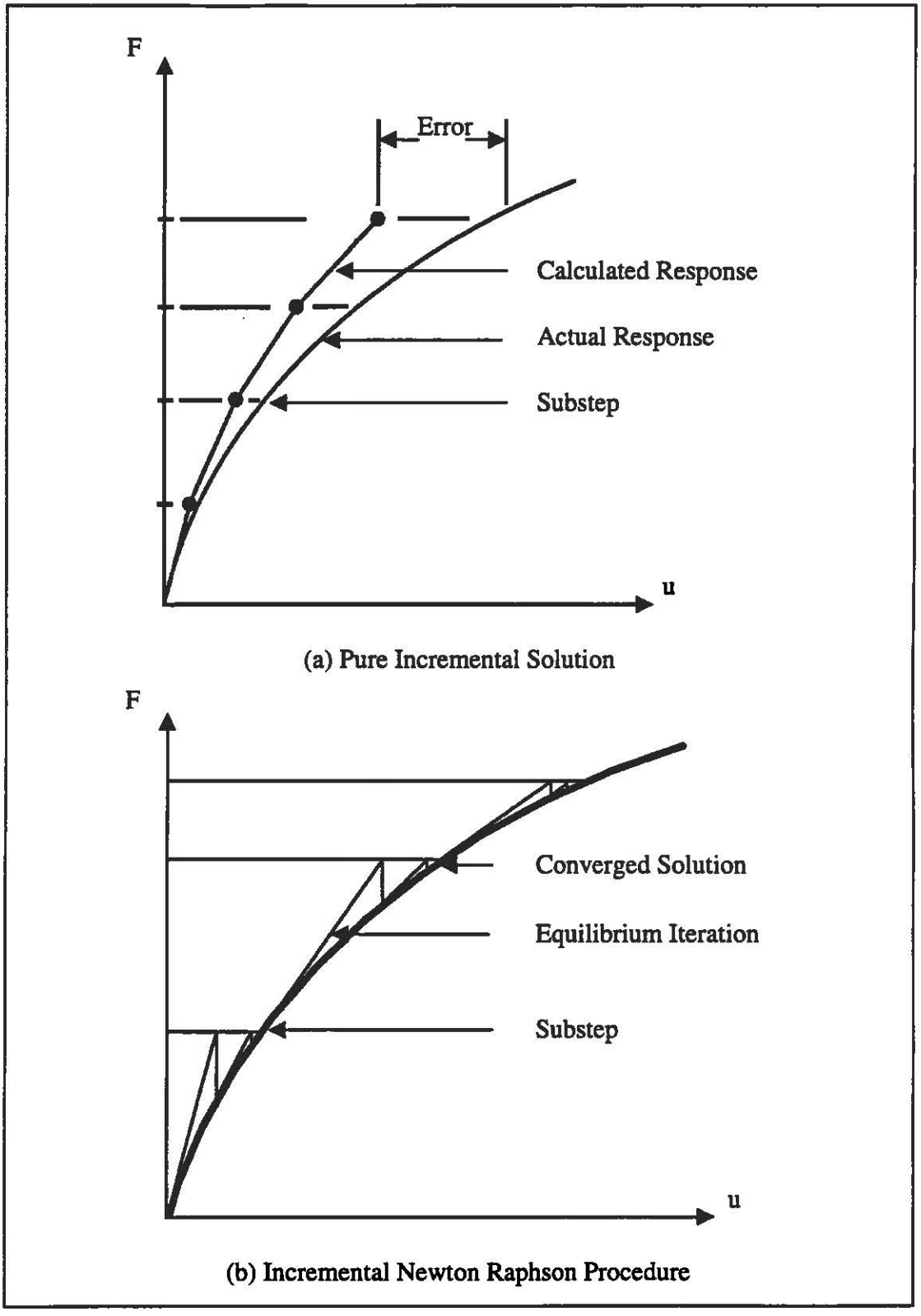

Figure 3.7 Nonlinear Solution Techniques (ANSYS Inc.,1996)

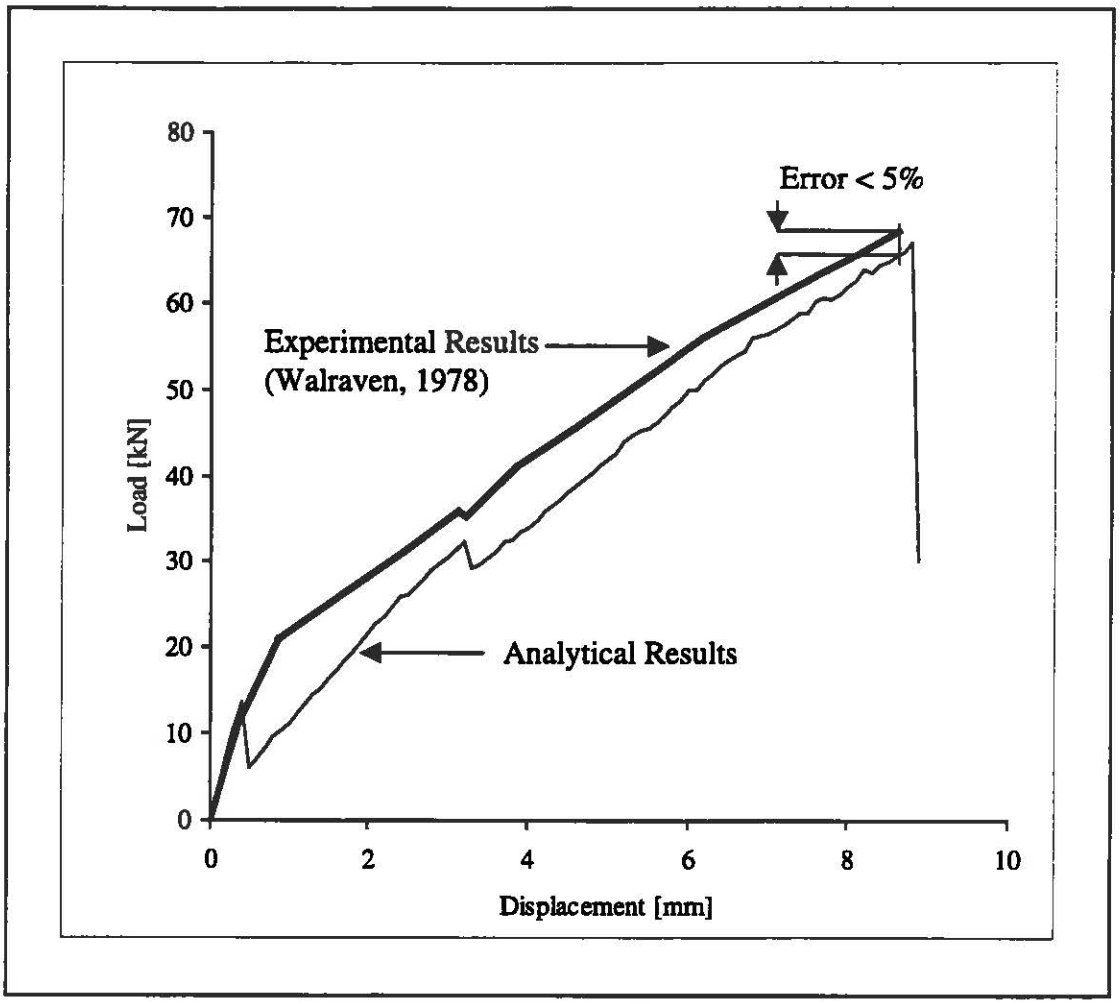

Figure 3.8 Comparison Experimental Results - Analytical Results

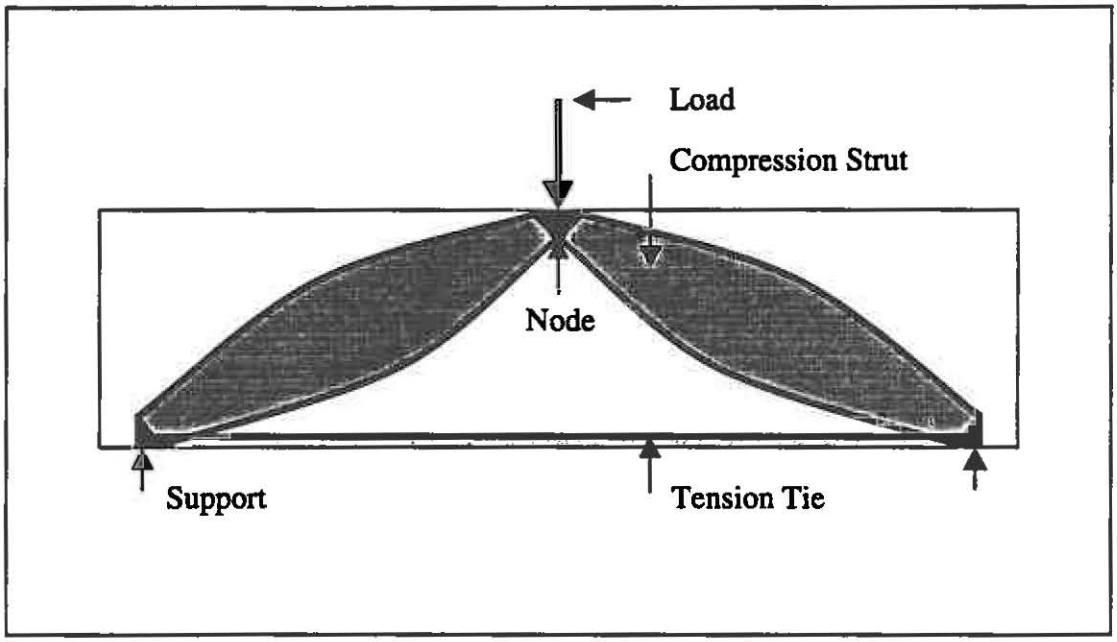

Figure 4.1 Strut and Tie Model for a Beam in Three Point Bending

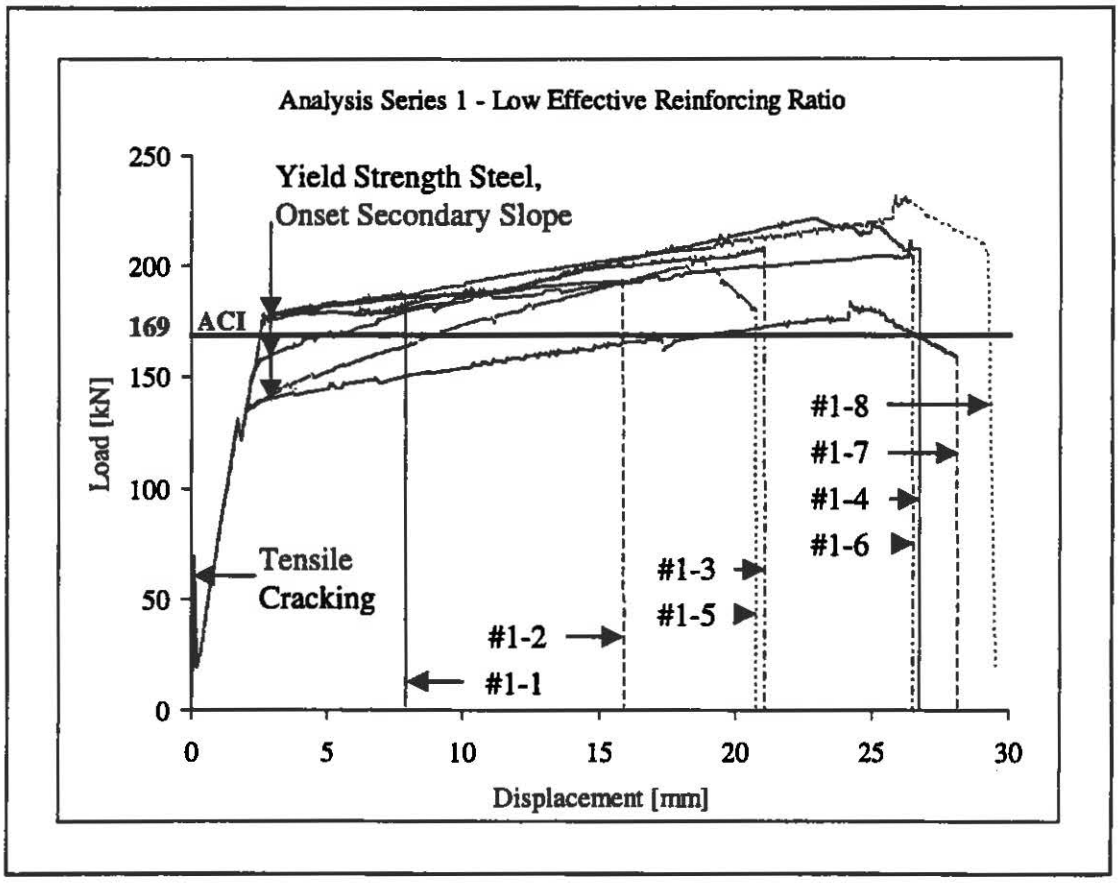

Figure 4.2 Analysis Series 1- Overview Results

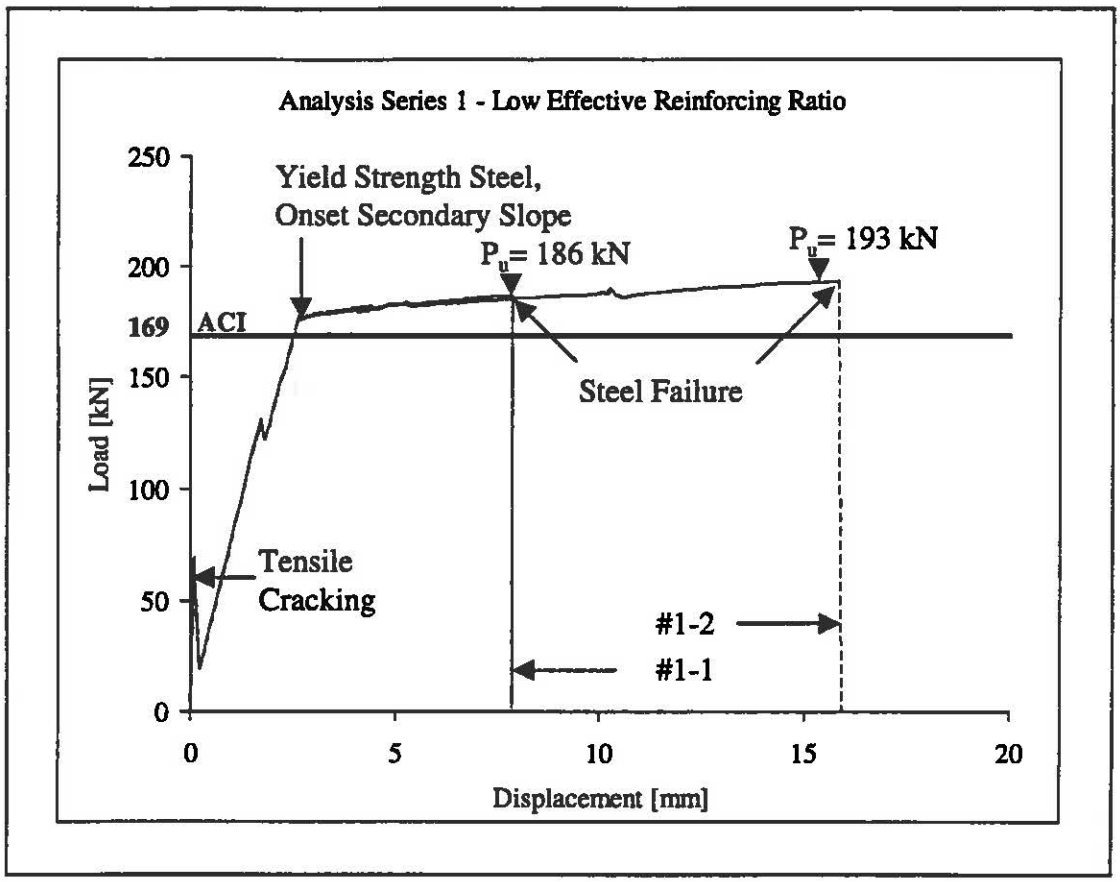

Figure 4.3 Analysis Series 1 - Structural Performance
(Steel without Yield Plateau)

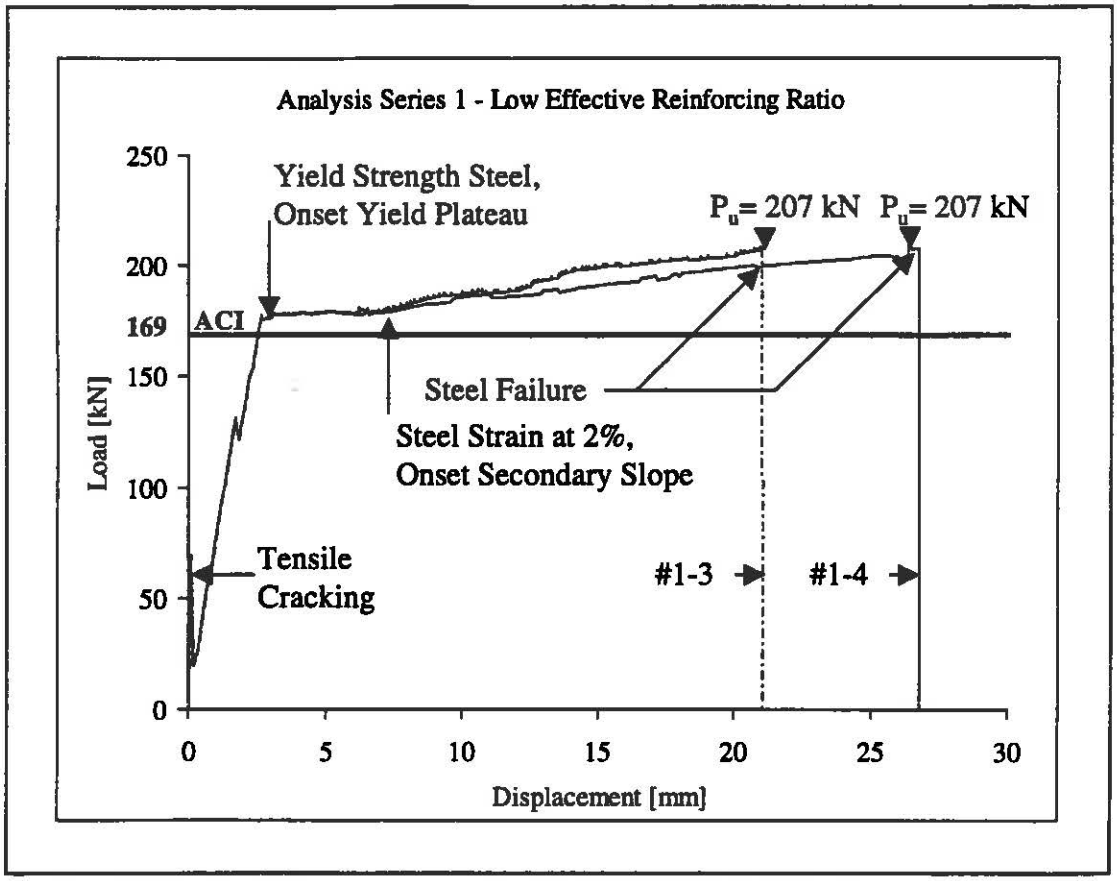

Figure 4.4 Analysis Series 1 - Structural Performance (Steel with Yield Plateau)

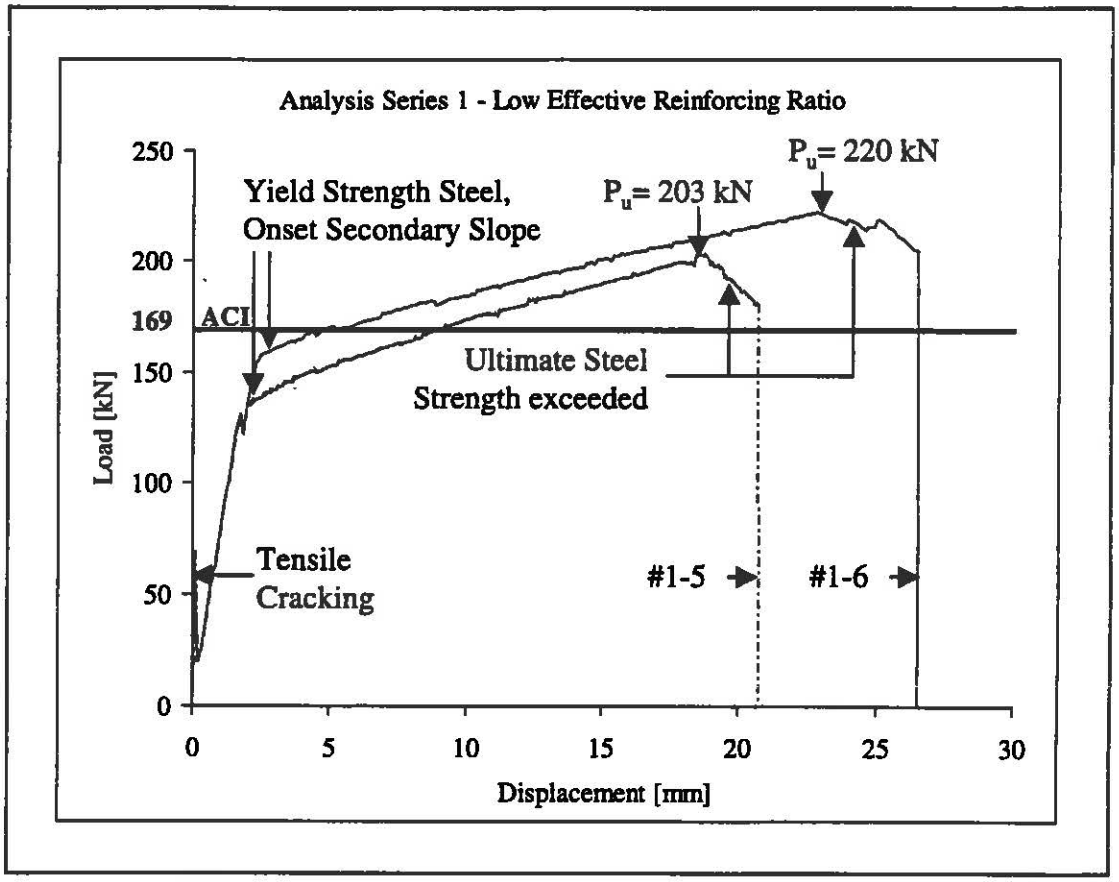

Figure 4.5 Analysis Series 1 - Structural Performance (A615 Steel)

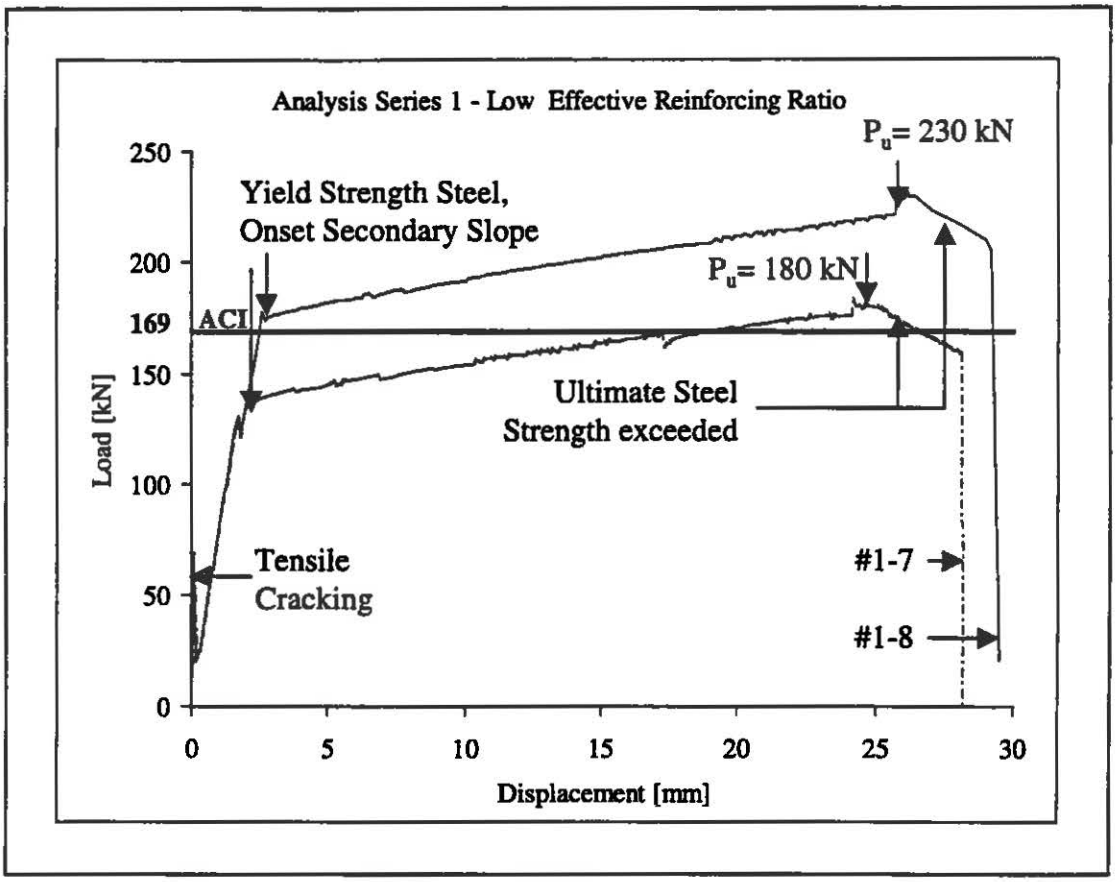

Figure 4.6 Analysis Series 1 - Structural Performance (A706 Steel)

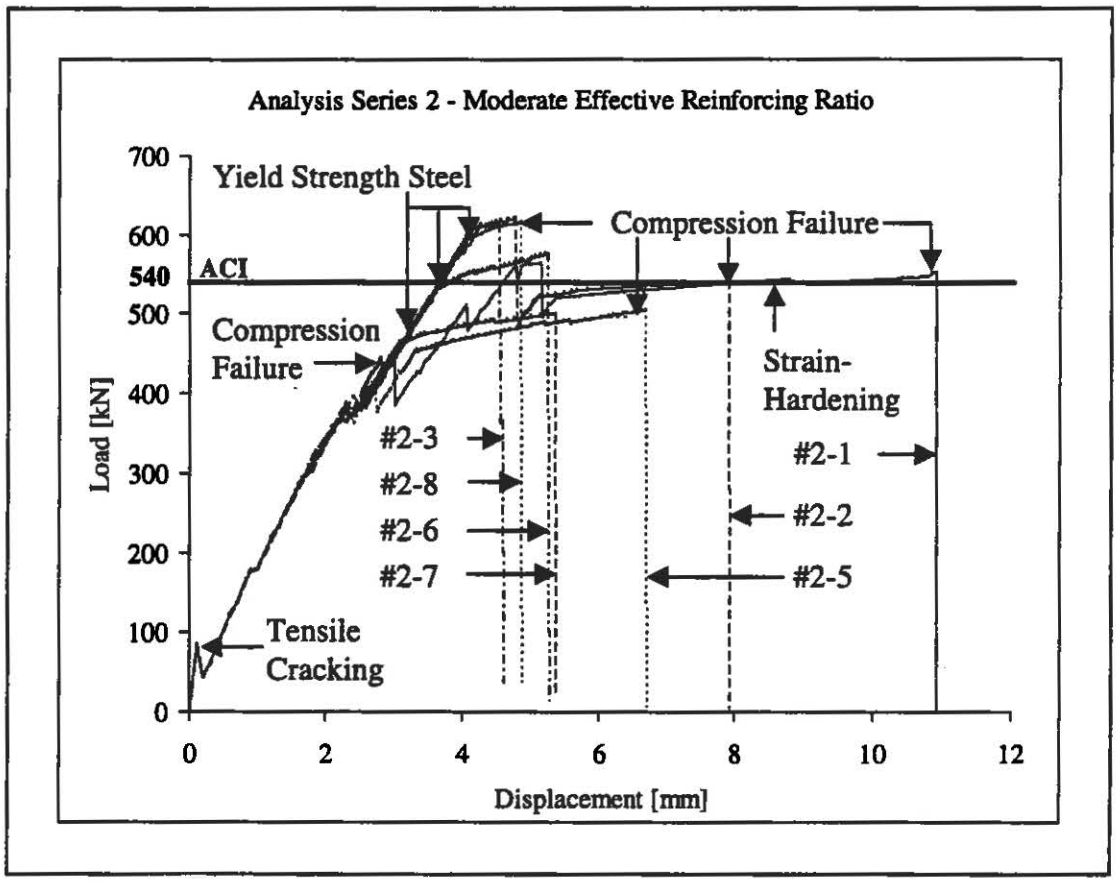

Figure 4.7 Analysis Series 2 - Overview Results

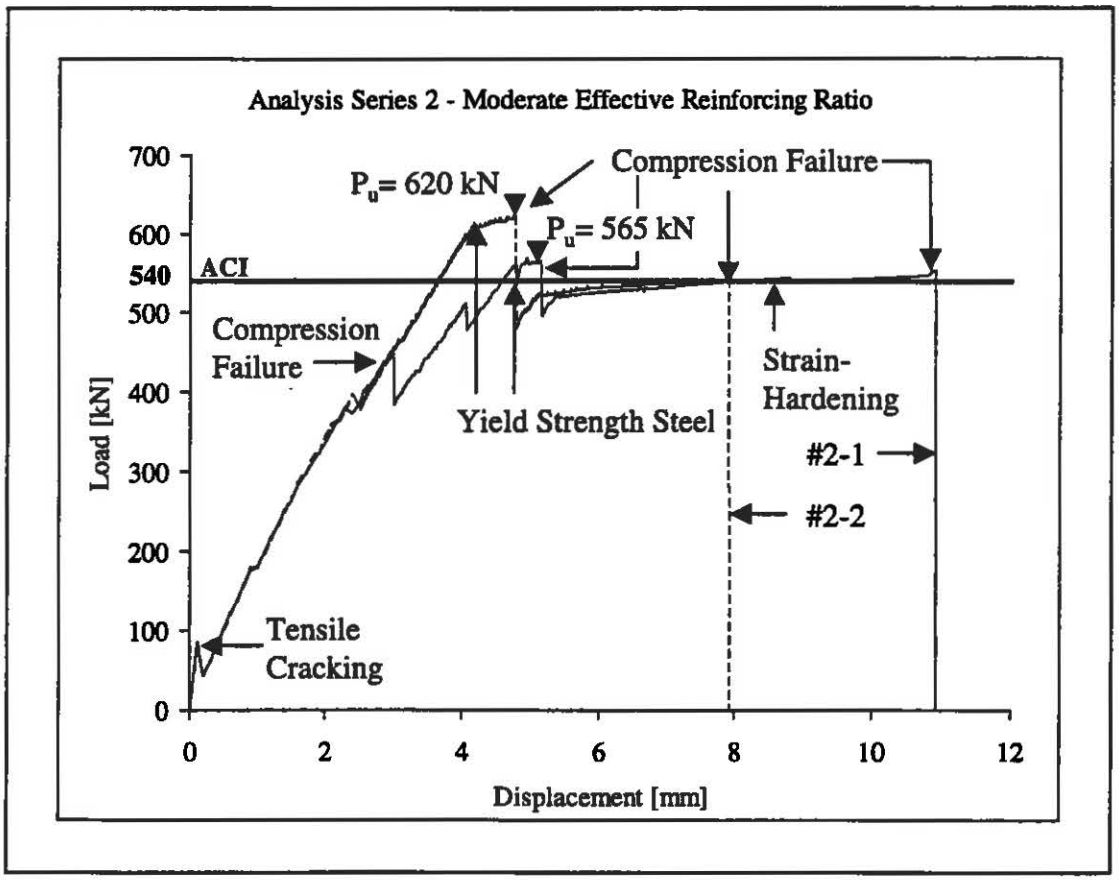

Figure 4.8 Analysis Series 2 - Structural Performance (Steel without Yield Plateau)

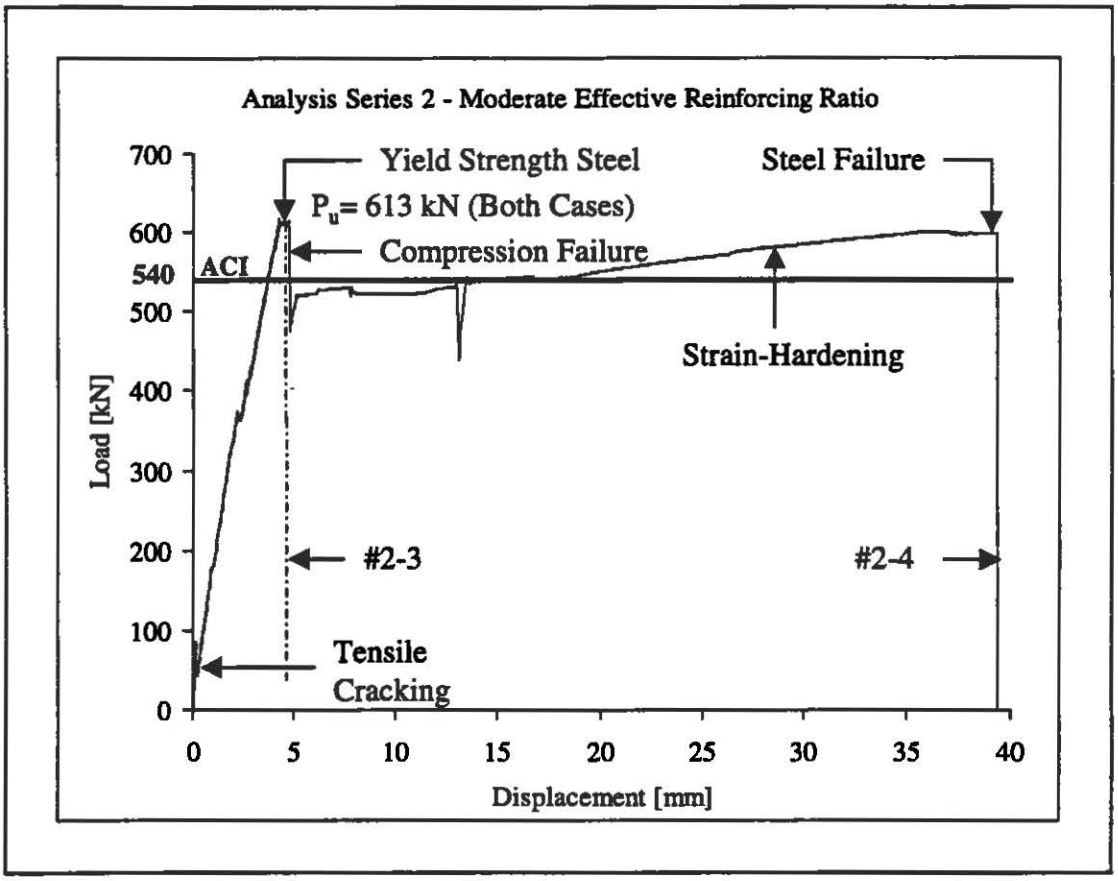

Figure 4.9 Analysis Series 2 - Structural Performance (Steel with Yield Plateau)

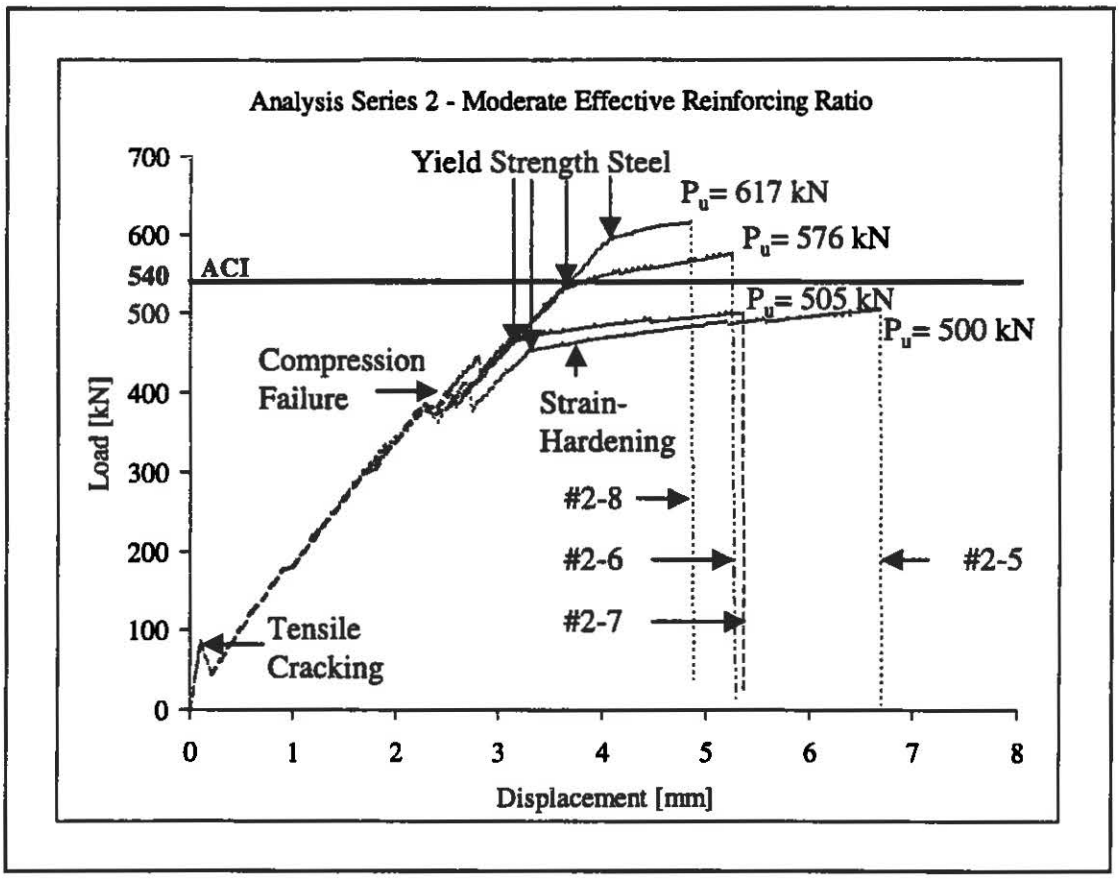

Figure 4.10 Analysis Series 2 - Structural Performance (A615/ A706 Steel)

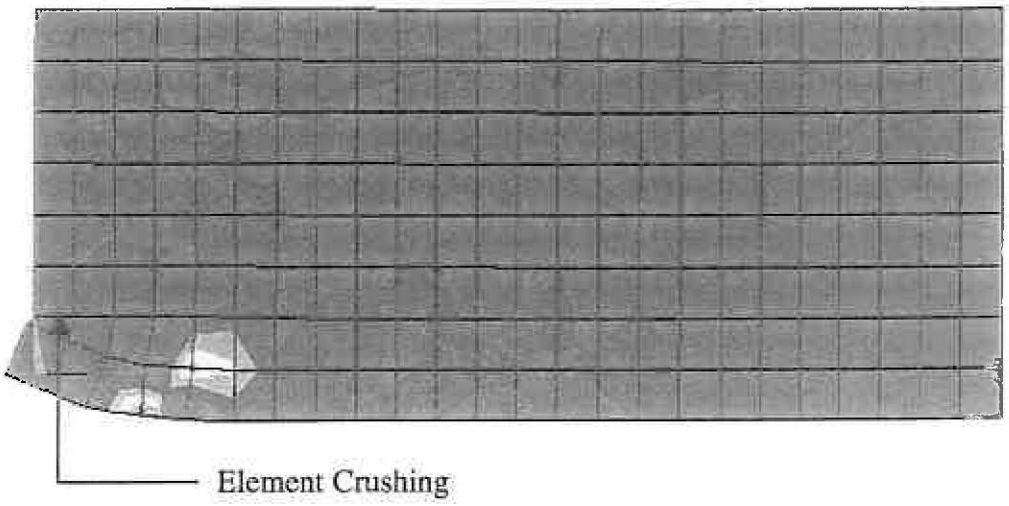

(a) Failure at Support - Analysis #3-6

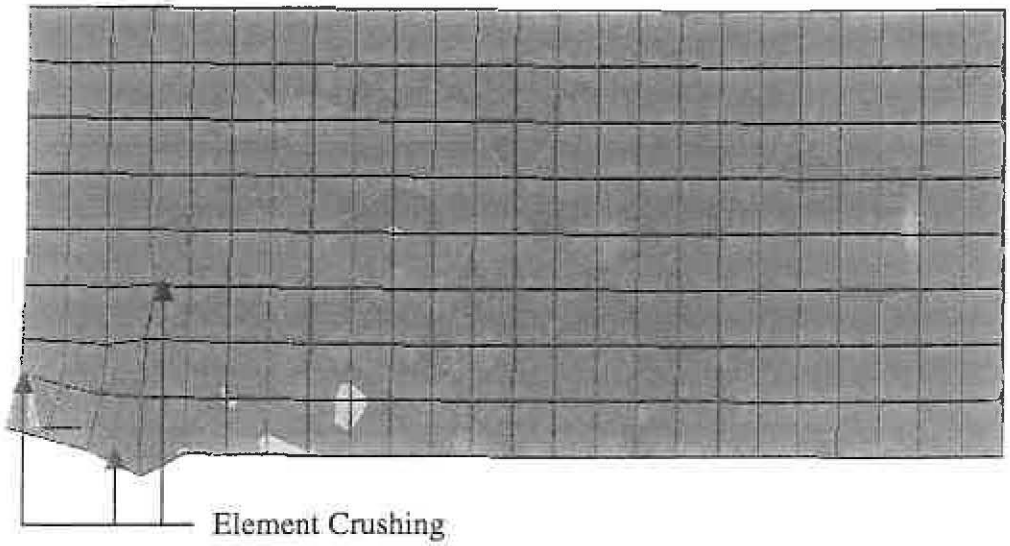

(b) Failure at Support - Analysis #4-5

Figure 4.11 Representative Overview of Compression Strut Failure

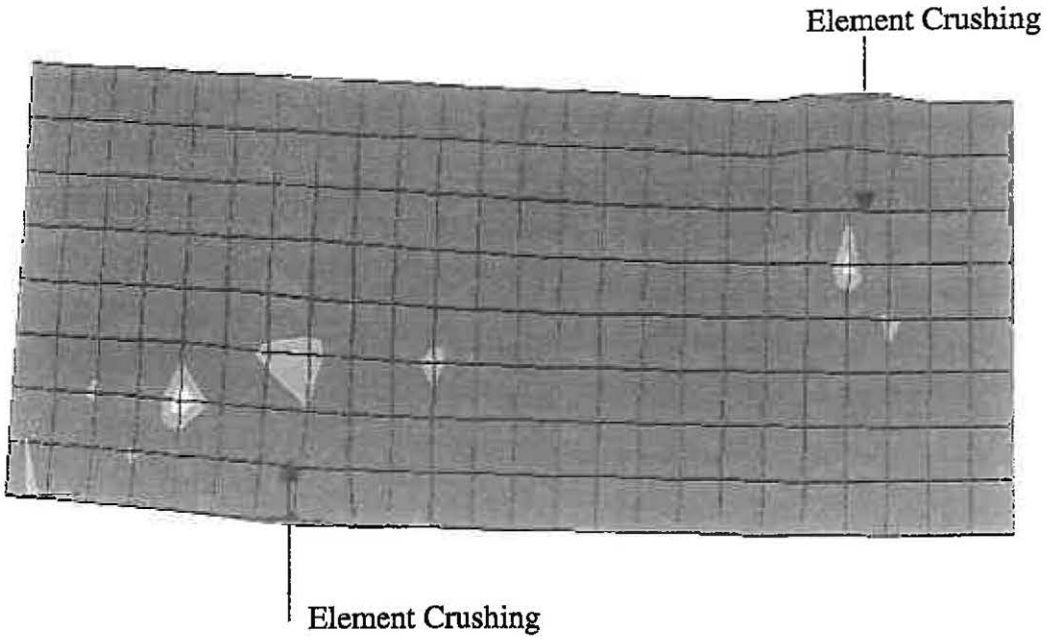

(c) Failure in Upper and Lower Portion - Analysis #3-7

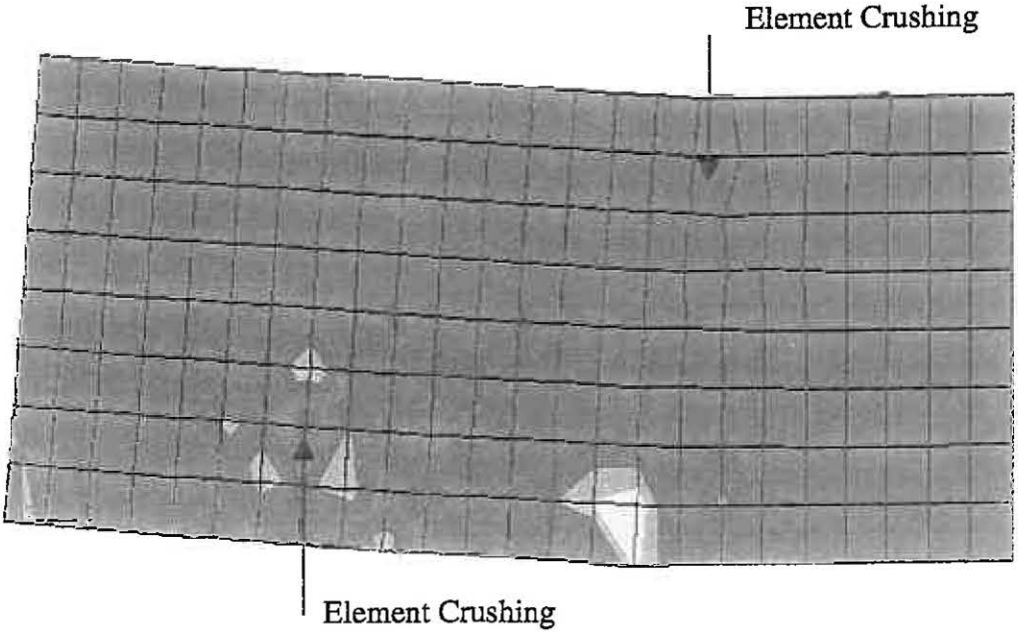

(d) Failure in Upper and Lower Portion - Analysis #4-2

Figure 4.11 Representative Overview of Compression Strut Failure - Cont'd

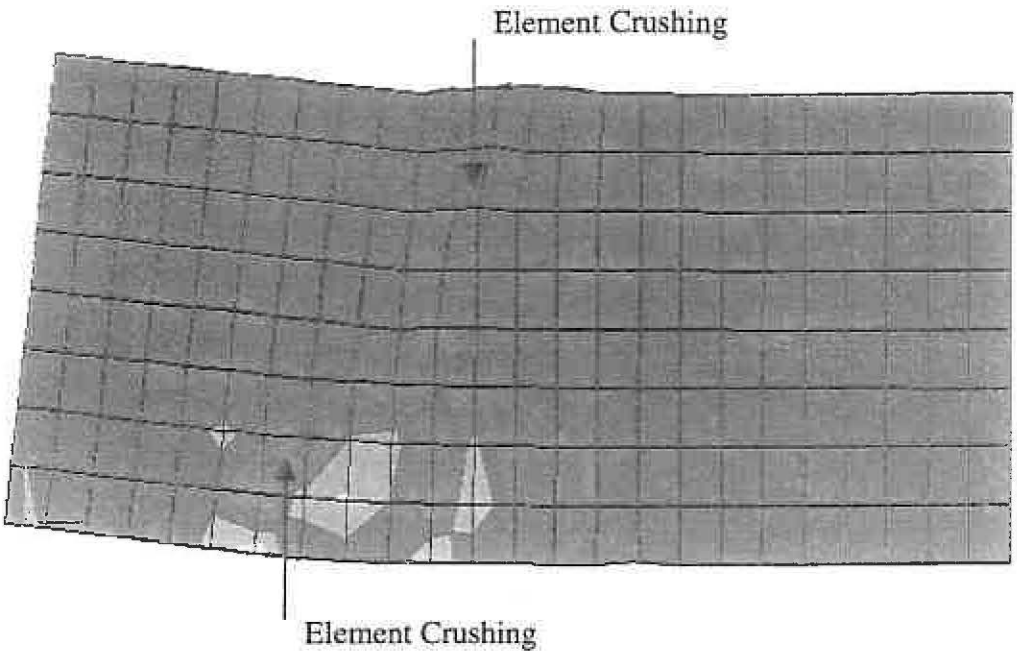

(e) Failure in Upper and Lower Portion - Analysis #4-3

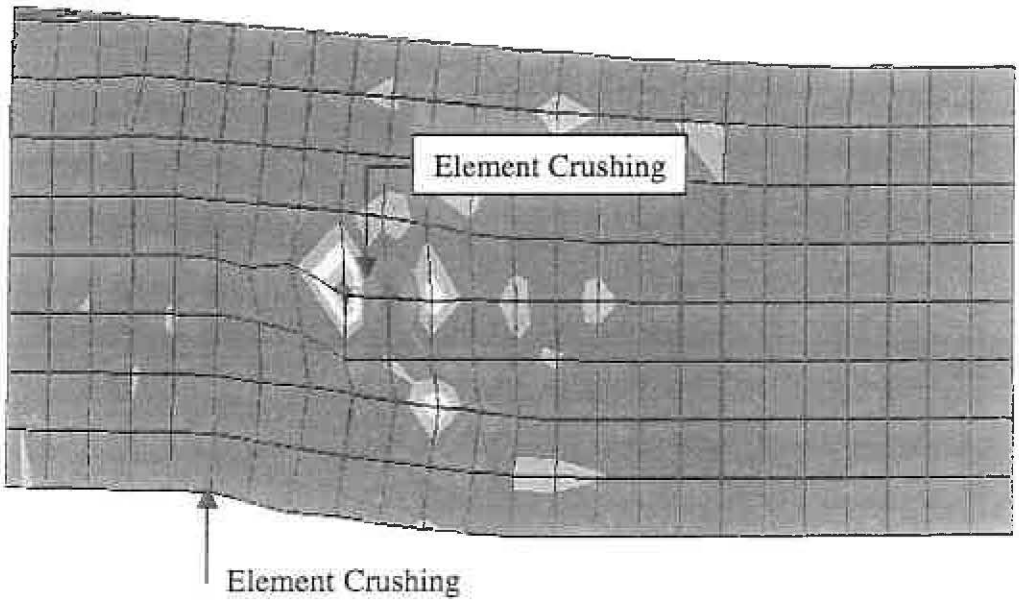

(f) Failure in Center - Analysis #4-4

Figure 4.11 Representative Overview of Compression Strut Failure - Cont'd

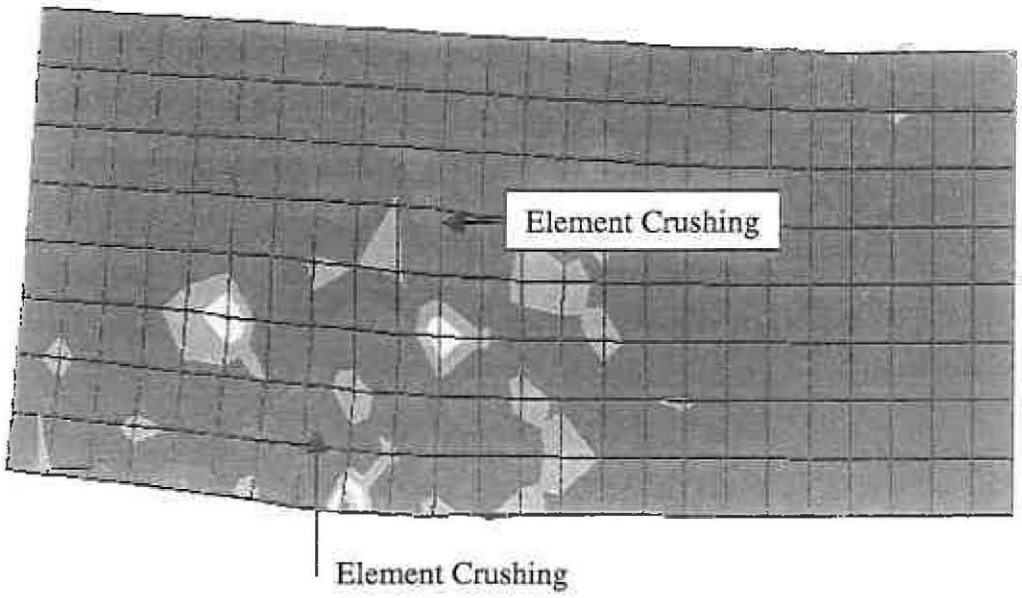

(g) Failure in Center and Lower Portion - Analysis #4-1

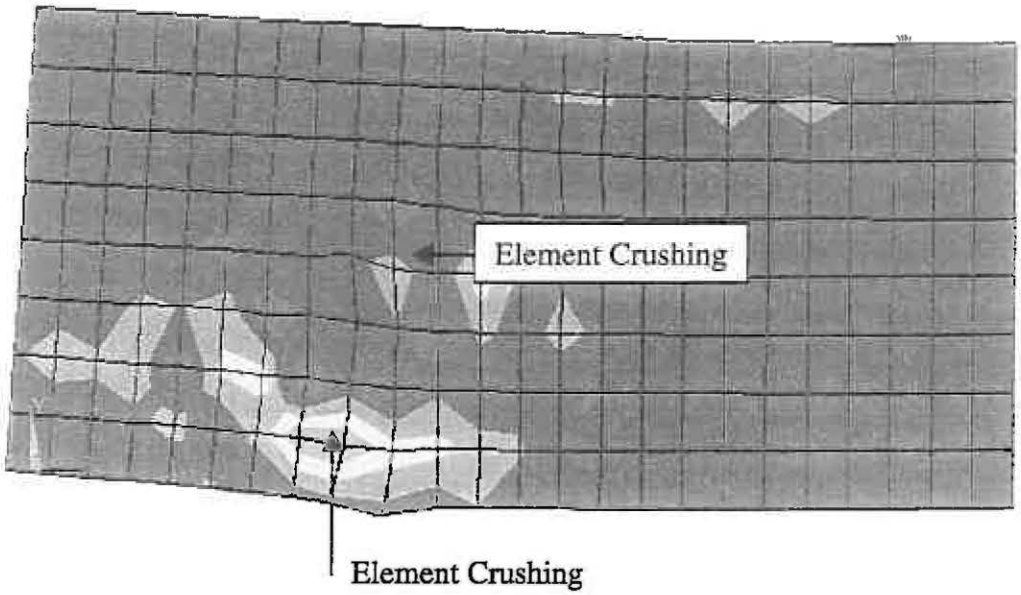

(h) Failure in Center and Lower Portion - Analysis #4-6

Figure 4.11 Representative Overview of Compression Strut Failure - Cont'd

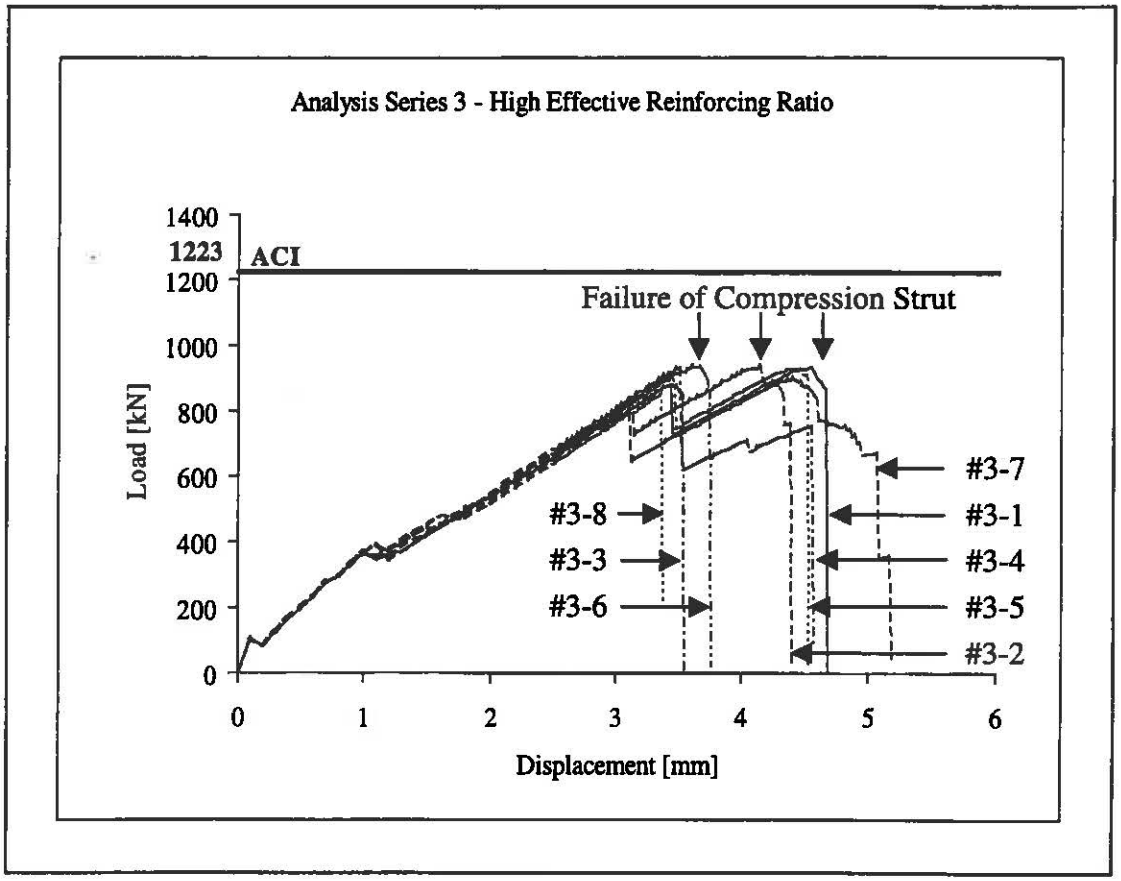

Figure 4.12 Analysis Series 3 - Overview Results

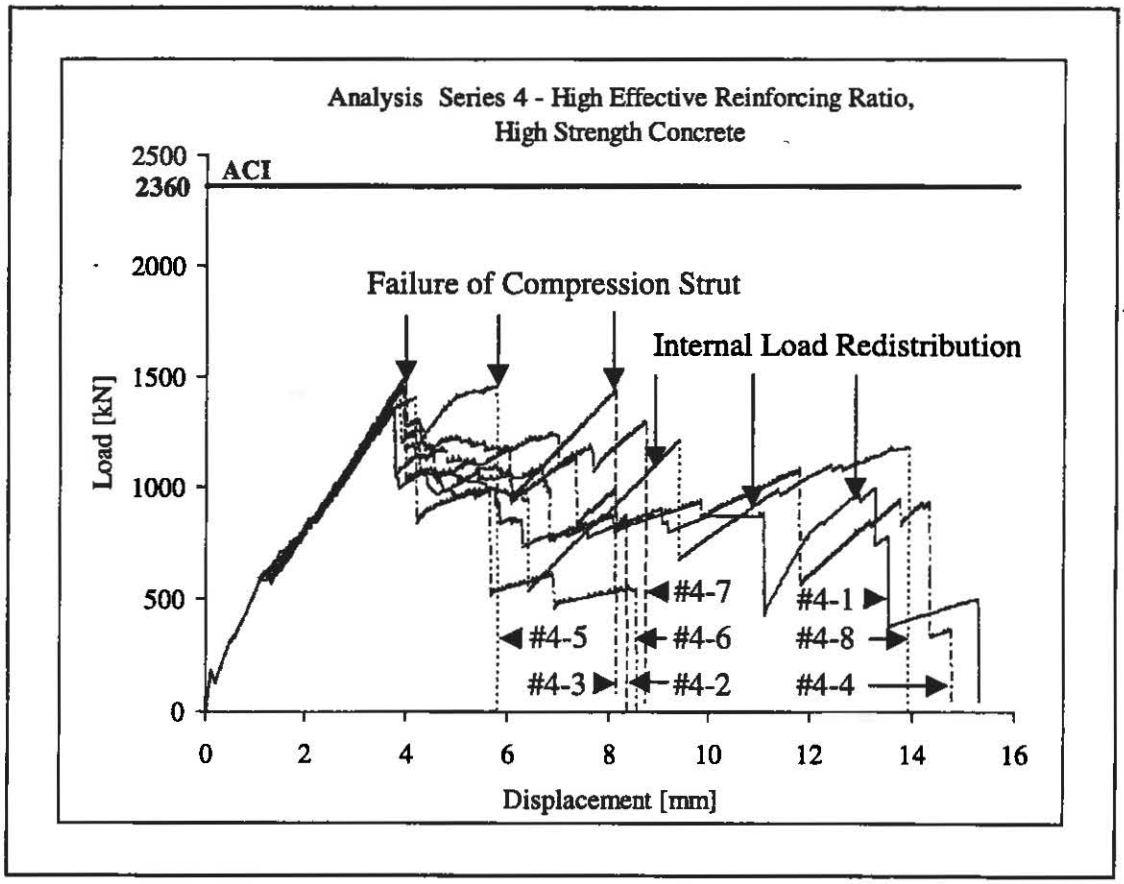

Figure 4.13 Analysis Series 4 - Overview Results

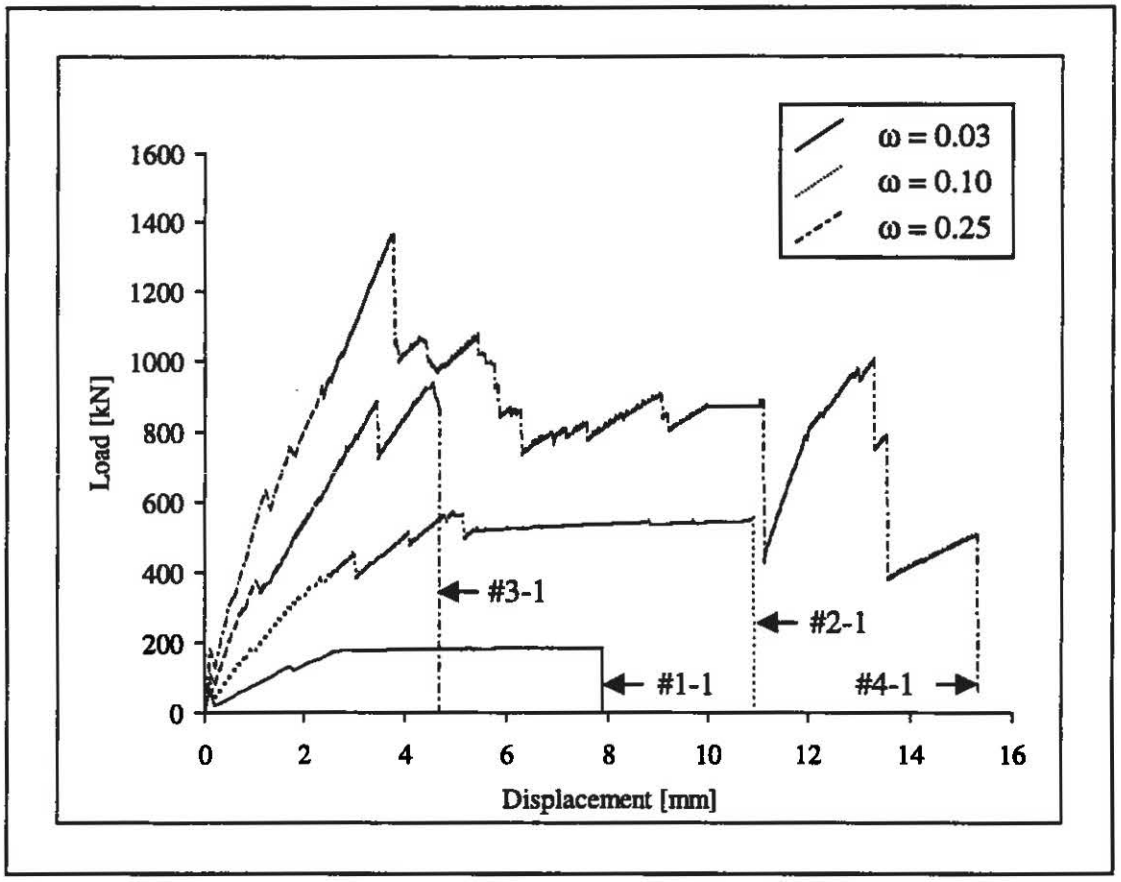

Figure 4.14 Comparison Test Results - Steel #1

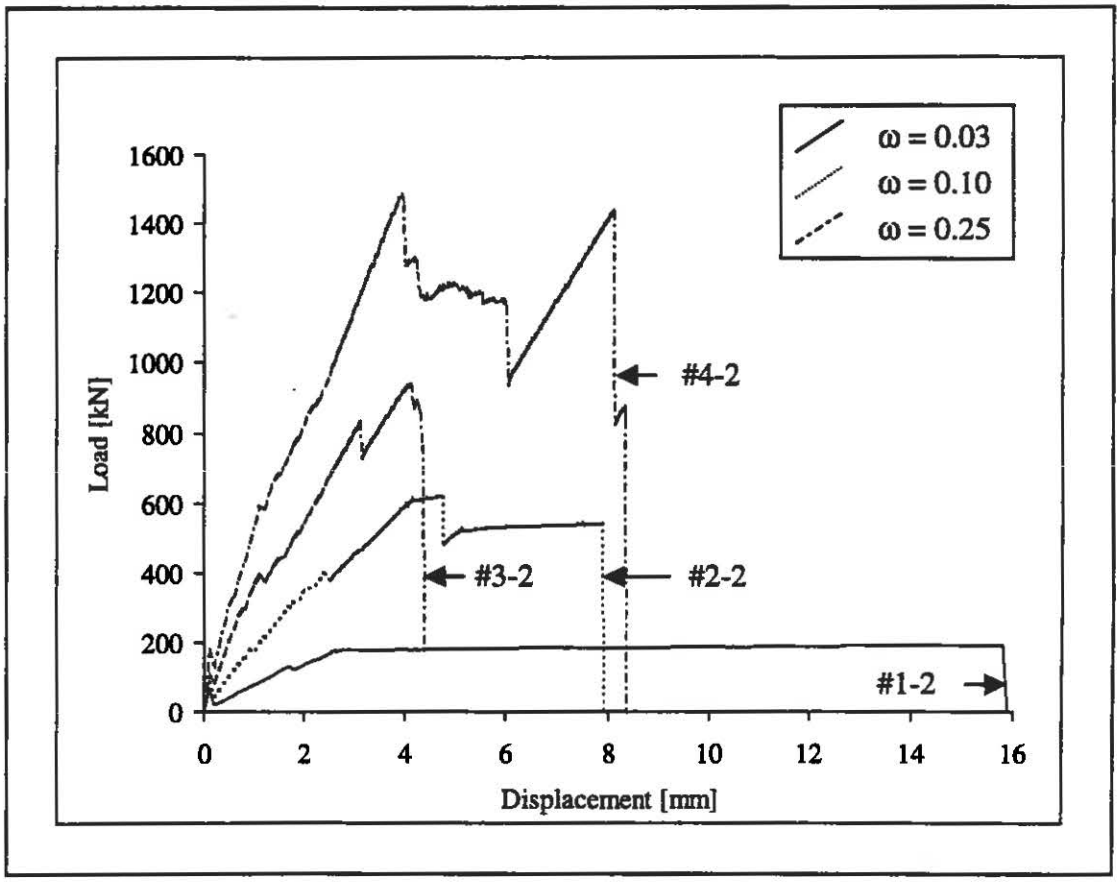

Figure 4.15 Comparison Test Results - Steel #2

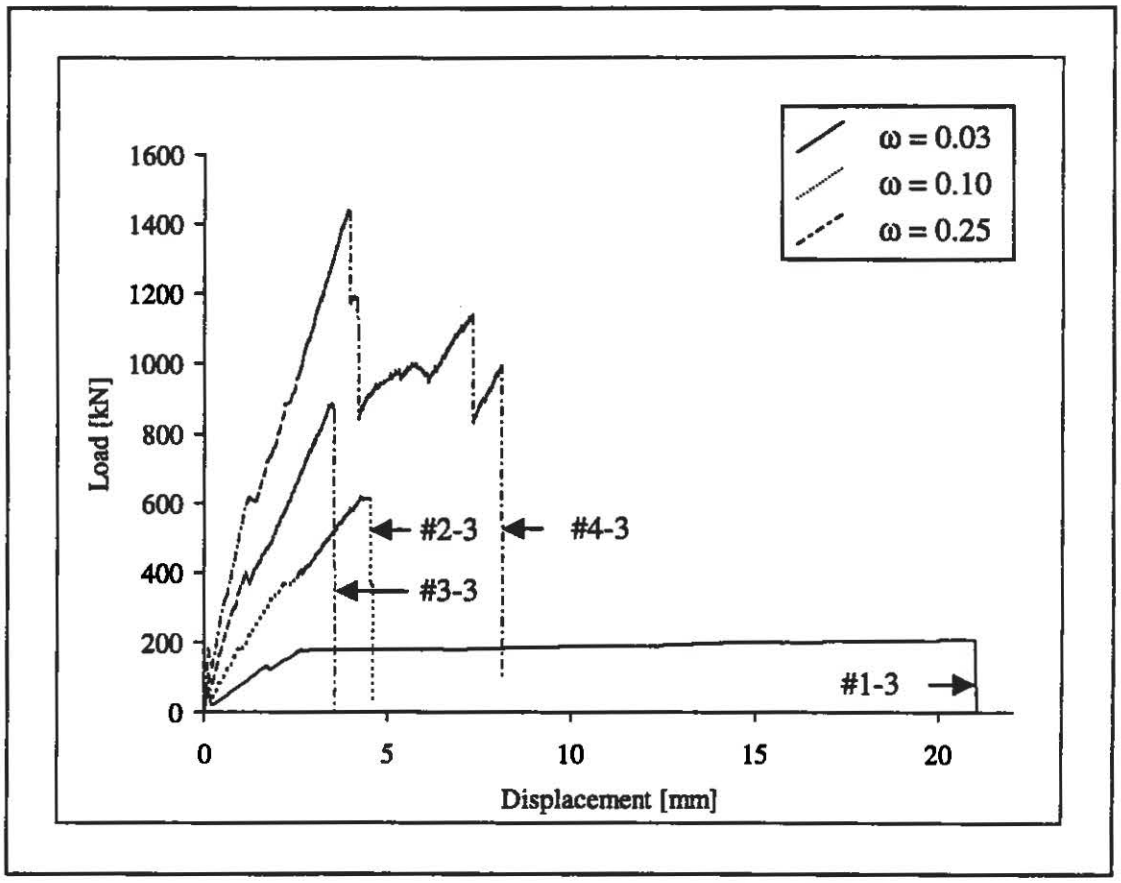

Figure 4.16 Comparison Test Results - Steel #3

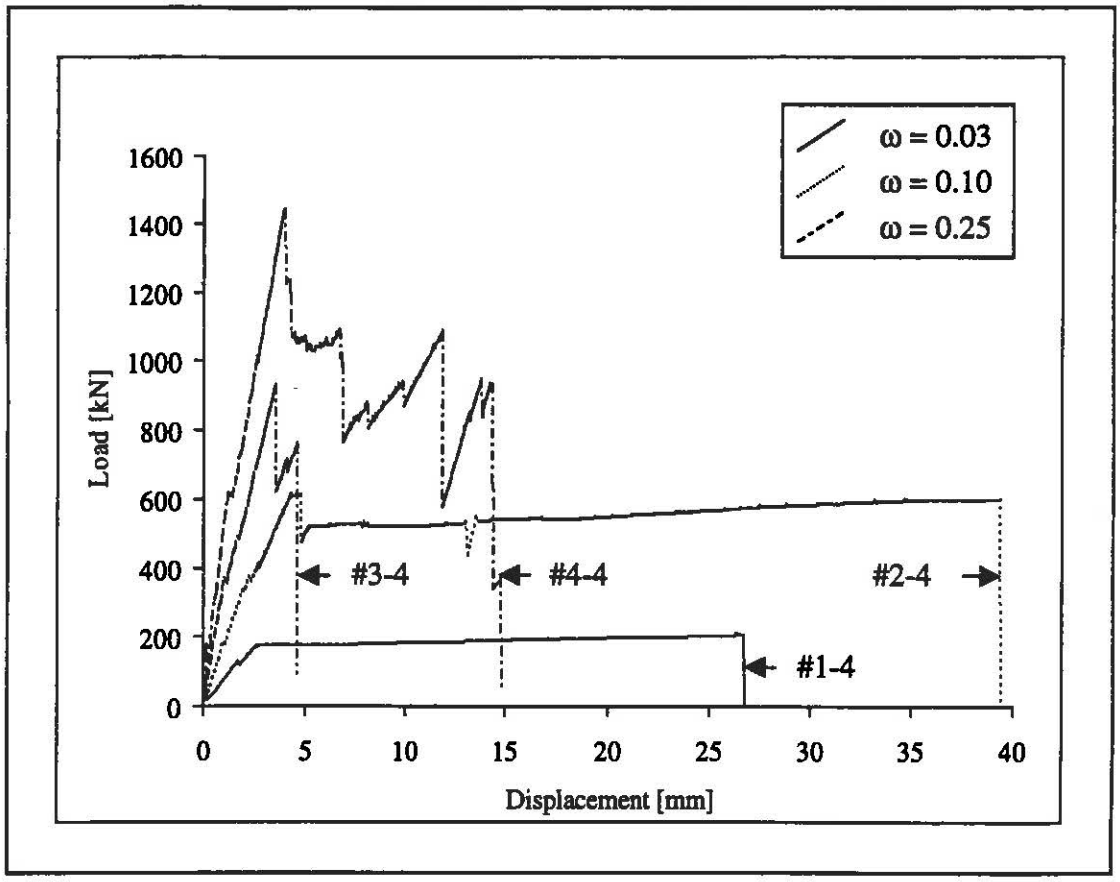

Figure 4.17 Comparison Test Results - Steel #4

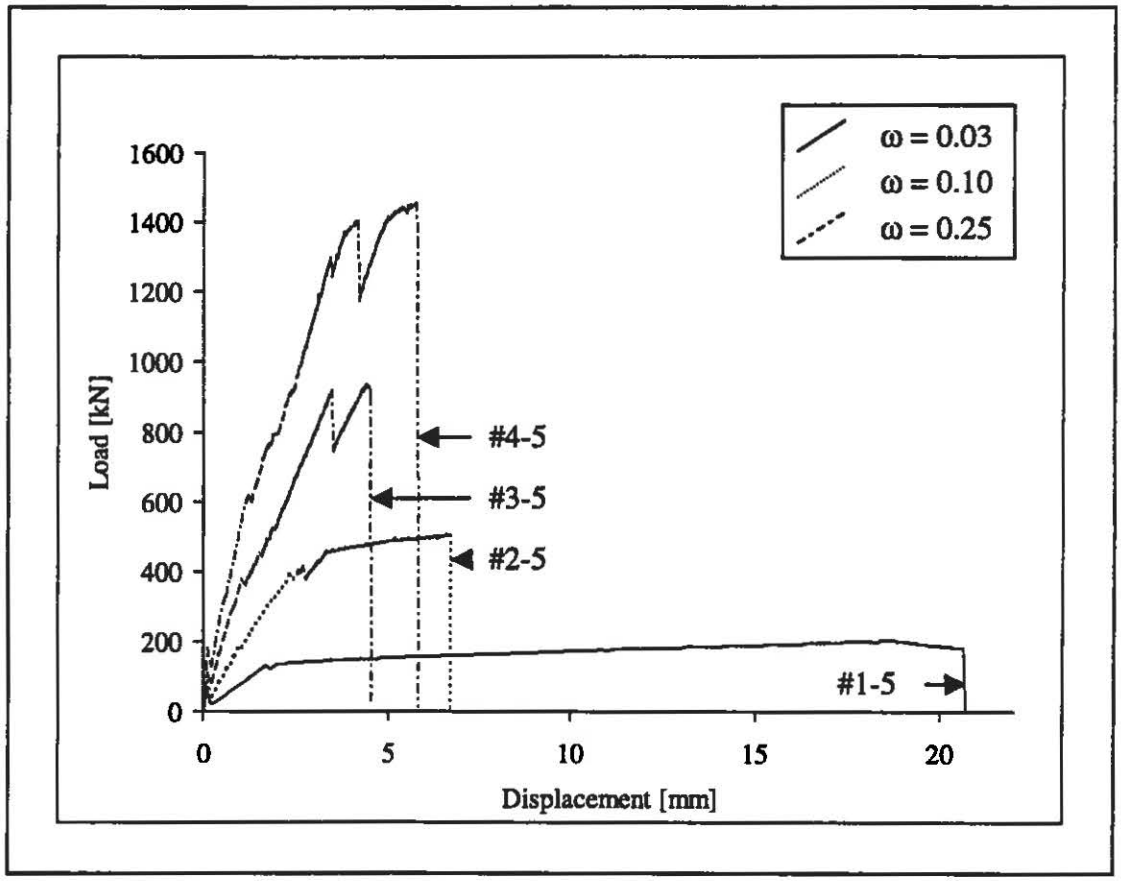

Figure 4.18 Comparison Test Results - Steel #5

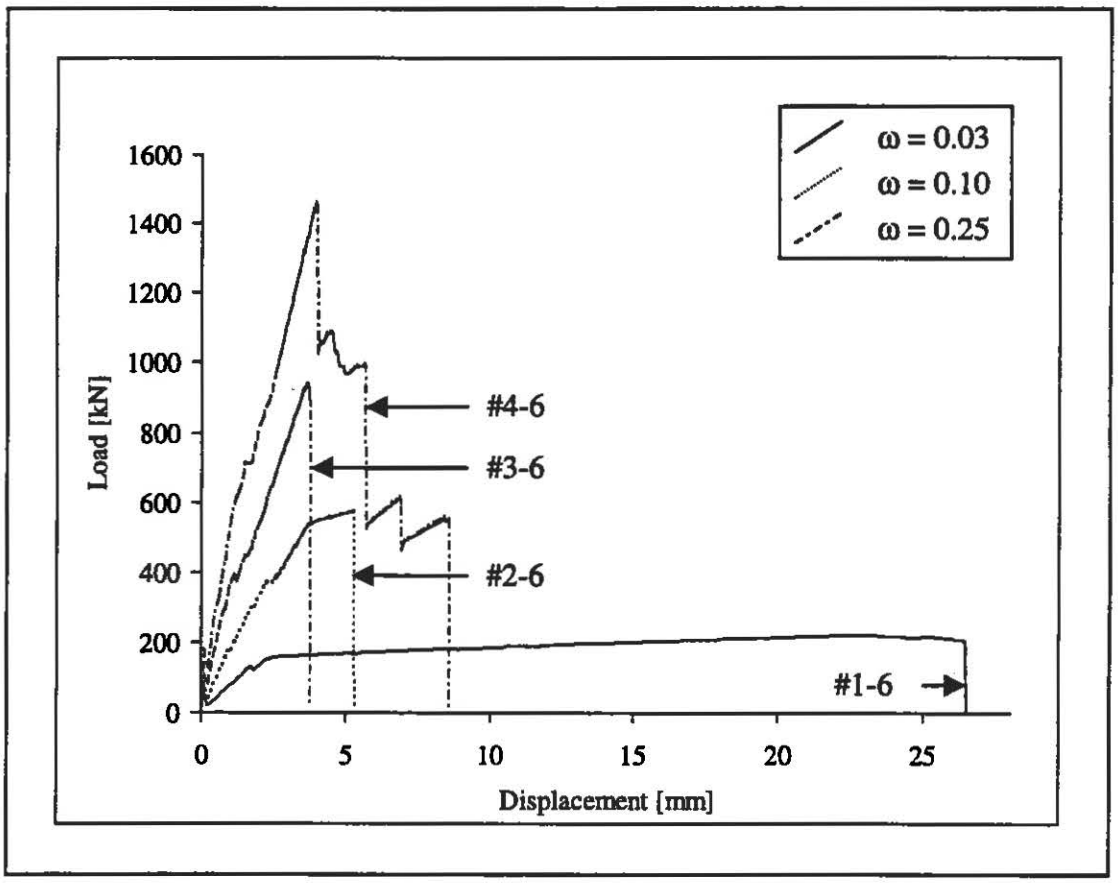

Figure 4.19 Comparison Test Results - Steel #6

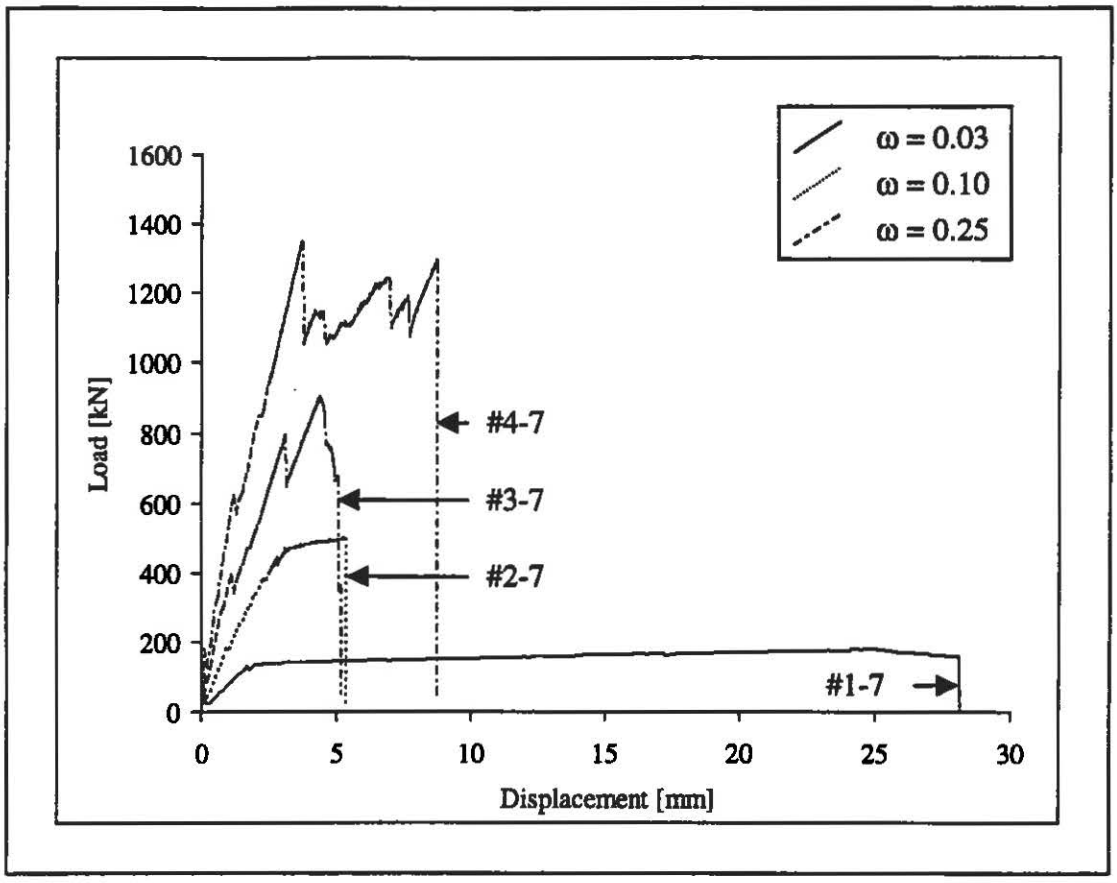

Figure 4.20 Comparison Test Results - Steel #7

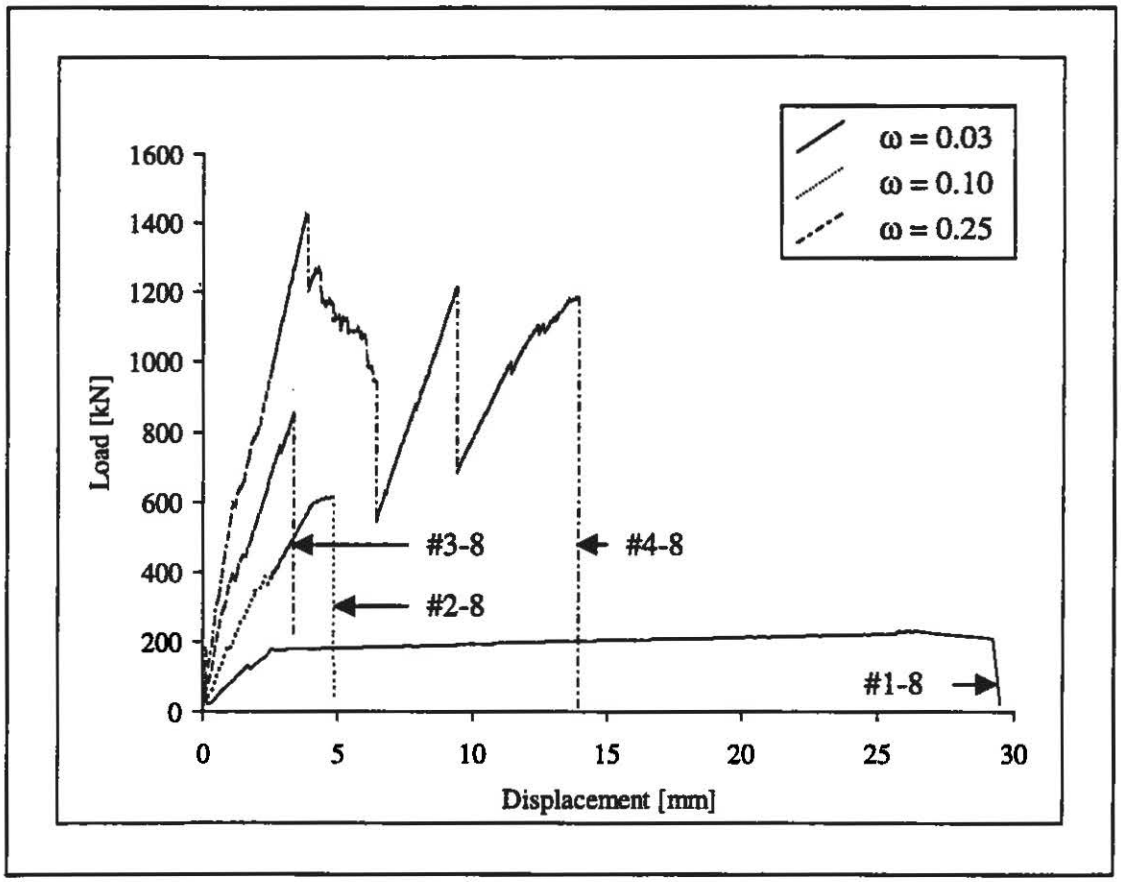

Figure 4.21 Comparison Test Results - Steel #8